AALBORG UNIVERSITY

DENMARK

Acquisition of Multi-Band Signals via Compressed Sensing

Grigoryan, Ruben

[Link to publication from Aalborg University](#)

Acquisition of Multi-Band Signals via Compressed Sensing

Ph.D. Dissertation
Ruben Grigoryan

Aalborg University
Department of Electronic Systems
Fredrik Bajers Vej 7B
DK-9220 Aalborg

Abstract

The Compressed Sensing (CS) approach allows sampling of signals below the conventional Nyquist rate, if signals are sparse in some basis. Basically, the CS framework comprises of two stages: a sub-Nyquist sampling and a signal reconstruction. The signal reconstruction is formulated as an underdetermined inverse problem, which can be solved by a variety of methods. Therefore in CS, the lack of signal samples is compensated by a more complicated reconstruction procedure in comparison to the Nyquist rate sampling.

The CS approach can improve characteristics of some acquisition instruments, for example Signal Analyzers (SA). SA is a measurement tool that can replace a spectrum and a vector analyzer. With the development of wireless communications, the demand for SA with better characteristics also increases. For example, the LTE specification uses high frequency and wide-band signals. However, the complexity and price of the analog front-end and ADCs that operate at such frequencies is high. Hence, it is beneficial to improve the SA capability by better utilizing the existing hardware, and CS may be a means for doing it.

In this thesis, we focused on two CS architectures that can be used for SA applications. These architectures are Single-channel Nonuniform Sampling (SNS) and Multi-Coset Sampling (MCS). One of their advantages is a relatively simple front-end that can be implemented with minimum modification of the SA hardware. The considered aspects include the performance and the reconstruction complexity of the various reconstruction methods. As the main scenario, we assume the acquisition of multi-band frequency sparse signals corrupted with additive white Gaussian noise. This scenario reflects the tendency of the modern wireless communication specifications, like LTE, to utilize a number of narrow bands distributed over a wide bandwidth.

With extensive numerical simulations, we highlight the performance of the various reconstruction methods under the different sampling conditions and provide the recommendations for the most appropriate reconstruction methods. We propose the multi-coset emulation as a means to reduce the reconstruction complexity for the SNS acquisition. Depending on the acquisition scenario, the multi-coset emulation may retain, improve or degrade the reconstruction quality. However, for all scenarios, this emulation reduces the reconstruction complexity by at least an order of magnitude.

Resumé

Det såkaldte Compressed Sensing (CS)-princip tillader opsamling af signaler under den konventionelle Nyquist-rate, hvis signalerne er såkaldt sparsomt repræsenteret i en given basis. Grundlæggende består princippet af to trin: Signalopsamling under Nyquist-raten og efterfølgende signalrekonstruktion. Signalrekonstruktionen formuleres som et underdetermineret invers problem, som kan løses med forskellige metoder. Således kompenseres de færre signal-samples i CS af en mere kompliceret rekonstruktionsprocedure sammenlignet med Nyquist-rate signalopsamling.

CS-tilgangen kan forbedre visse karakteristika ved nogle måleinstrumenter - for eksempel signalanalysatorer (SA). SA er måleværktøjer, der kan erstatte spektrum- og vektoranalysatorer. I takt med udviklingen inden for trådløs kommunikation stiger kravet om SA med bedre karakteristika også. For eksempel benytter LTE-specifikationen højfrekvente og bredbåndede signaler. Dog er kompleksiteten og prisen for den analoge "front-end" og analog-til-digital convertere, som arbejder ved så høje frekvenser, høj. Det er således fordelagtigt at forbedre SA ved bedre at udnytte eksisterende hardware, og her kan CS være et middel til at opnå dette.

I denne afhandling undersøger vi praktiske aspekter ved to CS-arkitekturer, der kan bruges til SA-applikationer. Disse arkitekturer er Single-channel Nonuniform Sampling (SNS) og Multi-Coset Sampling (MCS). En af fordelene ved disse er den relativt simple front-end, der kan implementeres med et minimum af modifikation af SA-hardwaren. De undersøgte aspekter inkluderer præstationsevne og rekonstruktionskompleksitet af forskellige rekonstruktionsmetoder. Som hovedscenariet betragter vi opsamling af flerbåndede signaler, der er sparsomt repræsenteret i frekvensdomænet og påvirket af additiv hvid Gaussisk støj. Dette scenarie reflekterer tendensen i moderne specifikationer for trådløs kommunikation - som LTE - ved at benytte et antal smalle frekvensbånd distribueret over en stor båndbredde.

Ved hjælp af omfattende numeriske simulationer sætter vi fokus på præstationerne for forskellige rekonstruktionsmetoder under forskellige signalopsamlingsforhold og uddrager heraf anbefalinger i forhold til de mest egnede metoder. Vi foreslår emulering af multi-coset som et middel til reduktion af beregningskompleksiteten i SNS signalopsamling. Afhængig af opsamlings-scenariet kan emulering af multi-coset bevare, forbedre eller forringe rekonstruktionskvaliteten. Under alle omstændigheder kan denne emulering dog nedbringe beregningskompleksiteten med en størrelsesorden.

Contents

II   Papers   45

A   Performance Comparison of Reconstruction Algorithms in Discrete Blind Multi-Coset Sampling   47

B   Reducing the Computational Complexity of Reconstruction in Compressed Sensing Nonuniform Sampling   65

C   Computational Complexity Reduction in Nonuniform Compressed Sensing by Multi-Coset Emulation   79

Thesis Details

Thesis Title:	Acquisition of Multi-Band Signals via Compressed Sensing
Ph.D. Student:	Ruben Grigoryan
Supervisor:	Torben Larsen, Aalborg University
Co-supervisor:	Thomas Arildsen, Aalborg University
	Tobias Lindstrøm Jensen, Aalborg University

The main body of this thesis consist of the following papers.

[A] Ruben Grigoryan, Thomas Arildsen, Deepaknath Tandur, Torben Larsen, " Performance Comparison of Reconstruction Algorithms in Discrete Blind Multi-Coset Sampling," *Proceedings of the IEEE International Symposium on Signal Processing and Information Technology*, pp. 147–152, 2012.

[B] Ruben Grigoryan, Tobias Lindstrøm Jensen, Thomas Arildsen and Torben Larsen, "Reducing the Computational Complexity of Reconstruction in Compressed Sensing Nonuniform Sampling," *Proceedings of the 21st European Signal Processing Conference (EUSIPCO)*, pp. 1–5, 2013.

[C] Ruben Grigoryan, Tobias Lindstrøm Jensen and Torben Larsen, "Computational Complexity Reduction in Nonuniform Compressed Sensing by Multi-Coset Emulation," submitted to *Signal Processing, Elsevier* journal, 2014.

This thesis has been submitted for assessment in partial fulfillment of the PhD degree. The thesis is based on the submitted or published scientific papers which are listed above. Parts of the papers are used directly or indirectly in the extended summary of the thesis. As part of the assessment, co-author statements have been made available to the assessment committee and are also available at the Faculty. The thesis is not in its present form acceptable for open publication but only in limited and closed circulation as copyright may not be ensured.

Preface

This thesis is submitted to the Doctoral School of Engineering and Science at Aalborg University in partial fulfilment of the requirements for the degree of Doctor of Philosophy. The work was carried out in the Department of Electronic Systems at Aalborg University.

This PhD project was conducted with collaboration with Agilent Technologies. As the result of the initial discussions, reconstruction performance and complexity issues in Compressed Sensing were considered as the perspective research topics. The conducted research followed this direction.

I would like to thank my supervisor, Professor Torben Larsen, for giving me an opportunity to make this PhD study. I truly appreciate his contributions to this research. I would also like to thank my co-supervisors, Thomas Arildsen and Tobias Lindstrøm Jensen, for there significant help and fruitful discussions. I want to express my gratitude to Deepaknath Tandur, Lieven Philips and Michael Dieudonne from Agilent Technologies and to my colleagues Pawel J. Pankiewicz, Francesco Tafuri, Hao Shen, Jacek Pierzchlewski, Karsten Fyhn and Peng Li. I would also like to thank my parents and my beloved wife Julieta for their support and encouragement.

Ruben Grigoryan
Aalborg University, March 15, 2015

Part I

Introduction

List of Abbreviations

Abbreviation	Meaning
AD	Analog-to-Digital
ADC	Analog-to-Digital Conversion
AWGN	Additive White Gaussian Noise
BPF	Band-Pass Filter
CS	Compressed Sensing
DUT	Device Under Test
FFT	Fast Fourier Transform
IF	Intermediate Frequency
LO	Local Oscillator
LPF	Low-Pass Filter
LTE	Long Term Evolution
MCS	Multi-Coset Sampling
MMV	Multiple Measurement Vectors
MRI	Magnetic Resonance Imaging
MWC	Modulated Wideband Converter
NR	Nyquist Rate
NRS	Nyquist Rate Sampling
OMP	Orthogonal Matching Pursuit
RD	Random Demodulator
RF	Radio Frequency
RIP	Restricted Isometry Property
SA	Signal Analyzer
SNR	Signal-to-Noise Ratio
SNS	Single-channel Nonuniform Sampling
SMV	Single Measurement Vector
SRR	Support Reconstruction Ratio

List of Notations

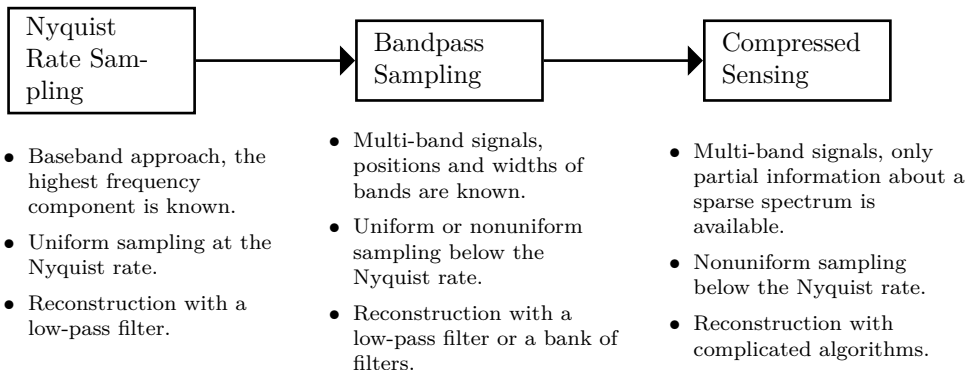| Notation	Description
$s(t)$	continuous time-domain signal
$s[n]$	discrete time-domain signal
$X(f)$	Fourier transform of $s(t)$
$\mathbf{x}$	column vector
$\mathbf{x}[n]$	nth element of $\mathbf{x}$
$\mathbf{x}_K$	vector formed by vertical concatenation of elements of $\mathbf{x}$ with indices in a set K
$\mathbf{A}$	matrix
$\mathbf{A}^{-1}$	inverse of $\mathbf{A}$
$\mathbf{A}^{\mathrm{T}}$	transpose of $\mathbf{A}$
$\mathbf{A}^{\mathrm{H}}$	Hermitian transpose of $\mathbf{A}$
$\mathbf{A}^K$	matrix formed by horizontal concatenation of columns of $\mathbf{A}$ with indices in a set K
$\mathbf{A}^j$	jth column $\mathbf{A}$
$\mathbf{A}_j$	jth row of $\mathbf{A}$
$\mathbf{A}_{i,p}$	element of $\mathbf{A}$ on ith row and pth column
$\mathbf{F}$	DFT matrix
$\mathbf{F}^{-1}$	IDFT matrix
K	support of a sparse signal
k	number of non-zero (dominant) elements in the sparse representation of a signal, k equal to the size of K
N	number of Nyquist rate samples of a signal
M	number of acquired samples/measurements of a signal, $M \leq N$
f_{C}	central band frequency
f_{S}	sampling rate
$H_k(\cdot)$	thresholding operator that preserves k largest elements (in the ℓ_2-norm) of a vector and set other to zero

1   Background

This chapter describes an evolution of approaches towards converting analog signals to digital representations – from Nyquist rate sampling to Compressed Sensing (CS). We also describe how CS approach may extend the capabilities of Signal Analyzers (SA) and what issues has to be resolved to make it possible. This motivated the conducted research.

1.1   Overview of Analog-to-Digital Acquisition Approaches

Signals in the real word have an analog nature, meaning that they are represented as a continuous function of time, space etc. However, the most of the modern telecommunication and computational platforms are digital. Therefore, analog signals have to be converted into a digital form prior to processing. This process is called an Analog-to-Digital (AD) conversion. A correct conversion implies that any analog signal has an unique digital representation and thus can be correctly reconstructed. The most common way of the digital representation of analog signals is a time discretization followed by a quantization [38]. This operation is done by a device called Analog-to-Digital Converter (ADC). A perfect ADC estimates values of a signal at the predefined moments. This procedure is called sampling. The precision of the estimation of signal value is defined by the resolution of ADC. If ADC samples are taken correctly, an input analog signal can be uniquely interpolated from the signal's samples up to some mismatch due to the quantization. In this sense, the process of AD conversion can be called a signal acquisition process. So, the key questions are: 1) how the samples should be taken; and 2) which interpolation method should be used to recover an analog signal based on the acquired samples.

Since the 1930s, several AD approaches have been developed. The evolution of these approaches is illustrated in Fig. 1. The classical Nyquist Rate Sampling (NRS) corresponds to uniform sampling at a rate higher than twice the highest frequency component in a signal. This sampling rate is called the Nyquist Rate (NR). For example, Fig. 2a illustrates a baseband signal with all the frequency components below the f_{H}. In this case, uniform sampling at a rate larger or equal to $2f_{\mathrm{H}}$ is a sufficient condition for a proper AD conversion. A reconstruction of the original signal is performed using low-pass filtering.

In telecommunication applications, RF signals are mostly multi-band rather than baseband (see Fig. 2b). Each band can for example be used to establish an independent data link. Multi-band signals can of course be sampled at NR. However, in some cases it is redundant as discussed in Section 3. NR sampling can be too costly for wide-band signals. In this case, sub-Nyquist bandpass sampling can be used [66]. Reconstruction in bandpass sampling is performed with one or more filters. The Bandpass sampling is a "non-blind" approach as it requires prior information about positions and widths of

Nyquist Rate Sampling	Bandpass Sampling	Compressed Sensing

- Baseband approach, the highest frequency component is known.
- Uniform sampling at the Nyquist rate.
- Reconstruction with a low-pass filter.

- Multi-band signals, positions and widths of bands are known.
- Uniform or nonuniform sampling below the Nyquist rate.
- Reconstruction with a low-pass filter or a bank of filters.

- Multi-band signals, only partial information about a sparse spectrum is available.
- Nonuniform sampling below the Nyquist rate.
- Reconstruction with complicated algorithms.

Fig. 1: Evolution of the AD approaches.

bands. This information is used to design the reconstruction filters.

In turn, CS allows "blind" sub-Nyquist sampling of sparse multi-band signals. This is achieved by formulating a signal reconstruction process as an underdetermined problem solved by complicated reconstruction algorithms. There are several different CS architectures for acquiring frequency sparse signals, but all of them obtain samples according to some pseudo-random time-domain sampling patterns. Due to this randomness, by sampling rate in CS we often talk about an average sampling rate. The CS approach has advantages compared to the both NR sampling and bandpass sampling [25, 26]:

- CS acquires signals at rates that may be significantly lower than the NR [13]. This reduction in sampling rate may simplify the hardware front-end of an acquisition device or extend the capabilities of the existing devices by introducing the CS mode.

- CS requires only partial prior information about the spectrum of a signal. In particular for multi-band signals, information on exact position of bands is not necessary. For example, the same device may acquire signals with different position of carriers without additional tuning [47].

However, CS also has some disadvantages [25, 26]:

- Only signals that are sparse in some basis can be acquired with CS [13]. There are two common definitions of sparsity: 1) signal's expansion in some basis contains only few non-zeros, 2) few of the expansion coordinates comprise the most of the signal's energy. For bandpass signals, sub-Nyquist sampling is impossible.

- CS requires non-trivial reconstruction procedures [13, 14] which compensate for the lack of measurements. In contrast, in NR sampling, the transition between

(a) A baseband signal.

(b) A multi-band signal with 4 carriers.
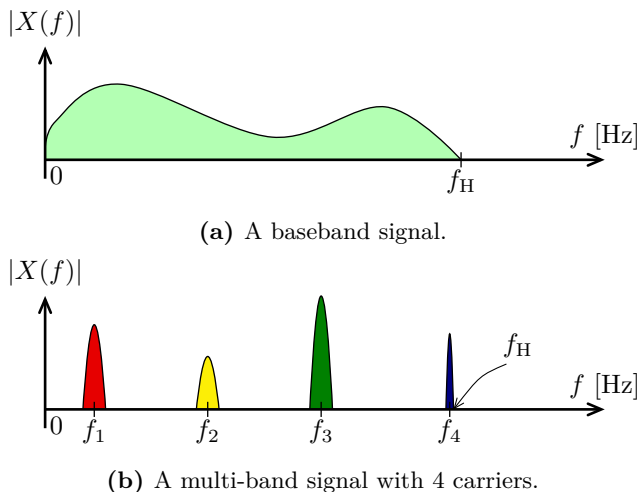
Fig. 2: Frequency domain representation, $X(f)$, of a bandpass and multi-band signals.

the frequency and time domain representations of a signal is performed with a pair of Fourier and inverse Fourier transformations [50]. As we show in subsection 4.3, the inverse Fourier transformation cannot be directly applied in CS. So there is a need for a complicated reconstruction algorithm that for example transform sub-Nyquist samples taken at the time domain to the full representation of a signal in the frequency domain.

In the following subsection, we describe how CS approach may extend capabilities of SA.

1.2   Compressed Sensing Acquisition in Signal Analyzers

The theory of CS has been developing since the mid 2000s [13]. CS is a universal mathematical framework that can be used in many digital signal processing fields: image processing [25], parameter estimation [30], telecommunications [67] etc. CS can also be embedded into existing applications in order to improve their technical characteristics. For example, in SA applications. SA is a measurement tool that is used to acquire various information about signals : amplitude, phase, modulated symbols etc. The demand for a wide-band SA increases with the development of modern telecommunication specifications like Long Term Evolution (LTE) operating at an ultra-high frequency range (0.8 – 3.0 GHz) [31]. Consider the following example of SA. Assume that a signal's bandwidth is within the analysed bandwidth of the SA. Then, the SA operates in a conventional NR sampling with an analog down-conversion. If, however, the signal's

(a) If the signal's bandwidth $< f_S/2$, the SA operates in the NR mode.

(b) If the signal's bandwidth $\geq f_S/2$, the SA switches to the CS mode.
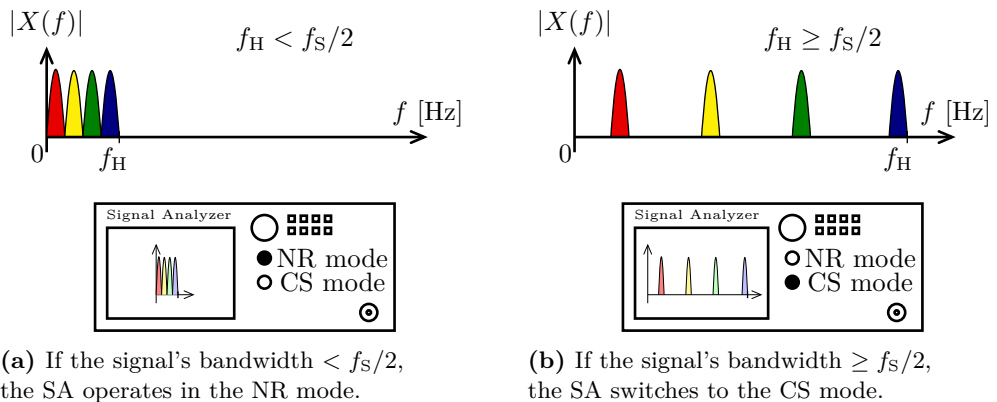
Fig. 3: Illustration of using CS acquisition in the SA.

bandwidth exceeds the default SA specifications, the SA switches to a CS mode (see Fig. 3). Therefore, a CS approach may improve the capabilities of the SA.

Two conditions must be fulfilled for the successful implementation of CS acquisition in real-life applications:

1. The CS acquisition can be only used with signals having sparse or approximately sparse representations in some basis. The sufficient level of sparsity depends on the application and cannot be specified explicitly for all cases. The general rule is that less sparse signals require higher average sampling rates. If signals are not "sufficient" sparse the necessary CS sampling rate can rise up to the NR. In this case, CS turns into NR sampling.

2. Sufficient computational resources have to be provided. As mentioned above, CS reconstructs undersampled signals by means of solving an underdetermined systems of equations. Various reconstruction algorithms exist which are based on different principles [25], [26]. Mathematical operations as Fast Fourier Transform (FFT), QR factorization, eigenvalues decomposition etc. are underlying the reconstruction algorithms. The complexity of the CS reconstruction depends on the specific algorithm and length of the acquired signals. If CS is used in real-time applications, the computational cost becomes a key issue, as a part of the signal has to be reconstructed before the next part is acquired.

We now try to see how this conditions are met for the CS acquisition in the SA. A typical measurement setup consists of a Device Under Test (DUT) connected with a cable to the SA, see Fig. 4. Assume that a signal from DUT is sparse. The cable has a wave impedance equal to the output impedance of the DUT and input impedance of SA. The typical value of this impedance is 50 Ω. Cables used with the SA for
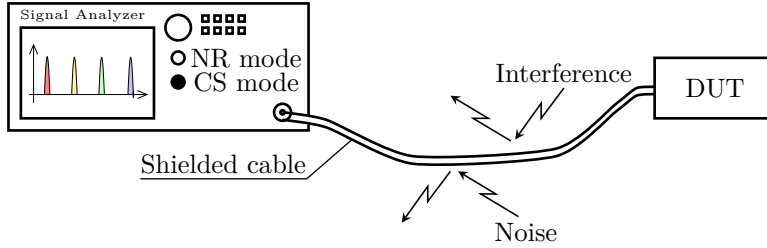
Fig. 4: Illustration of DUT measuring with the SA. The shielded cable prevents noise and interference from affecting the measurements.

RF measurements are usually coaxial, meaning that they have one central signal wire surrounded by a ground wire. The ground wire also acts as a shield that prevents external interference and noise signals from affecting the signal from the DUT. Therefore, a sparse signal from DUT remains sparse at the SA input even in an environment with wide-band noise.

An increase of computational resources comes with the increase of physical space and weight. SAs are produced mainly in three types: stationary, portable and handled. Additional space and weight is less crucial for stationary SA than for portable and handled versions. Nevertheless, an extension of the analysed bandwidth can bring more benefits than disadvantages related to the additional space and weight.

Summarizing, CS can be successfully implemented as an acquisition technique in a SA:

1. Sparsity of analysed signals is not affected by external noise. If the DUT outputs sparse signals, CS can be used to acquire them.

2. Additional space and weight related to the additional computational resources can be allocated in the SA.

Knowing the aspects of the CS acquisition in SA, we can formulate the research aims and the main hypothesis of this PhD thesis.

1.3 Research Aims and Hypothesis

The aim of this PhD thesis is to investigate the quality and computational complexity issues of the CS acquisition. These issues are interrelated and depend on many factors: specific CS architectures and their parameters, reconstruction algorithms, parameters of the acquired signals (length, types, level of noise etc), computational platform etc.

CS-based acquisition has already proved its efficiency in some image applications like Magnetic Resonance Imaging (MRI) [44] and single-pixel imaging [17, 24]. However, these application are non–real–time, meaning that the computational costs of

signal reconstruction is not critical. At the same time, for real–time applications, for example a SA, the complexity of reconstruction is significant. In a worst case scenario, computational costs maybe high enough to depreciate advantages of low sampling rates making a CS approach meaningless.

The main hypothesis of this thesis is that the the computational complexity of the CS acquisition can be reduced without degrading the reconstruction quality. This efficient reduction of complexity is achieved by reformulating the signal reconstruction problem.

This PhD research comprises the versatile analysis of the proposed hypothesis applied to acquisition of multi-band frequency-sparse signals.

2 Nyquist Rate Sampling

This chapter describes the well-known Nyquist sampling theorem and the practical aspects of Nyquist rate acquisition.

2.1 Nyquist Sampling Theorem

Many researches have worked independently on the topic of the unique interpolation of a signal from uniformly taken samples [36]. The result of this research can be stated as the Nyquist sampling theorem – if a signal has all frequency components below f_H, it is completely determined by its uniform samples taken at the rate $2f_H$ or higher [50, 56]. This rate is called Nyquist Rate (NR). The analog signal can be perfectly reconstructed from samples with a low-pass filter.

The Nyquist theorem is illustrated in Fig. 5. Suppose that a signal $s(t)$ is sampled

(a) Sampling of the analog signal.

(b) The Fourier transform $X(f)$ is bandlimited to f_H.

(c) Alias-free sampling, $T < 1/(2f_H)$.

(d) Sampling with aliasing distortions, $T \geq 1/(2f_H)$
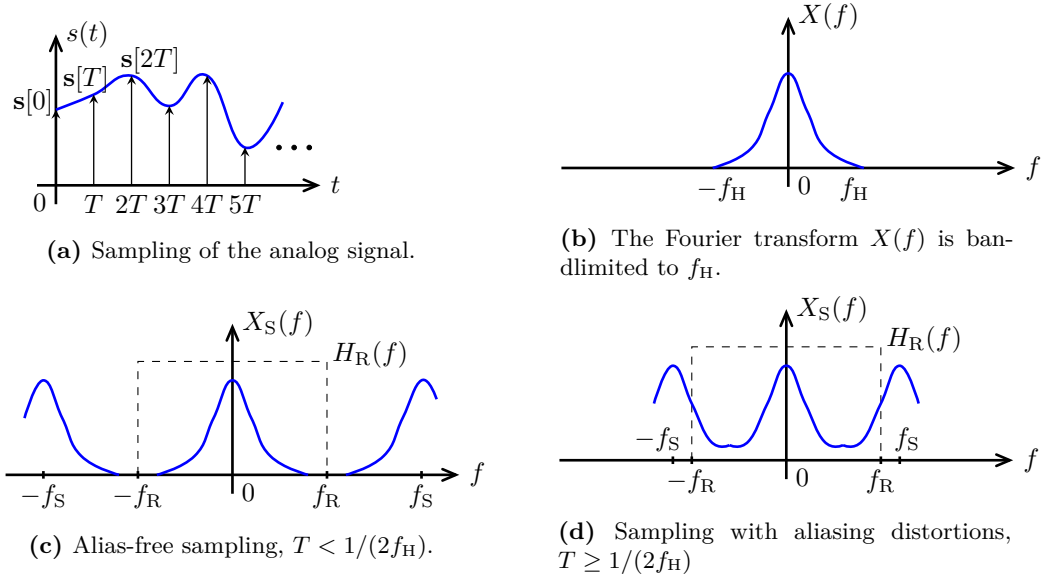
Fig. 5: Illustration of the Nyquist-Shannon theorem.

with some period T as in Fig. 5a and the Fourier transform $X(f)$ is bandlimited to f_H (see Fig. 5b). In turn, $X_S(f)$, which is the Fourier transform of the sequence of samples $s[0], s[T], s[2T], \ldots$, is a sum of the infinite numbers of the copies of $X(f)$ shifted by integer multipliers of the sampling rate $f_S = 1/T$ [50]. If $f_S > 2f_H$, the shifted copies of $X(f)$ do not overlap (see Fig. 5c). In this case, $s(t)$ is successfully obtained by passing the acquired samples through a recovery low-pass filter $H_R(f)$ with a cut-off frequency

f_R such that $f_H < f_R < f_S - f_H$. However, if the sampling rate is not sufficiently high, the replicas of $X(f)$ overlap resulting in aliasing distortions (see Fig. 5d). Because of the aliasing, all the replicas of $X(f)$ in $X_S(f)$ are distorted, and it is no longer possible to reconstruct (t) by a low-pass filter.

In digital systems, signals are often represented by finite-length sequences of samples. In this case, the Discrete Fourier Transform (DFT) substitutes the Fourier transform [50]. DFT is given by:

$$\mathbf{x}[p] = \sum_{n=0}^{N-1} \mathbf{s}[n]\exp\left(-j\frac{2\pi np}{N}\right), \tag{1}$$

$$\mathbf{s}[p] = \frac{1}{N}\sum_{n=0}^{N-1} \mathbf{x}[k]\exp\left(j\frac{2\pi np}{N}\right), \tag{2}$$

where $\mathbf{s} \in \mathbb{C}^{N\times 1}$ is a vector comprising the time domain samples of $s(t)$, $\mathbf{x} \in \mathbb{C}^{N\times 1}$ is the DFT of $\mathbf{s}$ and N is the number of acquired samples, i.e. the length of $\mathbf{s}$. For fast computation of DFT, methods have been developed under the general title Fast Fourier Transform (FFT) [50]. Alternatively, the DFT can be described in a matrix form:

$$\mathbf{x} = \mathbf{Fs}, \tag{3}$$

where the matrix $\mathbf{F} \in \mathbb{C}^{N\times N}$ is called the DFT matrix. Its elements are given by:

$$\mathbf{F}_{n,p} = \exp\left(-j\frac{2\pi}{N}(n-1)(p-1)\right), \tag{4}$$

where $n, p \in \{1, \ldots, N\}$.

2.2 Practical Aspects of the Analog-to-Digital Conversion

An actual sampling of a signal is performed by device called Analog-to-Digital Converter (ADC). There are many types of ADC [38]: flash, successive-approximation, pipeline, sigma-delta etc. Each of these types has its own advantages and drawbacks, but all of them consist of two main parts: a Sample and Hold (S/H) circuit and quantizer (see Fig. 6). The S/H circuit holds the actual value of the analog input signal $s(t)$ at the specific moments of time denoted by t_{samp}, so that $s_{SH}(t_{samp}) = s(t_{samp} + \tau), \tau \in [0, T)$, where T is a time period between two consecutive samples. The purpose of the S/H circuit is to provide a constant signal level for some time, which is necessary for correct quantization. A quantizer maps the value of $s_{SH}(t_S)$ to some digital code resulting in the output of the ADC – a sequence of samples $\mathbf{s}[n]$. The ADC sampling rate equals $f_{samp} = 1/T$.

In a NR acquisition, an input signal is filtered with a low-pass anti-aliasing filter prior to sampling. This ensures that $s(t)$ contains only frequency components below $f_{samp}/2$.
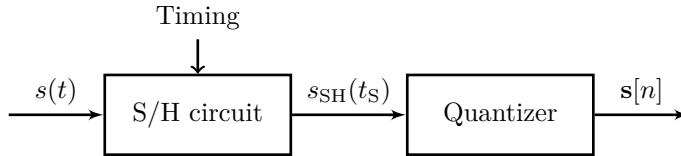
Fig. 6: A simplified ADC diagram [50].

In practice, signals are sampled at rates higher than NR [5]. This oversampling allows use of low-pass filters with a wider transition band and decrease of noise in samples [5].

The power consumption and the cost of the ADC depends on the input bandwidth, sampling rate, resolution, quantization noise, linearity etc. Table 1 provides information

Part's name	Sampling rate, GSPS	Full Power BW, GHz	Resolution, Bits	Power Consumption, W	Price, USD
ADC12D800RF[1]	1.6	2.7	12	2.5	2000
ADC12D1600[1]	3.2	2.8	12	3.8	3000
LM97600[1]	5	1.3	8	3	3300
AD6641[2]	0.5	0.25	12	0.7	130
AD9683[2]	0.25	1	14	0.45	70

Table 1: Specifications of some of the state-of-the-art high speed ADCs. Data from [1]www.ti.com and [2]www.analog.com.

about some of the state-of-the-art high speed ADCs. Though, high speed and wide input bandwidth ADCs are available (the first three items in Table 1), there are obstacles in the direct use of the NR sampling in telecommunication applications:

- Commercial off-the shelf available ADCs do not cover the entire range up to 3GHz.

- High speed ADCs provide output data at high rates. For example, if ADC12D800RF operates at the highest sampling rate, a control unit (MCU/FPGA etc) has to handle and store the ADC's data at the rate $12 \cdot 1.6 \cdot 10^9 = 19.2$ Gb/s. This introduces additional requirements to control units.

- High speed ADCs have a high cost and high power consumption.

Baseband signals can be acquired without aliasing distortion only at a NR. At the same time, telecommunication signals are bandpass or multi-band rather than baseband. In this case, down-conversion is used.

A typical example of NR sampling with the superheterodyne down-conversion technique is illustrated in Fig. 7. An input signal consequently passes an amplifier A1,

14
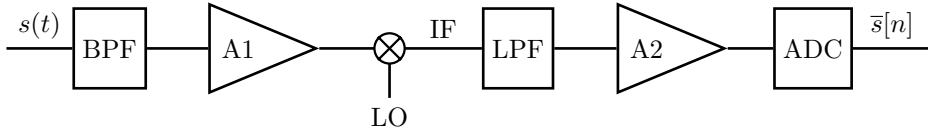
Fig. 7: Acquisition of a bandpass signal with the super-heterodyne technique [55].

a Band-Pass Filter (BPF), a frequency mixer, where it is shifted down to the Intermediate Frequency (IF) by a Local Oscillator (LO), an anti-aliasing Low-Pass Filter (LPF), another amplifier A2 and finally enters an ADC. The ADC outputs samples $\bar{s}[n]$ corresponding to $s(t)$ down-shifted to IF.

The superheterodyne technique has been used in many of the radio receivers and acquisition devices like SA [2, 63]. Despite its popularity, the superheterodyne architecture has several drawbacks: a high power consumption, leakage of LO and IF signals and theirs harmonics, difficulties in implementing filters in an integrated circuit and an overall large number of components etc.

3   Bandpass Sampling

Assume that a bandpass signal with the central frequency f_C and the bandwidth $B = f_H - f_L$ is sampled uniformly at the rate $f_{samp} < 2f_H$. Then, an aliasing occurs. However, depending on the position of the band, its width and the sampling rate, aliasing may not result in distortion. In this case, aliasing down-converts the band. This approach is called bandpass sampling and is illustrated in Fig. 8 [41, 43, 66].
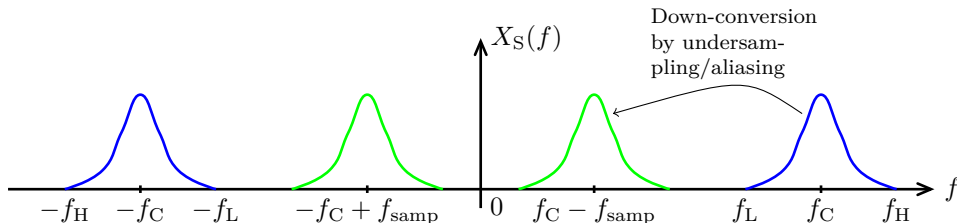
Fig. 8: Illustration of the down-conversion undersampling [53]. Original bands – blue, aliased – green.

In a bandpass signal, the position of a band can be specified by its width. A so-called integer band positioning means that the band is shifted from the origin by a value cB, $c \in \mathbb{Z}$ [66]. If $c = 0$, a signal is baseband.

We can now geometrically derive the minimum uniform sampling rate for a bandpass signal. As can be seen in Fig. 9, $f_S = 2B$ is the minimum theoretical sampling rate which does not cause distortions in case of an integer band position [41]. In practice, signals are always sampled at a rate higher than the theoretical minimum, as any imperfections of the acquisition device result in corruption [66]. If a signal does not possesses an integer band position, it is impossible to correctly acquire a signal with uniform sampling at the rate $f_{samp} = 2B$.

In [41], the authors introduced a second-order (nonuniform) sampling (see Fig. 10). In this sampling approach, an input signal is sampled with two ADCs. The ADCs output two streams of samples, $s_1[n]$ and $s_2[n]$. These streams of samples are obtained uniformly
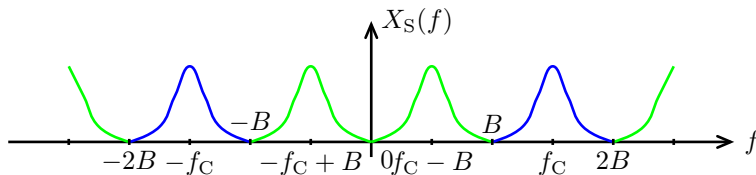
Fig. 9: Illustration of the uniform band-pass sampling at the rate $f_S = 2B$. The sampled signal possesses an integer band position.
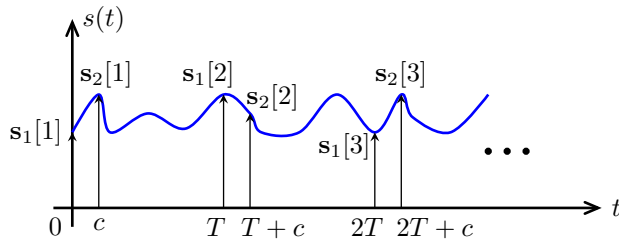
(a) Illustration of the second-order sampling.
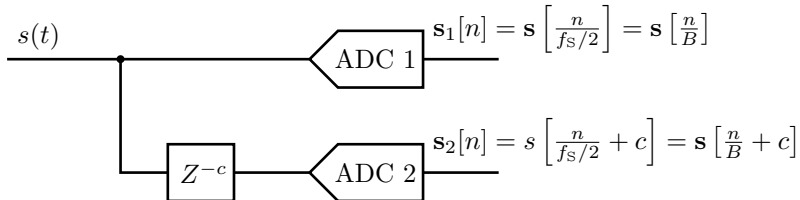
(b) Architecture of the second-order sampler, an average rate $f_S = 2B$.

Fig. 10: Second-order sampling at the average rate $f_S = 2B$.

at the rate $f_{\text{samp}}/2$, but one of them have a time offset denoted by c. Kohlenberg showed in [41] that a second-order approach with the average sampling rate $f_{\text{samp}} = 2B$ can acquire a signal correctly with an arbitrary band position. However, in this case, a signal reconstruction is performed with two synthesis filters which is more complicated than a reconstruction in uniform sampling. An original signal is interpolated by [66]:

$$s(t) = \sum_n s\left[\frac{n}{B}\right] I\left(t - \frac{n}{B}\right) + s\left[\frac{n}{B} + c\right] I\left(-t + \frac{n}{B} + c\right), \tag{5}$$

where $n \in \mathbb{N}$ is an index of a sample, $I(t) = I_0(t) + I_1(t)$,

$$I_0(t) = \frac{\cos[2\pi(rb - f_L)t - r\pi Bc] - \cos[2\pi f_L t - r\pi Bc]}{2\pi Bt \sin(r\pi Bc)}, \tag{6}$$

$$I_1(t) = \frac{\cos[2\pi(f_L + B)t - (r+1)\pi Bc] - \cos[2\pi(rB - f_L)t - (r+1)\pi Bc]}{2\pi Bt \sin((r+1)\pi Bc)}, \tag{7}$$

r is an integer value specifying which replicas of $X(f)$ overlap in the region (f_L, f_H). In (6) and (7), denominators cannot be equal to zero. This observation restricts the possible value of the delay c, i.e.

$$c \neq \frac{z}{rB}, \; c \neq \frac{z}{(r+1)B}, \; z = 1, 2, \ldots \tag{8}$$

In [43], an idea of nonuniform sampling was generalized for the Lth order sampling and two-dimensional signals. Some of the practical bandpass sampling issues were discussed in [66]. It was also pointed out that SNR is not preserved in bandpass sampling due to the aliasing of out-of-band noise.

In [42], Landau investigated an interpolation of a function with the aggregated width of its non-zero Fourier transform equal to B. Landau showed that for correct interpolation, the minimum sampling rate for such a function, equals to $2B$. Therefore, bandpass sampling allows acquisition of signals at the lowest possible sampling rates, however, requires information about positions and widths of bands prior to sampling.

Examples of the bandpass sampling RF receivers are presented in [8, 9].

4   Compressed Sensing Primer

CS is the mathematical approach which allows to reconstruct a signal from less samples/measurements than is needed according to the Nyquist-Shannon theorem. In this section, we present various CS approaches for multi-band signals acquisition. We may say that for this application, CS can be seen as a further development of Bandpass sampling with the difference that CS requires only partial information regarding the signal's bands.

The CS theory is built upon describing a signal recovery process as estimation of a sparse solution to an underdetermined linear system. To understand this process, we first elaborate on what we mean by taking measurements of a signal and how do these measurement compose a corresponding underdetermined system. Then, we describe a general CS framework. Conditions for a unique signal recovery and popular CS reconstruction methods are discussed in Section 5. Finally, we present CS architectures that can be used to acquire multi-band signals.

4.1   Signals as Vectors

Usually, signals can be presented as vectors in a vector space [58]. This allows us to describe signal processing systems using linear algebra. Three continuous real-valued signals existing in some time interval $(0, T)$ are illustrated in Fig. 11. Denote by $\mathcal{S} = \{s_1(t), s_2(t), \ldots\}$ an infinite set of such signals. A set $\mathcal{S}$ is a vector space over a field of $\mathbb{R}$ as it obeys necessary axioms [29]:

- $\forall\, s_i(t), s_k(t) \in \mathcal{S}, \quad s_i(t) + s_k(t) \in \mathcal{S}$

- $\forall\, \alpha \in \mathbb{R}, s_i(t) \in \mathcal{S}, \quad \alpha s_i(t) \in \mathcal{S}$

- $\exists\, \mathbf{0} \in \mathcal{S} : \forall\, s_i(t) \in \mathcal{S}, \quad s_i(t) + \mathbf{0} = s_i(t)$

- $\exists\, \mathbf{1} \in \mathcal{S} : \forall\, s_i(t) \in \mathcal{S}, \quad \mathbf{1} s_\mathrm{i}(t) = s_i(t)$
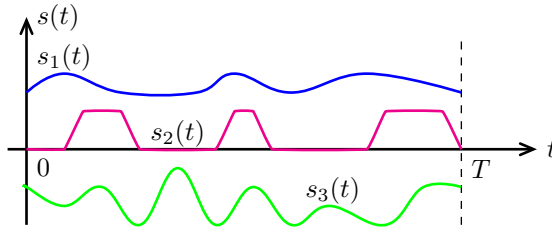
Fig. 11: Illustration of three vectors from a linear space of continuous real valued functions existing on $(0, T)$.

- commutativity and associativity of addition, distributivity and compatibility of multiplication, and the existence of additive inverse vectors are obvious.

Suppose, a continuous signal is replaced by its discretized versions in a form of a column vector, i.e. $s(t) \mapsto \mathbf{s} \in \mathbb{R}^{N \times 1}$ (or $\mathbb{C}^{N \times 1}$ in case of complex-valued signals). According to the axioms above, a set of discretized signals is also a vector space. The introduction of a vector space allows the use of various linear algebra tools to describe, compare and manipulate signals. For example:

- signals can be measured in terms of various vector norms. In general, a ℓ_p vector norm is given by:

$$\|\mathbf{s}\|_p = \left(\sum_{n=1}^{N} |\mathbf{s}[n]|^p \right)^{1/p}, \, p \geq 1. \tag{9}$$

Some of the popular norms are ℓ_2 and ℓ_1. The ℓ_2 norm corresponds to the energy of a signal; the ℓ_1 norm plays a central role in the CS theory. Norms with $0 < p < 1$ are called pseudo-norms as the absolute scalability and triangle inequality properties do not hold for them. For $p = 0$ triangular inequality holds but absolute scalability does not.

- an inner product of two vectors is defined as:

$$\langle \mathbf{s}, \mathbf{y} \rangle = \sum_{n=1}^{N} \mathbf{s}[n]\mathbf{y}[n]. \tag{10}$$

- a signal can be represented as a unique linear combination of the basis vectors. By definition, a basis is a set of linearly independent vectors that span the whole vector space [29]. Usually, the basis is selected to be orthonormal. In this case, the expansion of a signal in the basis is performed by taking consecutive scalar products of the signal and the basis vectors:

$$\mathbf{s} = \langle \mathbf{s}, \mathbf{e}_1 \rangle \mathbf{e}_1 + \langle \mathbf{s}, \mathbf{e}_2 \rangle \mathbf{e}_2 + \ldots + \langle \mathbf{s}, \mathbf{e}_N \rangle \mathbf{e}_N \tag{11}$$
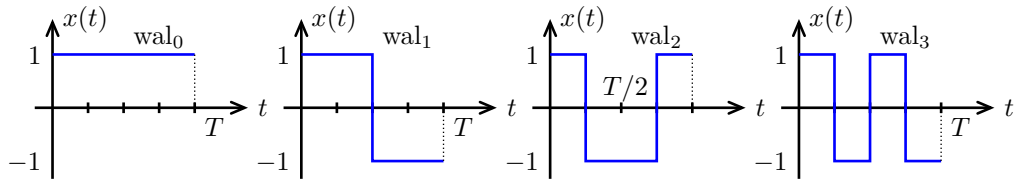
Fig. 12: Illustration of the first four Walsh functions, wal_i, $i = \{0, 1, 2, 3\}$.

The Walsh basis is an example of an orthonormal basis used in signal processing. The first four Walsh functions are illustrated in Fig. 12. Another, and one of the most used basis, is the DFT basis. It is given by the rows of the DFT matrix which are defined by (4). The rows and columns of $\mathbf{F}$ are orthogonal. Fig. 13 illustrates the 2nd and the 9th row of the DFT matrix of an order 64. Note that the elements of a DFT matrix are complex-valued.
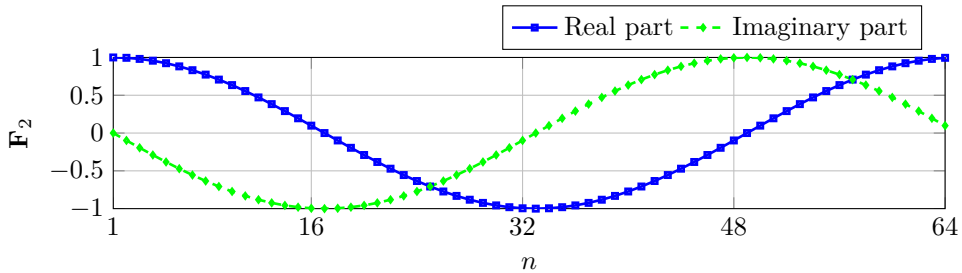
(a) 2nd DFT basis vector.
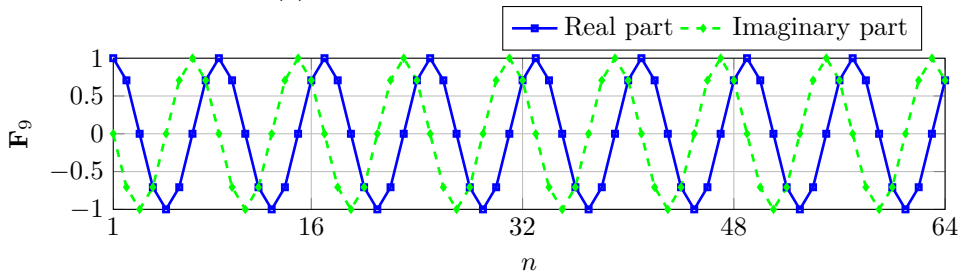
(b) 9th DFT basis vector.

Fig. 13: Illustration of the rows of the DFT matrix for $N = 64$.

As we show in the next subsection, linear algebra tools allow to present the sampling process as a linear transformation.

4.2   Sampling as a Linear Transformation

Let us consider the relation between the DFT of a sequence of samples and the DFT basis. Assume that you acquire N samples out of the ADC. The samples are taken at the NR and the DFT is without aliasing. From now on, by a vector $\mathbf{y} \in \mathbb{C}^{N \times 1}$, we denote a vector of the acquired samples in the time domain. Based on (3), the DFT coefficients can be found by:

$$\mathbf{x} = \mathbf{F}\mathbf{y}, \tag{12}$$

where $\mathbf{F} \in \mathbb{C}^{N \times N}$ is the DFT matrix. As $\mathbf{F}^{-1} = \mathbf{F}^{\mathrm{H}}$ (up to scalar coefficient), the transition between the frequency and time domain is described by:

$$\begin{bmatrix} \mathbf{y}[1] \\ \mathbf{y}[2] \\ \vdots \\ \mathbf{y}[N] \end{bmatrix} = \begin{bmatrix} \mathbf{F}_{1,1}^{-1} & \mathbf{F}_{1,2}^{-1} & \cdots & \mathbf{F}_{1,N}^{-1} \\ \mathbf{F}_{2,1}^{-1} & \mathbf{F}_{2,2}^{-1} & \cdots & \mathbf{F}_{2,N}^{-1} \\ \vdots & \vdots & \ddots & \vdots \\ \mathbf{F}_{N,1^{-1}} & \mathbf{F}_{N,2}^{-1} & \cdots & \mathbf{F}_{N,N}^{-1} \end{bmatrix} \begin{bmatrix} \mathbf{x}[1] \\ \mathbf{x}[2] \\ \vdots \\ \mathbf{x}[N] \end{bmatrix}. \tag{13}$$

Matrix $\mathbf{F}^{-1} \in \mathbb{C}^{N \times N}$ is called the Inverse DFT (IDFT) matrix. Note that the elements of $\mathbf{y}$ are given by:

$$\mathbf{y}[p] = \sum_{n=1}^{N} \mathbf{F}_{p,n}^{-1} \mathbf{x}[n], \tag{14}$$

which is a scalar product between the signal $\mathbf{x}$ and $\mathbf{F}_p^{-1}$, the pth IDFT basis vector. $\mathbf{F}^{-1}$ is a matrix of linear transformation mapping the frequency domain to the time domain. The IDFT matrix is unitary upon scaling on $1/\sqrt{N}$, which implies an important property of isometry [29]. This means that the IDFT preserves lengths and distances (in ℓ_2 sence). Thus, any time domain vector $\mathbf{y}_i$ has a unique image $\mathbf{x}_i$ in the frequency domain. This
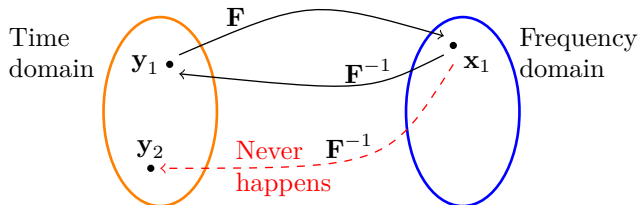
Fig. 14: Illustration of the isometric transformation $\mathbf{F}$.

is illustrated in Fig. 14, where $\mathbf{y}_1 \xrightarrow{\mathbf{F}} \mathbf{x}_1$ and the inverse transformation $\mathbf{F}^{-1}$ never maps $\mathbf{y}_1$ to any other vector than $\mathbf{x}_1$.

But what happens if a signal is undersampled? Assume that a signal $\mathbf{x}$ is sampled at a rate twice below the NR. Therefore, only $N/2$ samples are acquired. Applying an
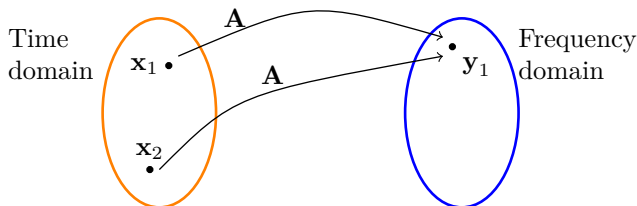
Fig. 15: Illustration of the non-isometric transformation $\mathbf{A}$.

IDFT operation on such an undersampled data is equivalent to:

$$\mathbf{y} = \mathbf{D}\mathbf{F}^{-1}\mathbf{x} = \mathbf{A}\mathbf{x}, \tag{15}$$

where $\mathbf{y} \in \mathbb{C}^{N/2 \times 1}$ is a vector of decimated time-domain samples, $\mathbf{D} \in \{0,1\}^{N/2 \times N}$ is a decimation matrix:

$$\mathbf{D} = \begin{bmatrix} 1 & 0 & 0 & 0 & \dots & 0 & 0 \\ 0 & 0 & 1 & 0 & \dots & 0 & 0 \\ \vdots & \vdots & \vdots & \vdots & \ddots & \vdots & \vdots \\ 0 & 0 & 0 & 0 & \dots & 1 & 0 \end{bmatrix}. \tag{16}$$

Here, the decimation selects every second sample. The linear transformation $\mathbf{A}$ is no longer isometric, so the inverse transformation $\mathbf{A}^{-1}$ is not defined. In this case, two different signals $\mathbf{x}_1$ and $\mathbf{x}_2$ may have the same $\mathbf{y}_1$ (see Fig. 15) and it is impossible to determine an input signal based on its image. A system (15) is called an underdetermined linear system [61]. In general, such a system does not have a unique solution. However in case of sparse signals, the CS theory provides conditions and methods for unique signal recovery (see Section 5).

4.3 Signal Acquisition with Compressed Sensing

Denote by $k-$sparse signal $\mathbf{x} \in \mathbb{C}^{N \times 1}$ that have at the most k non-zero elements, i.e. $\|\mathbf{x}\|_0 = k$ [13]. Note that it is not feasible and not necessary to define a specific value of k/N that indicates whether a signal is sparse or non-sparse.

Many signals in the real world may have a sparse representation in some basis. For example, a multi-tone signal can be sparse in the DFT basis, an image can be sparse in wavelets bases [13] etc. Observe that, if such signals are sampled at NR, the number of measurements exceeds the actual "information" the signals contain. This gives the indication that the number of measurements can be reduced.

Assume that a $k-$sparse signal $\mathbf{x}$ is acquired via the following system:

$$\mathbf{y} = \mathbf{A}\mathbf{x} = \mathbf{R}\mathbf{\Phi}\mathbf{\Psi}\mathbf{x}, \tag{17}$$

where $\mathbf{A} \in \mathbb{C}^{M \times N}$ is called a sensing matrix, $\mathbf{R} \in \mathbb{R}^{M \times N}$ is an extracting matrix, $\boldsymbol{\Phi} \in \mathbb{C}^{N \times N}$ is a measurement matrix, $\boldsymbol{\Psi} \in \mathbb{C}^{N \times N}$ is a dictionary matrix, M is a number of measurements, N is a length of a signal and $M < N$ [13]. As the number of rows of $\mathbf{A}$ is always lower than the number of columns, (17) may have an infinite number of solutions.

Summarizing, in order to develop a CS acquisition system, we have to answer the following questions [13, 25]:

1. What conditions are necessary for a unique solution $\mathbf{x}$?

2. How does noise and other real-world imperfections affect a signal acquisition?

3. Which methods can recover $\mathbf{x}$ from the undersampled measurements $\mathbf{y}$?

In the following subsections, we describe how these questions are considered in CS.

Spark of a Sensing Matrix

In CS, it is common to describe a uniqueness condition with the use of spark or mutual coherence [25]. We use the following definition

Definition 1 (Reproduced from Definition 2.2 of [25]). The spark of a given matrix $\mathbf{A}$ is the smallest number of columns from $\mathbf{A}$ that are linearly dependent.

In other words, all possible combinations of (spark$(\mathbf{A})$-1) columns of $\mathbf{A}$ are linearly independent. This is an important property that allows to derive the following uniqueness condition

Theorem 1 ([25, 32]). A system $\mathbf{y} = \mathbf{A}\mathbf{x}$ has only one solution $\mathbf{x}$ such that $\|\mathbf{x}\|_0 <$ spark$(\mathbf{A})/2$.

Proof. Assume $\exists\, \mathbf{x}_1, \mathbf{x}_2 \colon \mathbf{x}_1 \neq \mathbf{x}_2, \;\; \|\mathbf{x}_1\|_0 < $ spark$(\mathbf{A})/2, \;\; \|\mathbf{x}_2\|_0 < $ spark$(\mathbf{A})/2$ and $\mathbf{y} = \mathbf{A}\mathbf{x}_1 = \mathbf{A}\mathbf{x}_2 \Rightarrow \mathbf{A}\mathbf{x}_1 - \mathbf{A}\mathbf{x}_2 = \mathbf{A}(\mathbf{x}_1 - \mathbf{x}_2) = 0 \Rightarrow (\mathbf{x}_1 - \mathbf{x}_2) \in \text{Null}(\mathbf{A})$ $\Rightarrow \|\mathbf{x}_1 - \mathbf{x}_2\|_0 \geq$ spark$(\mathbf{A})$. At the same time, according to the triangular inequality, $\|\mathbf{x}_1 - \mathbf{x}_2\|_0 \leq \|\mathbf{x}_1\|_0 + \|\mathbf{x}_2\|_0 <$ spark$(\mathbf{A})$. This is a contradiction. Thus, either $\mathbf{x}_1$, or $\mathbf{x}_2$ has more than spark$(\mathbf{A})/2$ non-zero elements. $\qquad\square$

Therefore, if we found a solution $\mathbf{x}$ with less than spark$(\mathbf{A})/2$ non-zero elements, we are sure that this solution is unique.

By definition, spark$(\mathbf{A}) \in [2, M + 1]$ [25]. For some types of sensing matrices there is an analytically derived value of spark. For example, if $\mathbf{A}$ is a random matrix with elements from Gaussian ($\mathcal{N}(\mu, \sigma^2)$) or Bernoulli ($\pm 1$s) distribution, then spark$(A) = M + 1$ with probability 1. Another example is a so-called two-ortho case with $\boldsymbol{\Phi} = \mathbf{I}$ – an identity matrix, and $\boldsymbol{\Psi} = \mathbf{F}$ the inverse DFT basis. We have considered a similar
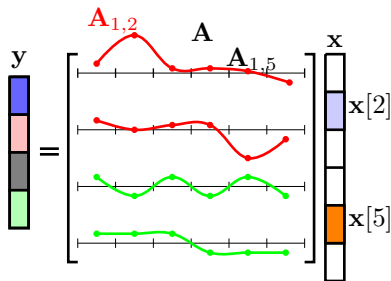
Fig. 16: Illustration of the impact of mutual incoherence on CS acquisition.

combination in (15), but $\mathbf{R}$ can represent any selection of rows, not strictly a uniform decimation. So, in case of $\mathbf{A} = \mathbf{RF}$, $\mathrm{spark}(A) = 2\sqrt{M}$, and if M is prime, $\mathrm{spark}(A) = M + 1$.

For arbitrary and large size $\boldsymbol{\Phi}$ and $\boldsymbol{\Psi}$, it can be infeasible to find $\mathrm{spark}(\mathbf{A})$ as it requires a brute-force search. In this approach, one have to check linear dependency of $\binom{M}{p}$ combinations of the columns of $\mathbf{A}$, while increasing p from 2 to M. Therefore, there is a need for alternative, probably less strong, condition on uniqueness of a sparse solution.

Incoherence

Consider Fig. 16 in order to understand the impact of incoherence between the dictionary and measurement matrices on the CS acquisition. Assume all the rows of a sensing matrix $\mathbf{A}$ have ℓ_2 norms equal to 1. Then, the lower the value of the largest elements in any rows, the more "flat" the rows are. If, for instance, a matrix $\mathbf{A}$ is used to acquire $\mathbf{x}$ with two non-zero elements, the contribution of different sensing vectors (rows of $\mathbf{A}$) is different. For example, the first row "transfers" $\mathbf{x}[2]$ to $\mathbf{y}$ well, but $\mathbf{x}[5]$ is suppressed as its contribution to $\langle \mathbf{A}_1, \mathbf{x} \rangle$ is small due to the small value of $\mathbf{A}_{1,5}$. The same is true for $\mathbf{A}_2$ and $\mathbf{x}[5]$. In contrast, more flat 3rd and 4th rows are more universal and preserve information about both $\mathbf{x}[2]$ and $\mathbf{x}[5]$. Therefore intuitively, it is preferable to have $\mathbf{A}$ with as "flat" rows as possible. The maximum element of the sensing matrix describes the overall "flatness". Recall that $\mathbf{A} = \mathbf{R}\boldsymbol{\Phi}\boldsymbol{\Psi}$. A value

$$\mu(\mathbf{A}) = \max_{1 \leq i,k \leq N} |\langle \boldsymbol{\Phi}^i, \boldsymbol{\Psi}^k \rangle| \tag{18}$$

is called a mutual coherence between the measurement and dictionary bases [15]. Consequently, $\max(\mathbf{A}) \leq \mu(\mathbf{A})$. Therefore in CS, the lower the coherence between $\boldsymbol{\Phi}$ and $\boldsymbol{\Psi}$, the lower the necessary sampling rate is. An alternative definition of mutual coherence

is given in [25]:

$$\mu(\mathbf{A}) = \max_{1 \leq i,k \leq N, i \neq k} \frac{|(\mathbf{A}^i)^T \mathbf{A}^k|}{\|\mathbf{A}^i\|_2 \|\mathbf{A}^k\|_2}. \tag{19}$$

With this definition, a low $\mu(\mathbf{A})$ implies that $\mathbf{A}$ is close to isometric, which is also intuitively favours the acquisition process.

Theorem 2 (Reproduced from Theorem 2.5 of [25]). If a system of linear equations $\mathbf{y} = \mathbf{A}\mathbf{x}$ has a solution $\mathbf{x}$ obeying $\|\mathbf{x}\|_0 < \frac{1}{2}(1 + 1/\mu(\mathbf{A}))$, this solution is necessarily the sparsest possible.

Examples of the pairs of bases that have low mutual coherence are identity with DFT bases, wavelet bases with noiselets, random matrices with any fixed dictionary [13].

Stability of Reconstruction

Up to now, we have been considering noise-free acquisition of purely sparse signals. However in real-life applications, signals can be compressible rather than sparse, maybe corrupted by wide-band noise and affected by imperfections of measurement hardware:

$$\mathbf{y} = \mathbf{A}\mathbf{x} + \mathbf{e} \tag{20}$$

where $\mathbf{e} \in \mathbb{C}^{M \times 1}$ denotes a noise/imperfection vector. In this case, it is impossible to recover the exact $\mathbf{x}$. Instead, an estimated sparse solution $\hat{\mathbf{x}}$ have to be found such that

$$\|\mathbf{y} - \mathbf{A}\hat{\mathbf{x}}\|_2 \leq \epsilon, \tag{21}$$

for some error tolerance $\epsilon > 0$ [25]. The error tolerance implies the stability of the CS acquisition that can be established with the notion of Restricted Isometry Property (RIP) [14].

Definition 2 (Reproduced from Definition 2 of [13]). For each integer $k = 1, 2, \ldots$ define the isometry constant δ_k of a matrix $\mathbf{A}$ as the smallest number such that

$$(1 - \delta_k)\|\mathbf{x}\|_2^2 \leq \|\mathbf{A}\mathbf{x}\|_2^2 \leq (1 + \delta_k)\|\mathbf{x}\|_2^2 \tag{22}$$

holds for all k-sparse vectors $\mathbf{x}$.

If δ_k is close to zero, then $\mathbf{A}$ preserves distances between k-sparse signals. Consequently, $\mathbf{A}$ acts similar to an isometric transformation (see Fig. 14).

Suppose that an approximate k-sparse solution $\hat{\mathbf{x}}$ satisfying (21) can be obtained by means of some reconstruction procedure. Then, it is needed to assess the distance $\|\mathbf{x} - \hat{\mathbf{x}}\|_2$ between the approximate and true solutions. Assume that $\mathbf{A}$ obeys $2k$-RIP with $\delta_{2k} < 1$. According to [25]:

$$(1 - \delta_{2k})\|\mathbf{x} - \hat{\mathbf{x}}\|_2^2 \leq \|\mathbf{A}(\mathbf{x} - \hat{\mathbf{x}})\|_2^2 \leq 4\epsilon^2 \Rightarrow$$

$$\|\mathbf{x} - \hat{\mathbf{x}}\|_2^2 \leq \frac{4\epsilon^2}{1 - \delta_{2k}}. \tag{23}$$

The above inequality puts the upper bound on the error between the real and reconstructed signals if $\mathbf{A}$ has a proper isometry constant.

It is computational infeasible to find δ_{2k} for a relatively large $\mathbf{A}$ and k. However, as in case of spark and mutual coherence, analytical assessment of isometry constants are available for random matrices [13, 14].

Reconstruction of signal in CS is described in details in Section 5.

4.4   CS architectures for acquiring multi-band signals

As discussed in Section 1, acquisition of multi-band signals is an application where CS can be used to extend the capabilities of SA. So, this subsection presents CS architectures designed for acquiring this type of signals.

Single-Channel Nonuniform Sampler

Single-Channel Nonuniform Sampler (SNS) consists of one input channel (see Fig. 17a) [45, 60, 67]. SNS pseudo-randomly acquires M samples out of N NR samples such that the average sampling rate is below the Nyquist sampling rate, $M < N$ (see Fig. 17b). A sampling pattern $\Lambda_{\mathrm{SNS}} \subset \mathbb{N}_0^{N-1}, |\Lambda_{\mathrm{SNS}}| = M$ specifies the acquired samples, where $\mathbb{N}_j^k$ denotes a set of the integer numbers $\{j, j+1, \ldots, k\}$.

SNS acquisition is described by the Single Measurement Vector (SMV) model [67]:

$$\mathbf{y} = \mathbf{A}\mathbf{x} + \mathbf{e} = \mathbf{R}\mathbf{F}\mathbf{x} + \mathbf{e}, \tag{24}$$

where $\mathbf{y} \in \mathbb{C}^{M \times 1}$ is a vector of time domain measurements, $\mathbf{A} \in \mathbb{C}^{M \times N}$ is a sensing matrix, $\mathbf{x} \in \mathbb{C}^{N \times 1}$ is an input sparse signal in frequency domain, $\mathbf{e} \in \mathbb{C}^{M \times 1}$ corresponds to noise in measurements, $\mathbf{R} \in \mathbb{R}^{M \times N}$ is a selection matrix corresponding to the sampling pattern Λ_{SNS} and $\mathbf{F} \in \mathbb{C}^{N \times N}$ is the DFT matrix.

An advantage of SNS is its relative simplicity. However, it requires obtaining samples from the Nyquist grid.

Multi-Coset Sampler

Multi-Coset Sampler (MCS) consists of P parallel channels that sample an input signal at the same rate but with different time offsets (see Fig. 18a) [12, 27, 47]. The MCS sampling pattern time $\Lambda_{\mathrm{MCS}} \subset \mathbb{N}_0^{L-1}, |\Lambda_{\mathrm{MCS}}| = P$ defines these time offsets. If the number of sampling channels is L, then MCS turns to be a time-interleaved NR sampler. An integer value L is called a multi-coset sampling period. Each ADC acquires W samples. The MCS mathematical model is described in Paper A. In short, MCS is defined by:

$$\mathbf{Y} = \mathbf{B}\mathbf{X} + \mathbf{E}, \tag{25}$$
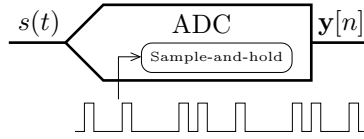
(a) Simplified SNS diagram.
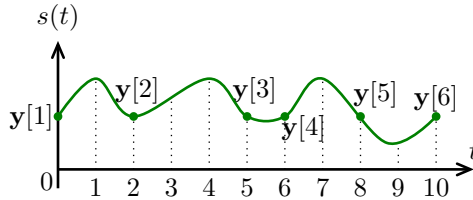
(b) An example of SNS acquisition, $M = 6$, $N = 10$,
$\Lambda_{\text{SNS}} = \{0, 2, 5, 6, 8, 10\}$.

Fig. 17: Illustration of SNS architecture and acquisition process.

where $\mathbf{Y} \in \mathbb{C}^{P \times W}$ is the matrix of known measurements, $\mathbf{B} \in \mathbb{C}^{P \times L}$ is a sensing matrix, $\mathbf{L} \in \mathbb{C}^{L \times W}$ denotes a matrix of an input signal in frequency domain and $\mathbf{E} \in \mathbb{C}^{P \times W}$ corresponds to noise. The matrix $\mathbf{X}$ is formed by slicing the spectrum of an input signal on L equal frequency slices and rearranging the slices (see Fig. 18b). In this case, the support of a sparse $\mathbf{X}$ is a set of indices of non-zero rows. Reconstruction of $\mathbf{X}$ from (25) is called a Multiple-Measurement Vectors (MMV) problem [21].

In [6], the authors proposed to use the MCS scheme for power spectrum blind sampling by computing the cross spectral densities between the outputs of sampling channels. The power spectrum directly provides the support of a signal and, thus, allowing signal reconstruction with the least squares approximation. The cross spectral densities approach reconstructs the power spectrum even of non-sparse signals. However, this method is based on minimal sparse ruler problem which limits the possible values of P and L and makes it less universal than the general MCS acquisition.

An advantage of MCS related to the advantage of time-interleaved ADCs – one fast ADC is replaced by several with a lower sampling rate. However, MCS requires to have precise time shifts between ADCs' sampling moments.
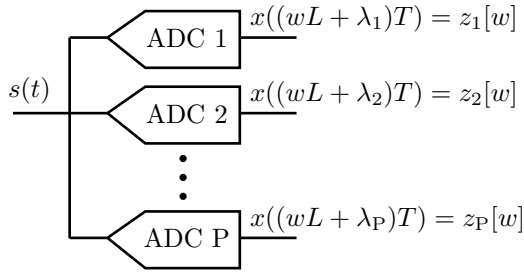
(a) Simplified MCS diagram.
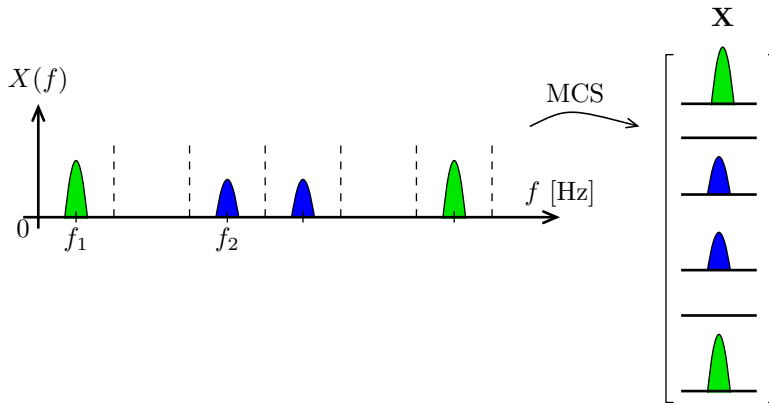
(b) MCS slicing of DFT of an input signal.

Fig. 18: Illustration of the MCS acquisition.

Random Demodulator

In a Random Demodulator (RD) scheme, an input signal is multiplied by a pseudo-random chipping sequence $p_c(t) \in \{\pm 1\}^N$, then passed through an anti-aliasing low-pass filter and sampled uniformly at low sampling rate (see Fig. 19) [39, 62]. Multiplying a
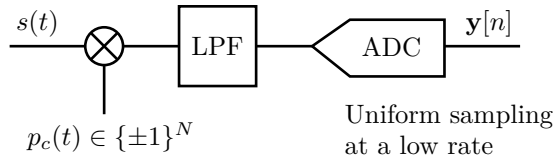
Fig. 19: Simplified RD diagram.

chipping sequence with an input signal is a direct-sequence spread-spectrum technique [52]. This implies that the information from the input signal is distributed over a wider band and an input signal can be reconstructed only from the part of spread spectrum. LPF cuts the baseband part of a spectrum and ADC acquires the selected part of the spectrum. RD acquisition is described by the SMV model [62]:

$$\mathbf{y} = \mathbf{H}\mathbf{D}\mathbf{F}^{-1}\mathbf{x}, \tag{26}$$

where $\mathbf{y} \in \mathbb{C}^{M \times 1}$ is a vector of the ADC's samples, $\mathbf{H} \in \mathbb{R}^{M \times N}$ represents a low-pass filtering operation, $\mathbf{D} \in \mathbb{R}^{N \times N}$ corresponds to the multiplication by a chipping sequence $p_c(t)$ and $\mathbf{x} \in \mathbb{C}^{N \times 1}$ is the unknown sparse signal in the frequency domain. Matrices $\mathbf{H}$ and $\mathbf{D}$ have the following form for example with $N{=}6$ and $M{=}3$

$$\mathbf{H} = \begin{bmatrix} 1 & 1 & 0 & 0 & 0 & 0 \\ 0 & 0 & 1 & 1 & 0 & 0 \\ 0 & 0 & 0 & 0 & 1 & 1 \end{bmatrix} \quad \mathbf{D} = \mathrm{diag}([1, -1, -1, 1, -, 1, 1]^{\mathrm{T}}).$$

The main advantage of the RD is that the ADC samples not a wide-band signal but a signal from the LPF. This allows to use ADCs which do not have high input bandwidths. However, imperfections of LPF degrade the acquisition quality [51].

Modulated Wideband Converter

Modulated Wideband Converter (MWC) can be seen as a hybrid of MCS and RD (see Fig. 20) [48]. An input signal falls into P channels where it is mixed with different periodic signals $p_i(t), i \in \{1, \ldots, P\}$. These operations spread the spectrum of an input signal. The resulting signals are sampled synchronously by P ADCs. MWC acquisition is described by row-sparse MMV.

The MWC architecture has two main advantages: (i) ADCs operates synchronously – there is no need for preserving accurate time-shifts as in MWC, (ii) ADCs sample
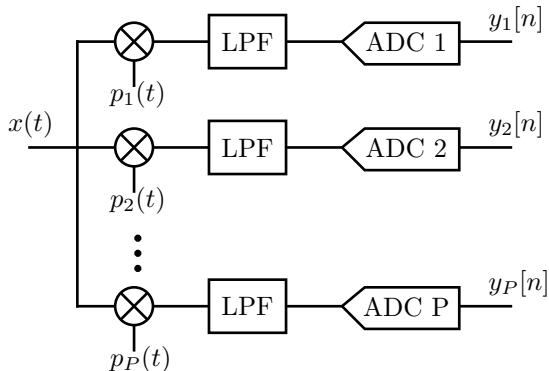
Fig. 20: Simplified MWC diagram.

baseband signals – no need for wide-band devices. However, the disadvantage is a complicated hardware.

4.5   Compressed Sensing Architectures for Signal Analyzers

Above we described four CS architectures that can be used for signal acquisition in SA applications. As can be seen from [2], a modern SA has sophisticated analog front-end and sampling parts. This hardware allows SA to perform in a frequency range up to 50 GHz [3]. However, further complication of hardware is undesirable due to the increasing costs and it is beneficial to simplify analog front-end. MCS and SNS are two architectures that have relative simple hardware.

An MCS acquisition device can be built by removing or adding some parallel channels of a full time-interleaved ADC [47]. An SA with 80 channels time-interleaved ADCs has been used for measurement applications for more than 10 years [54]. Therefore, there are no technological obstacles in implementing the MCS acquisition. The same is true for SNS.

(a) ℓ_1-ball. (b) $\ell_{0.4}$-ball. (c) ℓ_2-ball.
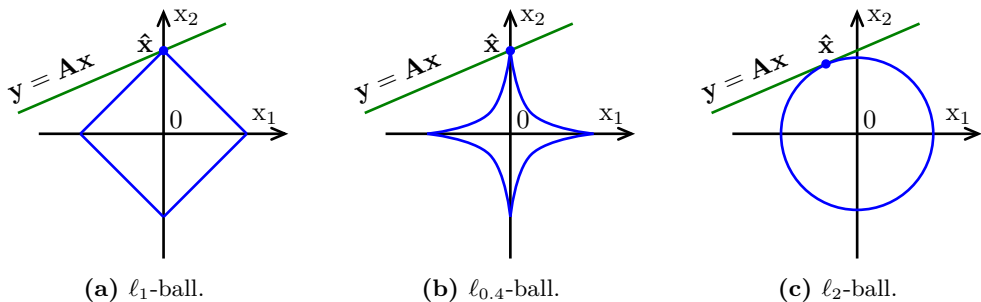
Fig. 21: Illustration of types of solution obtained with different norms as various functions. The green line denotes the constraint linear system.

5   Compressed Sensing Reconstruction

Knowing the requirements for unique and stable sparse solutions, we now turn to reconstruction approaches that find these solutions. These approaches can be classified in two groups: optimization and greedy methods. The first methods reconstruct a signal by solving optimization problems with various objective and constraints functions. Greedy methods either consequently find the columns of $\mathbf{A}$ that constitute $\mathbf{y}$, or follow the logic of thresholding non-zero elements and updating the solution.

5.1   Reconstruction Methods

Optimization methods

An intuitive way of CS reconstruction is to solve an optimization problem that directly promotes sparsity via the ℓ_0-norm [25]:

$$(P_0): \quad \underset{\mathbf{x}}{\text{minimize}} \ \|\mathbf{x}\|_0 \ \text{subject to} \ \mathbf{y} = \mathbf{A}\mathbf{x}. \tag{27}$$

Apart from its straightforward formulation, (P_0) is a NP-hard problem [25]. Solving a NP-hard problem requires a combinatorial search and tests for feasibility of solution that makes (P_0) unreal candidate for practical reconstruction procedure [25]. Therefore, it is beneficial to use other objective functions that promote sparsity. For example, ℓ_p-norms with $p \leq 1$. Consider Fig. 21 where the green line denotes the CS acquisition systems, $\mathbf{y} = \mathbf{A}\mathbf{x}$. Clearly, minimization of ℓ_1- and $\ell_{0.4}$-norms leads to a sparse solution with only $\mathrm{x}_2 \neq 0$. Minimization of ℓ_2-norm (squared ℓ_2-norm is an energy) results in a solution vector that have many non-zeros with small values, i.e. non-sparse. Therefore, it is not used in CS.

Minimization of the ℓ_1-norm, as oppose to ℓ_p-norms with $p < 1$, is a convex problem which implies that local minimum is necessary a global minimum [11]. Considering a

non-ideal CS acquisition (20), the reconstruction problem can be written as

$$(P_1^\epsilon): \quad \underset{\mathbf{x}}{\text{minimize}} \ \|\mathbf{x}\|_1 \ \text{ subject to } \ \|\mathbf{y} - \mathbf{Ax}\|_2 \le \epsilon. \tag{28}$$

(P_1^ϵ) is known by name of Basis Pursuit DeNoising (BPDN) [19]. Interestingly, the reconstruction error via (P_1^ϵ) can be theoretically bounded.

Theorem 3 (Based on Theorem 1.2 of [16]). Denote by $\hat{\mathbf{x}}_k$ the best k-sparse approximation of $\mathbf{x}$, assume that $\delta_{2k} < \sqrt{2} - 1$ and $\|e\|_2 \le \epsilon$. Then the solution $\hat{\mathbf{x}}$ to (P_1^ϵ) obeys

$$\|\hat{\mathbf{x}} - \mathbf{x}\|_2 \le C_0 k^{-1/2} \|\hat{\mathbf{x}}_k - \mathbf{x}\|_1 + C_1 \epsilon$$

for some constants C_0 and C_1.

This theorem establishes ℓ_1-minimization as a method that recovers k-sparse signals from non-ideal sub-Nyquist measurements. In general, ℓ_1-minimization has a high reconstruction performance [10].

There are several open source software packages that can be used for for solving (P_1^ϵ) problems: CVX [33, 34], SPGL1 [64, 65], YALL1 [68], GPSR [28] etc.

As mentioned above, the ℓ_p-minimization for $p < 1$ is not a convex problem and thus there is no guaranties for convergence to a global minimum. However, such methods are used due to the simplicity of implementation [25]. For example, FOCUSS [32].

Greedy methods

The problem of recovering $\mathbf{x}$ from an underdetermined system $\mathbf{y} = \mathbf{Ax}$ (or $\mathbf{y} = \mathbf{Ax} + \mathbf{e}$) can be solved with other approaches. If $\mathbf{x}$ is sparse, then

$$\mathbf{y} = \mathbf{Ax} = [\mathbf{A}^1 \, \mathbf{A}^2 \dots \mathbf{A}^N] \begin{bmatrix} \mathbf{x}[1] \\ \mathbf{x}[2] \\ \vdots \\ \mathbf{x}[N] \end{bmatrix} = \mathbf{A}^K \mathbf{x}_K, \tag{29}$$

where a set K is called a support of $\mathbf{x}$ – a set comprising indices of non-zero elements of $\mathbf{x}$; a matrix $\mathbf{A}^K \in \mathbf{C}^{M \times k}, k \le M$, consists of columns of $\mathbf{A}$ with indices from K and a vector $\mathbf{x}_K \in \mathbf{C}^{k \times 1}$ consists of non-zero elements of $\mathbf{x}$. In general, a system $\mathbf{y} = \mathbf{A}^K \mathbf{x}_K$ is overdetermined and does not have a solution. However, if $\mathbf{y} \in \text{range}(\mathbf{A}^K)$, which is a case in CS, the unique solution exists. The easiest way to find this unique solution is to use a least squares method [61].

The question is how to find the support of $\mathbf{x}$, K, i.e.   the indices of columns of $\mathbf{A}$ that form $\mathbf{y}$. One of the popular algorithms is an Orthogonal Matching Pursuit (OMP) [18, 21, 49]. OMP finds one element from K per iteration as in Fig. 22. OMP
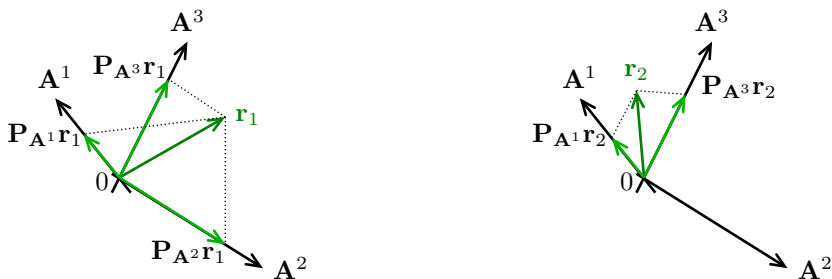
(a) First OMP iteration,
$\mathbf{r}_1 = \mathbf{y}$,
$\|\mathbf{P}_{\mathbf{A}^2}\mathbf{r}_1\|_2 > \{\|\mathbf{P}_{\mathbf{A}^1}\mathbf{r}_1\|_2, \|\mathbf{P}_{\mathbf{A}^3}\mathbf{r}_1\|_2\} \Rightarrow$
$K = \{2\}$.

(b) Second OMP iteration,
$\mathbf{r}_2 = \mathbf{r}_1 - \mathbf{P}_{\mathbf{A}^K}\mathbf{r}_1$,
$\|\mathbf{P}_{\mathbf{A}^3}\mathbf{r}_2\|_2 > \|\mathbf{P}_{\mathbf{A}^1}\mathbf{r}_2\|_2 \Rightarrow$
$K = K \cup \{3\} = \{2, 3\}$.

Fig. 22: Illustration of the two OMP iterations.

starts by setting the residual vector $\mathbf{r}_1 = \mathbf{y}$. Then, $\mathbf{r}_1$ is orthogonally projected on the columns of $\mathbf{A}^i, i \in \{1, 2, \ldots, N\}$ by $\mathbf{P}_{\mathbf{A}^i}\mathbf{r}_1$ and the ℓ_2-norms of the projection are evaluated. The largest projection corresponds to the index of a column that becomes the first element of K. In case of Fig. 22a, $K = \{2\}$. At the beginning of the second iteration, the residual is updated by projecting $\mathbf{r}_1$ to the space orthogonal complement to $\mathbf{A}^K$, i.e. $\mathbf{r}_2 = \mathbf{r}_1 - \mathbf{P}_{\mathbf{A}^K}\mathbf{r}_1$, and the projection of $\mathbf{r}_2$ are computed. Then, the second iteration follows the first one. The process continues until a termination criteria is met. The criteria can be the number of selected columns, the Frobenius norm of the residual etc [21].

Thresholding methods

Thresholding algorithms are another reconstruction approaches in CS [26]. In these methods, some of the non-zero elements of an estimated solution are thresholded at each iteration meaning that they are forced to zero. An example of such a method is an Iterative Hard Thresholding (IHT) [10]. The basic IHT iteration is given by:

$$\hat{\mathbf{x}}^{i+1} = H_k(\hat{\mathbf{x}}^i + \mu \mathbf{A}^H(\mathbf{y} - \mathbf{A}\hat{\mathbf{x}}^i)), \tag{30}$$

$\hat{\mathbf{x}}^i \in \mathbb{C}^{N \times 1}$ is an estimated solution at ith iteration, $i = 0, 1, \ldots, \hat{\mathbf{x}}^0 = \mathbf{0}$, $H_k(\cdot) \in \mathbb{C}^{N \times 1}$ is a thresholding operator that preserves k largest elements of a vector and set other to zero, $\mu \in \mathbb{R}$ is a step size. IHT can be seen as the gradient projection method applied to the problem:

$$\underset{\hat{\mathbf{x}}}{\text{minimize}} \ \|\mathbf{A}\hat{\mathbf{x}} - \mathbf{y}\|_2^2 \ \text{subject to} \ \text{card}(\hat{\mathbf{x}}) \leq k. \tag{31}$$
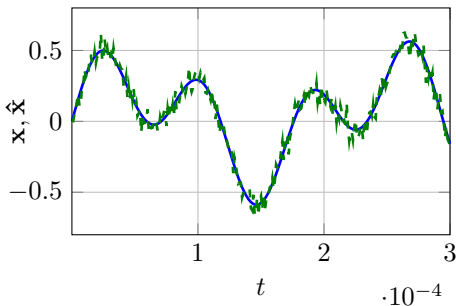
(a) $e = 0.16$, a signal $\hat{\mathbf{x}}$ is formed from $\mathbf{x}$ by adding AWGN such that SNR= 16 dB.
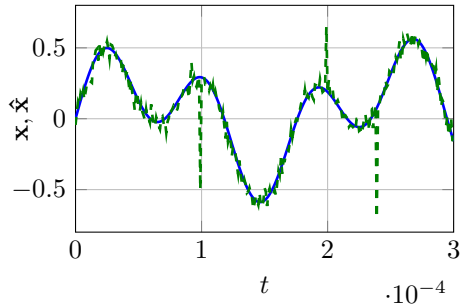
(b) $e = 0.27$, a signal $\hat{\mathbf{x}}$ is formed from $\mathbf{x}$ by adding AWGN such that SNR= 16 dB plus three random spike errors.

Fig. 23: Illustration of the RRMS errors, blue line – original signal, green line – reconstructed signal.

Notice that the gradient of the objective function is $2\mathbf{A}^{\mathrm{H}}(\mathbf{A}\hat{\mathbf{x}}-\mathbf{y})$. IHT consequently approaches $\hat{\mathbf{x}}$ that minimizes the objective function by "stepping" to the direction opposite to gradient and preserving sparsity of the solution with $H_k(\cdot) \in \mathbb{C}^{N\times 1}$. Thresholding algorithms possess both low complexity and high reconstruction performance [26].

Reconstruction algorithms based on Bayesian statistics and graphical models are also used in CS [37]. For example, Approximate Message Passing which is reported to have almost the same performance as ℓ_1-minimization [23].

The comparison of several reconstruction methods (OMP, ℓ_1-minimization, M-FOCUSS [21], MUSIC [21] etc) applied to acquisition of multi-band signals are presented in Publications A and C.

5.2 Quality of Reconstruction

The aim of CS is to reconstruct a signal with only undersampled measurements. Various performance metrics can be used for evaluating the quality of CS acquisition. For example, Relative Root Mean Square error (RRMS):

$$e = \frac{\|\mathbf{x} - \hat{\mathbf{x}}\|_2}{\|\mathbf{x}\|_2}, \; e \in [0, +\infty), \qquad (32)$$

where $\mathbf{x} \in \mathbb{C}^{N\times 1}$ and $\hat{\mathbf{x}} \in \mathbb{C}^{N\times 1}$, are the original and reconstructed signals in some domain, respectively. RRMS describes well both rare and frequent errors. Assume that $\hat{\mathbf{x}}$ is obtained with some reconstruction procedures. Consider examples in Fig. 23 that illustrates RRMS for two cases for time domain real-valued signals. In the first case, signal $\hat{\mathbf{x}}$ is basically a signal $\mathbf{x}$ polluted by Additive White Gaussian Noise (AWGN) such that the resulting Signal-to-Noise Ratio (SNR) is 16 dB. In the second case, a signal $\hat{\mathbf{x}}$ was additionally corrupted with three random spikes.

The average RRMS, $E = \frac{1}{Q}\sum_{i=1}^{N} e_i$, can be used to assess an average quality of reconstruction of Q signals.

E can be used to compare quality of different acquisition approaches and reconstruction algorithms. For example, a bunch of test signals is acquired and reconstructed under various conditions and E is evaluated. The lower the value of E, the better is CS approach/reconstruction algorithm.

Recall that CS aims to acquire signals that are sparse or compressible in some basis. Thus, a quality of reconstruction can also be evaluated with the Support Reconstruction Ratio (SRR):

$$G = \frac{\text{number of correctly reconstructed supports}}{\text{number of test signals}}, \; G \in [0, 1]. \tag{33}$$

In some CS architectures, a support of a signal can be less sensitive to noise. For example in MCS, the support is the set of indices of frequency slices containing bands. Therefore, it is unlikely that the support of a noise free signal differs from the support of a signal with AWGN, unless the power of noise equals to the power of a clean signal. In contrast in SNS, support comprises non-zero DFT bins. AWGN can mask some of these bins. Thus, the support of noise-free and noisy signals can be different.
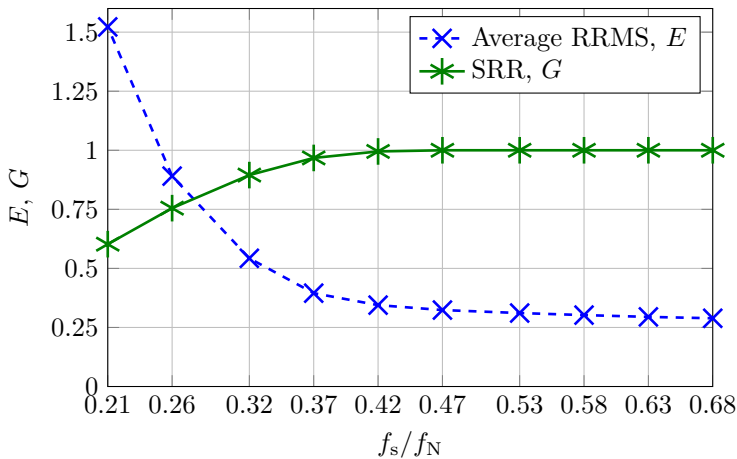
Fig. 24: Illustration of SRR and average RRMS vs. the average sampling rate in the MCS acquisition of two-band signals with SNR= 10 dB. Theoretical minimum RRMS is 0.27.

Fig. 24 illustrates the empirical relations between SRR and average RRMS vs. the average sampling rate in MCS acquisition of 100 instances of test two-band signals with SNR= 10 dB. The reconstruction is performed with the M-FOC-COR algorithm (see Paper **C**). SRR equals to 1 when at the point 0.42. This clear indicates the sampling rate

sufficient for correct detection of supports of all the test signals. The correct support reconstruction implies the successful signal reconstruction. However, it is problematic to detect this sampling rate with average RRMS as it requires to know a specific threshold. In its turn, the thresholds depends on SNR. Therefore, in MCS it is more beneficial to evaluate the quality of reconstruction with SRR despite of the fact that average RRMS is more universal.

5.3   Complexity of Reconstruction

CS reconstruction can be performed on various computational platforms: ASIC, FPGA, CPU/GPU unit. In general, the analysis of an algorithm's complexity allows to evaluate its applicability given constraints on computational resources and execution time.

In CS, complicated reconstruction algorithms are the means that allow to decrease sampling rates below NR. Different algorithms have different reconstruction performance and complexity. In case of real-time applications like SA, the complexity of reconstruction becomes an important issue. The selection of a specific algorithm for CS application is based on quality/complexity tradeoffs. The quality of reconstruction can be assessed with SRR and average RRMS. In its turn, complexity of an algorithm can also be evaluated in different ways [1]:

- number of floating point operations – arithmetic complexity [1, 20, 40]. This complexity metric is widely used to evaluate the total amount of computations performed by an algorithm.

- necessary memory space – memory complexity [1, 20].

The execution time of an algorithm is also depends on degree of parallelism [59] and memory bandwidth and latency [46]. Modern CPU/GPU perform arithmetic operations on data faster than this data is transferred between CPU/GPU and memory [4]. In multi-cores systems, the data access further complicates as some cores have to wait for their time for memory access. To cope with this queuing, some companies introduce technologies that allow a core to have an independent memory access, for example Intel Quickpath Interconnect [35]. Another issue is inter-process communication. With the increasing number of cores, data transferring between them becomes more complicated. Summarizing, the execution time of an algorithm depends not only on the amount of computations but also on the specific implementation.

In order to obtain more general results, we propose to evaluate computational costs of CS reconstruction algorithms with the number of floating point operations. Usually, arithmetic complexity of an algorithm is described with asymptotic notations, for example the big O notation.

Definition 3 (Big O notation [40]). Assume that $f(n) \in \mathbb{R}$ and $g(n) \in \mathbb{R}$ are functions of the positive integer n. Then, $f(n) = \mathcal{O}(g(n)) \Leftrightarrow \exists M \in \mathbb{R}$ and positive integer

n_0 such that

$$|f(n)| \leq M|g(n)| \quad \text{for} \quad n > n_0. \tag{34}$$

the Big O notation is very useful for comparison of complexities of algorithms if problem's size increasing towards infinity. Asymptotic complexities of many computational algorithms like eigenvalue decomposition, QR factorization etc. are already available [61]. At the same time, these notations can be misleading if argument is not "sufficient" large. For example, assume that arithmetic complexities of two algorithms is described with functions $f_1(n) = 10^5 n^2$ and $f_2(n) = n^3$. Then, $f_1(n) = \mathcal{O}(n^2)$ and $f_2(n) = \mathcal{O}(n^3)$, which implies that asymptotically second algorithm has larger computational cost. However, for $n = 10$ $f_1(10) = 10^7 > f_2(10) = 10^3$. For this reason, in this thesis we do not directly use asymptotic notations but rather count all the arithmetic operations that are performed by an algorithm. This allows to compare computational costs for the specific problem sizes.

6   Research Contributions

In this research, we were aiming at investigating issues related to the reconstruction quality and complexity of the CS acquisition. In particular, to investigate the performance–complexity tradeoffs and methods decreasing computational complexity. Acquisition of multi-band signals in SA has been chosen as one the potential CS application.

6.1   Publication A

We started our research by comparing the existing reconstruction approaches in MCS. The results of this part of the research are presented in Publication A. The comparison is performed with extensive numerical simulations. Similar research is performed in [57]. However in this article, the acquisition scenarios are limited to signals having a fixed, $N = 3$, number of bands. This limits the investigation of the behaviour of reconstruction algorithms. In particular as we show in Publication A, the necessary average sampling rates for some of the reconstruction algorithms scales non-linearly with the number of bands. The necessary sampling rates also depend on the level of noise in the signals. As the main outcome, the article provides recommendations on which algorithms result in better reconstruction performance depending on the number of bands and the level of noise in the signals. Apart from this, the article also studies how different approaches of sampling patterns selection impact the reconstruction quality.

This paper developed the framework allowing to compare quality of different reconstruction methods. The framework was used for Publication B and C.

6.2 Publication B

In this publication, we introduced multi-coset emulation in SNS as a means to reduce computational complexity of reconstruction. Previously, the computational costs of signal reconstruction in RD (SMV reconstruction model) and MWC (MMV reconstruction model) were compared in [26] and the advantage of MWC was pointed out. However, an idea of replacing the SMV reconstruction with MMV was not elaborated. We filled this gap in Publication B, where the proposed multi-coset emulation reformulates the reconstruction in SNS as a MMV problem (MCS reconstruction). As a result, a number of floating point operations in the SNS acquisition is decreased by several orders of magnitude without degradation of reconstruction performance. This confirms the main hypothesis of the thesis applied to CS acquisition of noise-free signals.

6.3 Publication C

This publication contains more thorough elaboration of the multi-coset emulation for the SNS acquisition. This article is motivated by several reasons.

Publication B considered scenarios with noise-free signals. In addition, frequency bands in these scenarios were aligned within the boundaries of multi-coset frequency slices. These simplifications do not fully comply with real-life conditions and requirements, so, they were eliminated in Publication C, where noisy signals with different bands' width and position were used in the numerical simulations. Such a broad variety of test signals allowed to point out the simulation scenarios where multi-coset emulation degrades or improves the reconstruction performance while the reduction of computational complexity is preserved. Therefore, multi-coset emulation in SNS introduces performance-complexity tradeoffs which were studied in this part of the research.

One more motivating factor for Publication C was that in Publication B only the OMP algorithm and its MMV version, M-OMP, were used for signal reconstruction. These methods were widely used in CS [25] until the appearance of iterative thresholding algorithms, like IHT [26]. From the computational point of view, one of the prominent feature of IHT is that its implementation based on FFT is possible while reconstructing signals from the Fourier basis. Thus, if IHT is not considered for the direct SNS acquisition, then the advantage is given to multi-coset emulation. This is why, IHT was used in the SNS reconstruction in Publication C in order to increase objectivity of the research.

This publication confirms the main hypothesis of the thesis applied to more realistic CS acquisition of noisy signals and CS reconstruction with prominent algorithms.

7 Conclusions

CS can be used to acquire frequency-sparse multi-band signals. With this approach, sampling rate can be decreased below NR. In CS, reconstruction quality and complexity are the crucial issues especially for real-time applications.

In this thesis, we studied these two CS issues applied to acquisition of frequency sparse multi-band signals. Sensing of multi-band signals is required, for example in SA applications. With the CS approach, SA may therefore acquire signals that are not possible to acquire with the classical NR sampling. We were focusing on scenarios comprising signals with different number, widths and position of bands and level of noise in signals.

The quality of SNS and MCS acquisition with different reconstruction algorithms has been evaluated. In addition, the impact of the different MCS sampling patterns on the reconstruction quality has been investigated.

This thesis confirms that the computational complexity of the CS acquisition can be reduced by an order of magnitude without degrading the reconstruction quality. This reduction is achieved by multi-coset emulation which corresponds to the reformulation of reconstruction problem. This emulation introduces performance-complexity tradeoffs that has been also studied. In some cases, the multi-coset emulation degrades the reconstruction quality while in other the emulation improves it. However, the reduction of computational complexity of signal reconstruction by orders of magnitude is preserved for the all considered acquisition scenarios. Thus, the multi-coset emulation may bring CS acquisition closer to real-life real-time applications.

The MATLAB code used for this PhD thesis is available only at http://dx.doi.org/ 10.5278/VBN/MISC/MSS.AMBSCS, DOI 10.5278/VBN/MISC/MSS.AMBSCS.

Future Perspectives

The conducted research can be further developed:

- The multi-coset emulation described in this thesis allows to reduce the number of floating point operations in the CS reconstruction by orders of magnitude. In this thesis, we considered signals that are sparse in the Fourier basis. However, the multi-coset emulation is universal and can be used with other CS applications. Therefore, it is of great interest to use this method for acquisition of signals that are sparse in basis aside from the Fourier basis.

- One more issue in CS is noise folding [7, 22], which is basically the aliasing of wideband noise due to sub-Nyquist sampling. Unfortunately, noise folding cannot be avoided in CS, so it is important to find the ways that mitigate noise folding.

References

[1] M. Abramov, *Lecture Notes on Algorithms Complexity*. Moscow Center for Continuous Mathematical Education (MCNMO), 2009.

[2] Agilent Technologies, "The architecture of a modern spectrum analyzer," *X-Series Spectrum Analyzers Seminar*, 2010. [Online]. Available: http://www.home.agilent.com/upload/cmc_upload/All/PPT2_AGILENT_Evolution-technologique-des-nouveaux-analyseurs-de-signaux.pdf?&cc=DK&lc=dan

[3] ——, "Spectrum analysis basics," *Application Note 150*, 2014. [Online]. Available: http://cp.literature.agilent.com/litweb/pdf/5952-0292.pdf

[4] F. Alted, "Why modern CPUs are starving and what can be done about it," *Computing in Science & Engineering*, pp. 68–71, Mar.–Apr. 2010.

[5] Analog Devices, "Fundamentals of sampled data systems," *Application Note, AN-282.*

[6] D. Ariananda, G. Leus, and Z. Tian, "Multi-coset sampling for power spectrum blind sensing," in *17th International Conference on Digital Signal Processing (DSP)*, July 2011, pp. 1–8.

[7] E. Arias-Castro and Y. Eldar, "Noise folding in compressed sensing," *IEEE Signal Processing Letters*, vol. 18, no. 8, pp. 478–481, 2011.

[8] N. Behjou, T. Larsen, and M. Hoegdal, "Design of a simultaneous multi-band RF sub-sampling receiver," in *Digest of IEEE MTT-S International Microwave Symposium*, June 2008, pp. 5–8.

[9] N. Behjou, T. Larsen, and O. Jensen, "RF sub-sampling receiver architecture based on milieu adapting techniques," in *Digest of IEEE MTT-S International Microwave Symposium*, June 2012, pp. 1–3.

[10] T. Blumensath and M. E Davies, "How to use the iterative hard thresholding algorithm," in *SPARS'09 - Signal Processing with Adaptive Sparse Structured Representations*, Saint Malo, France, 2009.

[11] S. Boyd and L. Vandenberghe, *Convex Optimization*. Cambridge University Press, 2004.

[12] Y. Bresler, "Spectrum-blind sampling and compressive sensing for continuous-index signals," in *Information Theory and Applications Workshop*, Jan. 27 2008-Feb. 1 2008, pp. 547–554.

[13] E. J. Candès and M. B. Wakin, "An introduction to compressive sampling," *IEEE Signal Process. Mag.*, vol. 25, no. 2, pp. 21–30, Mar. 2008.

[14] E. J. Candès and T. Tao, "Decoding by linear programming," *IEEE Transactions on Information Theory*, vol. 51, no. 12, pp. 4203–4215, 12 2005.

[15] E. Candès and J. Romberg, "Sparsity and incoherence in compressive sampling," *Inverse Problems*, vol. 23, no. 3, p. 969, 2007. [Online]. Available: http://stacks.iop.org/0266-5611/23/i=3/a=008

[16] E. J. Candès, "The restricted isometry property and its implications for compressed sensing," *Comptes Rendus Mathematique*, vol. 346, no. 9-10, pp. 589–592, 2008. [Online]. Available: http://www.sciencedirect.com/science/article/B6X1B-4S86288-6/2/3b39cda39e6bbd3b3388c4119ffbc198

[17] W. L. Chan, K. Charan, D. Takhar, K. F. Kelly, R. Baraniuk, and D. Mittleman, "A single-pixel terahertz imaging system based on compressed sensing," *Applied Physics Letters*, vol. 93, no. 12, pp. 121 105–121 105–3, Sep 2008.

[18] S. Chen and J. Wigger, "Fast orthogonal least squares algorithm for efficient subset model selection." *IEEE Trans. Signal Process.*, vol. 43, no. 7, pp. 1713–1715, 1995.

[19] S. S. Chen, D. L. Donoho, and M. A. Saunders, "Atomic decomposition by basis pursuit," *SIAM Review*, vol. 43, no. 1, pp. 129–159, 2001.

[20] T. H. Cormen, C. E. Leiserson, R. L. Rivest, and C. Stein, *Introduction to Algorithms*, 3rd ed.   The MIT Press, 2009.

[21] S. Cotter, B. Rao, K. Engan, and K. Kreutz-Delgado, "Sparse solutions to linear inverse problems with multiple measurement vectors," *IEEE Trans. Signal Process.*, vol. 53, no. 7, pp. 2477–2488, Jul. 2005.

[22] M. A. Davenport, J. N. Laska, J. R. Treichler, and R. G. Baraniuk, "The pros and cons of compressive sensing for wideband signal acquisition: Noise folding vs. dynamic range," available in arXiv: arXiv:1104.4842v2. [Online]. Available: arXiv:1104.4842v2

[23] D. L. Donoho, A. Maleki, and A. Montanari, "Message-passing algorithms for compressed sensing," in *Proceedings of the National Academy of Sciences of the United States of America*, vol. 106 no. 45, 2009, pp. 18 914 –18 919.

[24] M. Duarte, M. Davenport, D. Takhar, J. Laska, T. Sun, K. Kelly, and R. Baraniuk, "Single-pixel imaging via compressive sampling," *Signal Processing Magazine, IEEE*, vol. 25, no. 2, pp. 83 –91, march 2008.

[25] M. Elad, *Sparse and Redundant Representations: From Theory to Applications in Signal and Image Processing*.   Springer, 2010.

[26] Y. C. Eldar and G. Kutyniok, *Compressed Sensing: Theory and Applications*.   Cambridge University Press, 2012.

[27] P. Feng and Y. Bresler, "Spectrum-blind minimum-rate sampling and reconstruction of multiband signals," in *IEEE International Conference on Acoustics, Speech, and Signal Processing*, vol. 3, May 1996, pp. 1688–1691.

[28] M. Figueiredo, R. Nowak, and S. Wright, "Gradient projection for sparse reconstruction: Application to compressed sensing and other inverse problems," *IEEE Journal of Selected Topics in Signal Processing*, vol. 1, no. 4, pp. 586–597, Dec 2007.

[29] S. V. Friedberg, A. J. Insel, and L. E. Spence, *Linear Algebra (2nd ed.)*.   Englewood Cliffs, NJ, USA: Prentice-Hall, Inc., 1989.

[30] K. Gedalyahu and Y. Eldar, "Time delay estimation: Compressed sensing over an infinite union of subspaces," in *IEEE International Conference on Acoustics Speech and Signal Processing*, 2010, pp. 3902–3905.

[31] C. Gessner, *Long Term Evolution: A concise introduction to LTE and its measurement requirements.*   Rohde & Schwarz, 2011.

[32] I. Gorodnitsky and B. Rao, "Sparse signal reconstruction from limited data using FO-CUSS: a re-weighted minimum norm algorithm," *IEEE Trans. Signal Process.*, vol. 45, no. 3, pp. 600–616, Mar. 1997.

[33] M. Grant and S. Boyd, "Graph implementations for nonsmooth convex programs," in *Recent Advances in Learning and Control*, ser. Lecture Notes in Control and Information Sciences, V. Blondel, S. Boyd, and H. Kimura, Eds.   Springer-Verlag Limited, 2008, pp. 95–110, http://stanford.edu/~boyd/graph_dcp.html.

[34] ——, "CVX: Matlab software for disciplined convex programming, version 2.0 beta," http://cvxr.com/cvx, Sep. 2013.

[35] Intel Corparation, "An Introduction to the Intel Quickpath Interconnect," *Application Note 150*, 2009. [Online]. Available: http://www.intel.com/content/www/us/en/io/quickpath-technology/quick-path-interconnect-introduction-paper.html

[36] A. Jerri, "The Shannon sampling theorem – its various extensions and applications: A tutorial review," *Proceedings of the IEEE*, vol. 65, no. 11, pp. 1565–1596, 1977.

[37] S. Ji, Y. Xue, and L. Carin, "Bayesian compressive sensing," *IEEE Transactions on Signal Processing*, vol. 56, no. 6, pp. 2346–2356, June 2008.

[38] Kester, W.A. and Analog Devices, *Data Conversion Handbook*, ser. Analog Devices. Elsevier, 2005. [Online]. Available: http://books.google.dk/books?id=0aeBS6SgtR4C

[39] S. Kirolos, J. Laska, M. Wakin, M. Duarte, D. Baron, T. Ragheb, Y. Massoud, and R. Baraniuk, "Analog-to-information conversion via random demodulation," in *IEEE Dallas/CAS Workshop on Design, Applications, Integration and Software, 2006*, 10 2006, pp. 71–74.

[40] D. E. Knuth, *The Art of Computer Programming.*   Addison-Wesley Publishing Company, 1969, vol. 1.

[41] A. Kohlenberg, "Exact interpolation of band-limited functions," *Journal of Applied Physics*, vol. 24, no. 12, pp. 1432 –1436, dec 1953.

[42] H. Landau, "Necessary density conditions for sampling and interpolation of certain entire functions," *Acta Mathematica*, vol. 117, pp. 37–52, 1967.

[43] Y.-P. Lin and P. Vaidyanathan, "Periodically nonuniform sampling of bandpass signals," *IEEE Trans. Circuits Syst. II, Analog Digit. Signal Process*, vol. 45, no. 3, pp. 340–351, 1998.

[44] M. Lustig, D. Donoho, J. Santos, and J. Pauly, "Compressed sensing MRI," *Signal Processing Magazine, IEEE*, vol. 25, no. 2, pp. 72–82, March 2008.

[45] P. Maechler, N. Felber, H. Kaeslin, and A. Burg, "Hardware-efficient random sampling of Fourier-sparse signals," in *IEEE International Symposium on Circuits and Systems (ISCAS)*, May 2012, pp. 269–272.

[46] D. Malech, "DDR4 LRDIMMs Unprecedented Memory Bandwidth on Samsung DDR4 LRDIMM Enabled by IDT's Register and Data Buffer," *Whitpe Paper*, 2014. [Online]. Available: http://www.idt.com/document/whp/ddr4-lrdimms-both-memory-capacity-and-speed

[47] M. Mishali and Y. C. Eldar, "Blind multiband signal reconstruction: Compressed sensing for analog signals," *IEEE Trans. Signal Process.*, vol. 57, no. 3, pp. 993–1009, 2009.

[48] ——, "From theory to practice: Sub-nyquist sampling of sparse wideband analog signals," *IEEE Journal of Selected Topics in Signal Processing*, vol. 4, no. 2, pp. 375–391, 4 2010.

[49] B. K. Natarajan, "Sparse approximate solutions to linear systems," *SIAM J. Comput.*, vol. 24, no. 2, pp. 227–234, 1995.

[50] A. V. Oppenheim, R. W. Schafer, and J. R. Buck, *Discrete-time Signal Processing (2nd ed.)*.   Upper Saddle River, NJ, USA: Prentice-Hall, Inc., 1999.

[51] P. Pankiewicz, T. Arildsen, and T. Larsen, "Sensitivity of the random demodulation framework to filter tolerances," in *Proceedings of the European Signal Processing Conference (EUSIPCO)*, 2011, pp. 534–538.

[52] R. Pickholtz, D. Schilling, and L. Milstein, "Theory of spread-spectrum communications–a tutorial," *IEEE Transactions on Communications*, vol. 30, no. 5, pp. 855–884, May 1982.

[53] P. Poshala, "Why oversampling when undersampling can do the job?" Texas Instruments, Tech. Rep. SLAA594A, 7 2013.

[54] K. Poulton, R. Neff, B. Setterberg, B. Wuppermann, T. Kopley, R. Jewett, J. Pernillo, C. Tan, and A. Montijo, "A 20 GS/s 8 b ADC with a 1 MB memory in 0.18 μm CMOS," in *IEEE International Solid-State Circuits Conference, ISSCC-2003. Digest of Technical Papers.*, vol. 1, Feb. 2003, pp. 318–496.

[55] B. Razavi, "Challenges in portable RF transceiver design," *IEEE Circuits and Devices Magazine*, vol. 12, no. 5, pp. 12–25, Sep 1996.

[56] C. Shannon, "Communication in the presence of noise," *Proceedings of the IRE*, vol. 37, no. 1, pp. 10–21, Jan 1949.

[57] H. Shen, T. Arildsen, and T. Larsen, "Blind multi-band spectrum signals reconstruction algorithms comparison," *Proceedings of the European Signal Processing Conference (EUSIPCO)*, pp. 353–357, 2011.

[58] J. Smith, *Introduction to Digital Filters: With Audio Applications*, ser. Music signal processing series.   W3K, 2007. [Online]. Available: http://books.google.dk/books?id=pC1iCQUAsHEC

[59] Y. Sun and J. Su, "Computing Degree of Parallelism for BPMN Processes," in *Service-Oriented Computing*, ser. Lecture Notes in Computer Science, G. Kappel, Z. Maamar, and H. Motahari-Nezhad, Eds.   Springer Berlin Heidelberg, 2011, vol. 7084, pp. 1–15. [Online]. Available: http://dx.doi.org/10.1007/978-3-642-25535-9_1

[60] M. Trakimas, R. D'Angelo, S. Aeron, T. Hancock, and S. Sonkusale, "A compressed sensing analog-to-information converter with edge-triggered SAR ADC core," *IEEE Transactions on Circuits and Systems I: Regular Papers*, vol. 60, no. 5, pp. 1135–1148, May 2013.

[61] L. Trefethen and D. Bau, *Numerical Linear Algebra*.   Philadelphia: Society for Industrial and Applied Mathematics, 1997.

[62] J. Tropp, J. Laska, M. Duarte, J. Romberg, and R. Baraniuk, "Beyond Nyquist: Efficient sampling of sparse bandlimited signals," *IEEE Trans. Inf. Theory*, vol. 56, no. 1, pp. 520–544, Jan. 2010.

[63] M. Valkama and M. Renfors, "Advanced receiver architectures and I/Q signal processing," in *First International Symposium on Control, Communications and Signal Processing*, 2004, pp. 71–74.

[64] E. van den Berg and M. P. Friedlander, "SPGL1: A solver for large-scale sparse reconstruction," June 2007, http://www.cs.ubc.ca/labs/scl/spgl1.

[65] ——, "Probing the Pareto frontier for basis pursuit solutions," *SIAM Journal on Scientific Computing*, vol. 31, no. 2, pp. 890–912, 2008.

[66] R. Vaughan, N. Scott, and D. White, "The theory of bandpass sampling," *IEEE Trans. Signal Process.*, vol. 39, no. 9, pp. 1973–1984, Sep. 1991.

[67] M. Wakin, S. Becker, E. Nakamura, M. Grant, E. Sovero, D. Ching, J. Yoo, J. Romberg, A. Emami-Neyestanak, and E. Candè, "A nonuniform sampler for wideband spectrally-sparse environments," *IEEE J. Emerg. Sel. Topic Circuits Syst.*, vol. 2, no. 3, pp. 516–529, Sep. 2012.

[68] J. Yang and Y. Zhang, "Alternating direction algorithms for ℓ_1-problems in compressive sensing," *SIAM Journal on Scientific Computing*, vol. 33, no. 1, pp. 250–278, 2011. [Online]. Available: http://dx.doi.org/10.1137/090777761

Part II

Papers

Paper A

Performance Comparison of Reconstruction Algorithms in
Discrete Blind Multi-Coset Sampling

Ruben Grigoryan, Thomas Arildsen, Deepaknath Tandur, Torben Larsen

Abstract

This paper investigates the performance of different reconstruction algorithms in discrete blind multi-coset sampling. Multi-coset scheme is a promising compressed sensing architecture that can replace traditional Nyquist-rate sampling in the applications with multi-band frequency sparse signals. The performance of the existing compressed sensing reconstruction algorithms have not been investigated yet for the discrete multi-coset sampling. We compare the following algorithms – orthogonal matching pursuit, multiple signal classification, subspace-augmented multiple signal classification, focal underdetermined system solver and basis pursuit denoising. The comparison is performed via numerical simulations for different sampling conditions. According to the simulations, focal under-determined system solver outperforms all other algorithms for signals with low signal-to-noise ratio. In other cases, the multiple signal classification algorithm is more beneficial.

1 Introduction

Bandpass and multi-band signals can be successfully sampled at frequencies below the Nyquist-Shannon limit, so called sub-Nyquist sampling [1]. For this type of signals the minimum sampling rate depends on the accumulated bandwidth rather than the highest frequency component as in the classical Nyquist-Shannon-Kotelnikov theorem. Nonuniform periodic sampling is one of the method for sub-Nyquist sampling. This strategy can be implemented with parallel sampling channels each of them containing an analog-to-digital converter (ADC). The ADCs perform measurements at different moments of time. Such a scheme is called a multi-coset sampling scheme (see Fig. A.1) [2]. The problem of sub-Nyquist sampling of non-baseband signals has been discussed in a number of papers [2–6].

Consider multi-band signals. When the positions of bands in a signal are known in advance (non-blind sampling) the reconstruction can be performed with specially designed filters [3, 4]. In [2] Feng and Bresler introduced blind sampling where the positions of bands are unknown prior to sampling. Blind sampling can be seen as a compressed sensing problem for multiple-measurement vectors (MMV) [6].

The method proposed by Feng and Bresler allows to directly reconstruct a continuous input signal without discretization. This approach avoids the negative discretization issues such as the need for block processing, windowing and spectrum leakage. The same idea was used in [5, 7]. However, the purpose of some applications, e.g. spectrum analyzers, is to evaluate the frequency spectrum rather than to reconstruct the continuous input signal in time domain. For these applications the discrete Fourier transform (DFT) of a sequence of the samples of an input signal is computed. Thereby, discretization is introduced. From this perspective it is interesting to investigate the quality of the
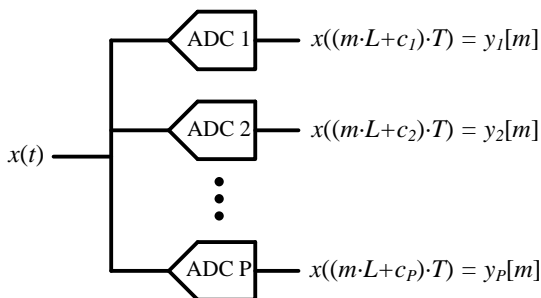
Fig. A.1: Multi-coset sampling scheme [2].

DFT evaluation when the traditional Nyquist-rate sampling is replaced by compressed sensing with the multi-coset scheme. i.e. the discrete multi-coset sampling. To date, such a discrete approach has not been considered. Throughout the paper, by signal reconstruction we mean the evaluation of the DFT of a sequence of samples. We wish to determine in which cases the multi-coset sampling can replace traditional Nyquist-rate sampling and extend the functionality of the existing sampling applications. For that purpose the performance of different reconstruction algorithms should be evaluated.

In multi-coset sampling the bandwidth of a single ADC should be higher than the bandwidth of the input signal. In [7] the modified multi-coset sampling scheme, named modulated-wideband converter, was presented. Modulated-wideband converter has a premixing stage before analog-to-digital conversions which allows using ADCs with a relatively low input bandwidth. The price for that is a more complicated front-end. However, an 80 channels time-interleaved ADC implemented as a single integrated circuit already exists [8]. The multi-coset scheme can be made from the time-interleaved scheme by simply removing some of the parallel channels. So, there are no technological obstacles in implementing multi-coset sampling.

In order to make one more step toward implementation of compressed sensing acquisition systems for real-life applications, we numerically investigate the quality of the DFT evaluation when the Nyquist-rate sampling is replaced by the sub-Nyquist multi-coset sampling. The objective is to investigate the relations between the number of sampling channels (an average sampling rate), the number of bands in signals, widths of bands, power of noise in signals on one side and reconstruction distortion on another. The reconstruction quality is evaluated by comparing the two DFT sequences. One is obtained with the Nyquist-rate sampling and is used as a reference. The second is obtained with the multi-coset sampling. We consider the following reconstruction algorithms: orthogonal matching pursuit for MMV (M-OMP) [9], multiple signal classification (MUSIC) [6], subspace-augmented MUSIC (SA-MUSIC) [10], basis pursuit denoising for MMV (M-BPDN) [11, 12] and focal underdetermined system solver for MMV (M-FOCUSS) [9]. To date these algorithms have not been compared in the ap-

plication of discrete multi-coset sampling. M-OMP and M-FOCUSS were described and compared in [9] but BPDN, MUSIC and SA-MUSIC were not considered. In [13] the authors proposed a new way of finding the solution to the MMV equation by solving a set of randomly formed singular-measurement vector problems. However, the success of this method depends on whether the number of random sub-problems is large enough. All the cases considered in [13] were noiseless and MUSIC-like algorithms were not considered.

The main contribution of this paper is that we formulate the discrete multi-coset approach and compare the performance of different reconstruction algorithms for the evaluation of the DFT. Our discrete multi-coset approach links together the unknown DFT of the sequence of samples of an input signal and the known DFTs of samples from sensing channels.

The outline is as follows. In Section II we review a multi-coset sampling scheme, describe discrete multi-coset sampling, test signals and performance measures. Algorithms that are used for the reconstruction are specified in Section III. In Section IV we present the complete simulation setup and the simulation results. Conclusions are stated in Section V.

2 Multi-coset scheme, test signals and performance measures

2.1 Multi-coset scheme

The main idea of the multi-coset scheme is to use multiple ADCs with a low sampling frequency rather than one that operates at a high frequency. As can be seen on Fig. A.1, a multi-coset scheme consists of P parallel sampling channels. The ADCs in these channels perform sampling of an input signal $x(t)$ at different moments of time specified by the set of time shifts $C = \{c_1, \ldots, c_P\}$, $c_p \in \{0, 1, \ldots, L - 1\}$, for channel $p = \{1, \ldots, P\}$. The positive integer L is called the multi-coset sampling period, $1 \leq P < L$. The combination of L and C denoted by (L, C) is called a multi-coset sampling pattern [6]. The time period $T = 1/(2 \cdot f_{\max})$ is the Nyquist sampling period and all the frequency components in an input signal are less than $f_{\max}$. In this paper we do not consider quantization effects.

Assume that $\mathcal{X}(f), f \in (-f_{\max}, f_{\max})$, is the unknown discrete-time Fourier transform of an input signal $x(t)$ (see Fig. A.2a). In the multi-coset scheme the relation between the input and the outputs is as follows [5, 6]:

$$\mathbf{y}(f) = \mathbf{A} \cdot \mathbf{x}(f) \tag{A.1}$$

$$\mathbf{y}(f) = [y_1(f), \ldots, y_P(f)]^{\mathrm{T}}, \ \mathbf{x}(f) = [x_1(f), \ldots, x_L(f)]^{\mathrm{T}}$$
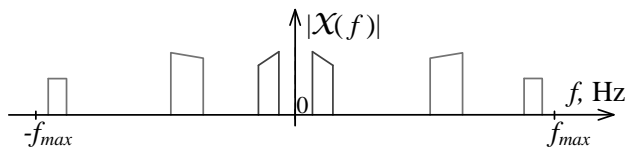
(a) Absolute values of the discrete-time Fourier transform of the three-band signal $x(t)$.

(b) Absolute values of the DFT coefficients of the three-band signal $x(t)$ sampled at the rate $1/T$, $\hat{f}$ denotes the discrete frequency.

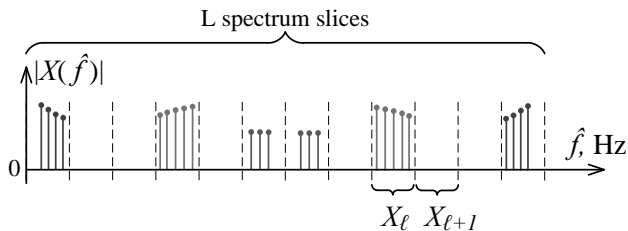**Fig. A.2:** Illustration of the Fourier transform and the discrete Fourier transform of the sequence of samples of the three-band signal $x(t)$.

$f \in F_0 = [0, \frac{1}{L \cdot T})$, $y_i(f) \in \mathbb{C}$ is the known discrete time Fourier transform of $y_i[m]$, $m \in \mathbb{Z}^+$, $x_\ell(f) = \mathcal{X}(f + \frac{\ell}{LT}) \in \mathbb{C}$ is the ℓth slice upon slicing $\mathcal{X}(f)$ into L equal-sized parts. The measurement matrix $\mathbf{A} \in \mathbb{C}^{P \times L}$ is given by:

$$A_{i,\ell} = \frac{1}{L \cdot T} \exp\left[j \frac{2\pi}{L} \cdot c_i \cdot (\ell - 1) \right]. \tag{A.2}$$

In (A.1) f is a continuous variable. Therefore this equation describes an infinite dimensional problem [6, 13]. In [2] the authors proposed a method that reduces the infinite dimensional problem to the finite dimensional MMV by computing the correlation matrix of the interpolated ADCs' output sequences. This allows to reconstruct the continuous input signal without discretization. However, there are practical applications where the DFT of the sequence of samples of an input signal is computed rather than the time-domain reconstruction, e.g. spectrum analyzers. From this perspective it is interesting to evaluate how the DFT of a multi-band frequency sparse signal can be estimated with the multi-coset sampling scheme. Denote by $X(\hat{f}) \in \mathbb{C}^K$ the DFT of the sequence of length K obtained by uniform sampling $x(t)$ with the sampling rate $1/T$. The discrete multi-coset problem can be formulated as follows:

$$\widehat{\mathbf{Y}} = \mathbf{A}\mathbf{X} \tag{A.3}$$

$$\widehat{\mathbf{Y}} = \begin{pmatrix} Y_1 \\ \vdots \\ Y_P \end{pmatrix} \circ \begin{pmatrix} \alpha_{1,1} & \dots & \alpha_{1,M} \\ \vdots & \ddots & \vdots \\ \alpha_{P,1} & \dots & \alpha_{P,M} \end{pmatrix}$$

$$\alpha_{p,m} = \exp\left[\frac{-2\pi j \cdot c_p \cdot (m-1)}{K}\right], \ p \in \{1, \dots, P\}, \ m \in \{1, \dots, M\}$$

$$\mathbf{X} = \begin{pmatrix} X_1 \\ \vdots \\ X_L \end{pmatrix} = \begin{pmatrix} X(1) & \dots & X(M) \\ \vdots & \ddots & \vdots \\ X((L-1)\cdot M + 1) & \dots & X(L \cdot M) \end{pmatrix}$$

where $\widehat{\mathbf{Y}} \in \mathbb{C}^{P \times M}$ and $\mathbf{X} \in \mathbb{C}^{L \times M}$, $\circ$ denotes Hadamard product (element-wise multiplication). $Y_P \in \mathbb{C}^M$ is the known DFT of the output sequence of the pth channel, i.e $Y_p = \mathcal{F}_{\text{DFT}}(y_p[1, 2, \dots, M])$, $\mathcal{F}_{\text{DFT}}$ denotes DFT. $X(j)$ is the jth element of $X(\hat{f})$. Then the matrix $\mathbf{X} \in \mathbb{C}^{L \times M}$ is formed by slicing and rearranging the unknown DFT transform $X(\hat{f})$, $X_\ell \in \mathbb{C}^L$ is the ℓth slice of $X(\hat{f})$ (see Fig. A.2b). We assume that the total number of the observed samples of $x(t)$ equals to $K = L \cdot M$. The coefficients $\alpha_{i,m}$ are introduced to compensate the time shift of the mth DFT bin in the pth sampling channel. The multi-coset sampling for discrete signals can be done in three steps:

1. Take M samples from each ADC;

2. Take DFTs of the obtained sequences;

3. Multiply each DFT bin by the corresponding time shift multiplier;

Equation (C.3) establishes the relation between the DFT transforms of the sequences of samples of an individual channel and the DFT transform of the input signal. This interpretation of the multi-coset sampling differs from the original idea that is to reconstruct a continuous input signal [2, 5, 6]. If $\mathbf{X}$ can be uniquely defined from (C.3) given $\widehat{\mathbf{Y}}$, the traditional Nyquist-rate sampling can be replaced by the sub-Nyquist multi-coset sampling in applications where DFT is needed. To our best knowledge, this discrete approach has not been used in the existing publications. Discretization introduces some undesirable features such as spectrum leakage, the need for block processing, windowing effects etc. At the same time, all these negative effects appears in the Nyquist-rate sampling as well.

Each column of the unknown matrix $\mathbf{X}$, a source vector, has the corresponding column of the known matrix $\widehat{\mathbf{Y}}$, the measurement vector. This is why (C.3) is named the multiple-measurement vectors problem [9]. The task of a reconstruction algorithm is to find the unknown $\mathbf{X}$ based on the known $\widehat{\mathbf{Y}}$ and $\mathbf{A}$. Recall that $P < L$. Therefore, in the general case of arbitrary $\mathbf{X}$ the system of linear equations (C.3) is under-determined, so it

does not have a unique solution. For the signal measurement application this means that the sampled signal can not be uniquely reconstructed. However, the rows $X_\ell \in \mathbb{C}^L$ of $\mathbf{X}$ are slices of the $X(\hat{f})$ (see Fig. A.2b). If $X(\hat{f})$ only has few non-zero bands, the matrix $\mathbf{X}$ only has few non-zero (whole or partly) rows. Under this assumption, blind multi-coset sampling for discrete multi-band signals becomes the compressed sensing problem. It was proven that a unique solution to (C.3) exists under certain conditions. Various theoretical aspects of compressed sensing, such as requirements for the measurement matrix, the necessary number of measurements, robustness to noise etc. are discussed in [14] and its references.

Denote by S a set of indices of non-zero rows of $\mathbf{X}$. This set is called the support of $\mathbf{X}$ and indicates the non-zero frequency slices. The matrix $\mathbf{X}_S$ is formed by selecting the rows of $\mathbf{X}$ with indices S and $\mathbf{A}^S$ is formed by selecting the columns of $\mathbf{A}$ with the same indices S. Then (C.3) is reduced to [5]:

$$\widehat{\mathbf{Y}} = \mathbf{A}^S \mathbf{X}_S \tag{A.4}$$

The properties of the matrix $\mathbf{A}^S$ affect the performance of the sampling system. The reconstruction fails if $\mathbf{A}^S$ does not have full column rank. In the presence of noise a high condition number of $\mathbf{A}^S$ will also lead to the reconstruction failure. It is of particular interest to select the sampling pattern (L, C) that yields a well-conditioned $\mathbf{A}^S$ for all possible variations of the support S. For our simulation we select the sampling pattern for each number of the sampling channels by searching over the all possible combinations and analysis of the condition numbers [6].

2.2   Test signals and performance measures

The level of frequency sparsity of a signal can be quantified by the spectral occupancy ratio Ω:

$$\Omega = \frac{\lambda(\mathrm{supp}\langle(X(\hat{f}))\rangle)}{\lambda([0, f_{\max}])}, \ \Omega \in [0, 1] \tag{A.5}$$

$\mathrm{supp}\langle\cdot\rangle$ is the support of $X(\hat{f})$, which is the set of frequency points where $X(\hat{f})$ is nonzero, $\lambda(\cdot)$ denotes the Lebesgue measure. In our case the Lebesgue measure is equal to the joint length of frequency bands. We assume that $X(\hat{f})$ does not contain noise when we calculate the value of Ω, so that broadband noise does not affect it. Denote by N the number of bands in a signal. Then Ω and N describe the structure of the signal (see Fig. A.3).

To evaluate the performance of the reconstruction algorithms we use multi-band test signals with different parameters. We vary occupancy ratio, number and positions of bands and power of noise in signals. Frequency bands are formed via $\mathrm{sinc}(\cdot)$ functions in the time domain and always centered at the middle of the frequency slices. Signals are
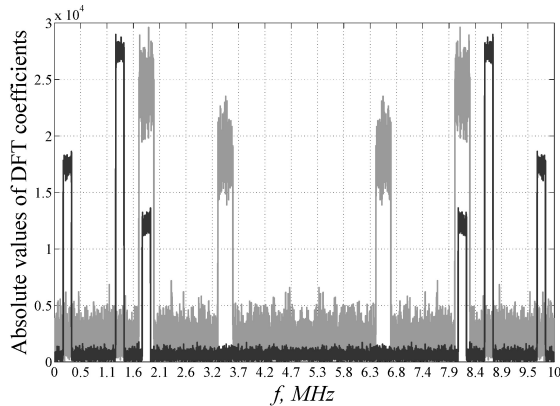
Fig. A.3: Illustration of the test signals. Black line – the signal with N=3, $\Omega = 0.1$, SNR = 20dB, grey line – the signal with N=2, $\Omega = 0.12$, SNR=10 dB, $f_{\max}$ =5 MHz. Test signals consist of $K = L \cdot M$ samples. Dashed lines show the positions of the frequency slices.

real-valued. We use the support reconstruction ratio as one of the performance measure:

$$R = \frac{\text{Number of correctly found support sets}}{\text{Number of test signals}}. \tag{A.6}$$

Support reconstruction ratio shows how well a reconstruction algorithm identifies the positions of bands in a signal.

As for the second performance measure we use *relative root mean square* (RRMS) value:

$$\text{RRMS} = \sqrt{\frac{\sum_{i=1}^{K}(\widehat{X}(i) - X(i))^2}{\sum_{i=1}^{K} X^2(i)}} \geq 0 \tag{A.7}$$

where $X(i)$ and $\widehat{X}(i)$ are original and estimated DFT coefficients of the test signal, $K = L \cdot M$ is the total number of DFT coefficients. In case of Nyquist-rate sampling RRMS is always equal to 0.

To simulate noisy environment we add white Gaussian noise to the test signals. The power of noise corresponds to the specified Signal-to-Noise Ratio (SNR) as illustrated in Fig. 3.

$$\text{SNR} = 10 \cdot \log_{10} \left(\frac{\text{P}_{\text{signal}}}{\text{P}_{\text{noise}}} \right) \tag{A.8}$$

where P_{signal} is power of a clean signal, P_{noise} is power of noise. Thus, we introduce noise folding:

$$\widehat{\mathbf{Y}}_N = \mathbf{A} \left(\mathbf{X} + \mathbf{N} \right) \tag{A.9}$$

where $\widehat{\mathbf{Y}}_N \in \mathbb{C}^{P \times M}$ is the matrix of measurements of a noisy signal and $\mathbf{N} \in \mathbb{C}^{L \times M}$ is the matrix that corresponds to broadband noise. Elements of $\mathbf{N} \in \mathbb{C}^{L \times M}$ are independent and identically distributed from the Gaussian distribution.

3 Reconstruction algorithms

We consider the following algorithms that are used in compressed sensing applications: 1) Orthogonal Matching Pursuit for MMV – M-OMP [9], 2) MUltiple Signal Classification – MUSIC [6], 3) Subspace Augmented-MUSIC [10], 4) FOCal Underdetermined System Solver for MMV – M-FOCUSS [9], 5) Basis Pursuit Denoising for MMV – M-BPDN [11, 12]. The MUSIC algorithm was used by Feng and Bresler in [2] when they proposed multi-coset blind sampling. SA-MUSIC is further development of MUSIC. The other three algorithms are used to solve general MMV problems. The detailed description of the reconstruction algorithms can be found in the corresponding references.

Algorithms 1–3 show the best performance when the number of non-zero rows of $\mathbf{X}$ is known prior to the reconstruction. Otherwise we have to estimate the number of non-zeros. However, the precision of this estimation is based on many factors: level of noise in a signal, width of bands in a signal, dynamic range of the input signal etc. In our simulation we assume that the number of non-zeros is known prior to the reconstruction, otherwise the performance of the reconstruction algorithm will be limited by the algorithm estimating this number.

In additional to the general regularized M-FOCUSS we implement a modification M-FOCUSS* that takes the number of non-zero rows of $\mathbf{X}$ as an input parameter and returns the indices of non-zero frequency slices. That allows to compare M-FOCUSS* to algorithms 1–3 in terms of the support reconstruction ratio.

We use our own implementations of the reconstruction algorithms except M-BPDN [11, 12]. Signal subspace estimation in SA-MUSIC is performed by thresholding eigenvalues. M-FOCUSS was implemented with Tikhonov regularization [9], the regularization parameter was picked empirically. The internal parameter of M-FOCUSS was set to 0.8 as it gives good tradeoffs between the sparsity of the solution and the convergence speed [9].

Signal reconstruction with M-OMP, MUSIC, SA-MUSIC and M-FOCUSS* is done in two steps. The first step is to find the frequency support S. Different algorithms do it in different ways. The second step is to solve the determined system (A.4). This step is the same for all these algorithms. So, the performance of M-OMP, MUSIC, SA-MUSIC and M-FOCUSS* can be compared in terms of the support reconstruction ratio R. M-FOCUSS and M-BPDN algorithms reconstruct a signal directly. Theirs performance is compared in terms of the RRMS values.

M-FOCUSS* and M-FOCUSS are initialized with the least square solution. For the algorithms $1, 2$ the correlation matrix $\mathbf{Q} = \widehat{\mathbf{Y}}_N \widehat{\mathbf{Y}}_N^H$ is computed. Algorithms 3–5 are

applied directly to (A.9).

4 Simulation

4.1 Simulation setup

For our simulations we use the multi-coset scheme with $L = 19$. Sampling patterns with a prime L yields to full column rank matrices $\mathbf{A}_S$ [5]. We vary the number of sampling channels from 1 to 19. Three types of sampling patterns are used: 1) optimal sampling patterns – patterns that are selected by exhaustive search for the lowest condition numbers, 2) random generated patterns, 3) bunched sampling patterns – $C = \{1, 2, \ldots, P\}$.

   We created signals with different parameters. For one set of parameters we create 1000 random signal instances. Variation of parameters: $N = \{1, 2, 3, 4\}$, $\Omega = \{0.05, 0.10, 0.15, 0.2\}$, SNR $= \{30, 16, 13, 10, 6\}$ dB. Positions of bands are picked randomly but always in the middle of frequency slices.

   This gives control over the support of $\mathbf{X}$. Amplitudes of bands are picked within the 20 dB dynamic range. All bands have the same width. Bands do not overlap. Test signals are stored in files. This allows to run simulations for different reconstruction algorithms independently. M-OMP, MUSIC, SA-MUSIC and M-FOCUSS* take the number of non-zero frequency slices as an input parameter. M-BPDN and M-FOCUSS run without any prior information about the signals. The algorithms are validated by sampling and reconstructing test signals without noise. The source code used for the simulation is available at http://www.sparsesampling.com/discretemulticoset.

4.2 Simulation results

Some of the simulation results are presented in Fig. 4–6. We do not include all the simulation results because of the limited paper space. However, the presented plots allow to make the correct conclusions as they preserve the tendency of behaviors of the reconstruction algorithms. Convergence analysis has shown the stability of the obtained data. For signals with a high SNR, MUSIC has the highest reconstruction rate (see Fig. A.4a) – reconstruction rate 1 is obtained with the 7 channels while other algorithms require more sampling channels. However, M-FOCUSS* outperforms the MUSIC algorithm in case of a low SNR. As can be seen in Fig. A.4b the reconstruction rate 1 for M-FOCUSS* is achieved with 10 sampling channel and for MUSIC with 12 channels. SA-MUSIC is a further development of MUSIC that overcomes some restrictions of the original algorithm. But on Fig. 4 we see that the performance of SA-MUSIC is lower than the performance of MUSIC. The reason for this is the thresholding approach for the estimation of the signal subspace in SA-MUSIC [10]. If the signal subspace is not correctly estimated then the whole reconstruction fails. The thresholding parameter should be picked for each set of signal's parameters.

The M-OMP algorithm has the lowest reconstruction rate. However, the reconstruction performance of OMP is less sensitive to SNR. Reconstruction rate 1 for signals with $N = 3$, $\Omega = 0.15$ and different SNR (30 dB and 10 dB) is achieved with the same number of the sampling channels (see Fig. A.4a and A.4b). In case of 1- and 2-band signals the reconstruction performance of other algorithms decrease to the M-OMP level when the signals have a low SNR (SNR$\leq$ 13 dB) (see Fig. A.4c). In this case, in order to have the reconstruction rate equal to 1 with M-OMP, MUSIC and M-FOCUSS* the multi-coset scheme should have 9 channels.

We compare the reconstruction rates for the sampling patterns of different types. Plots on Fig. 5 shows that the reconstruction rate for the random and bunched sampling patterns is lower than for the sampling patterns obtained by the analysis of the condition numbers. Moreover, as can be seen on Fig. A.5a the random sampling pattern for 12 sampling channels results in lower than expected reconstruction rate. This shows that relying on random selection of sampling patterns may lead to undesirable results.
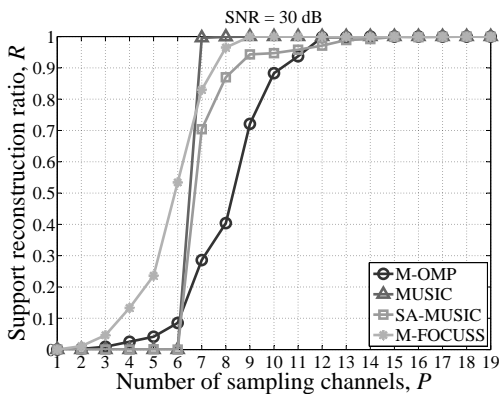
(a) $N = 3$, $\Omega = 0.15$, SNR=30 dB.
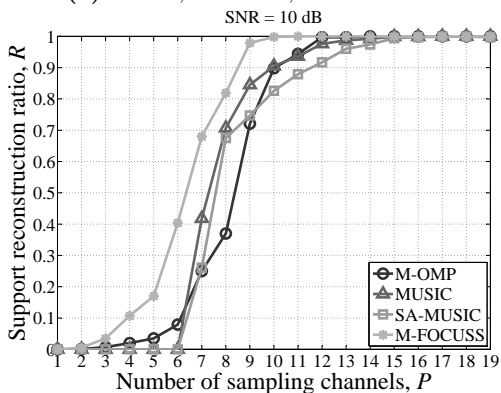
(b) $N = 3$, $\Omega = 0.15$, SNR=10 dB.
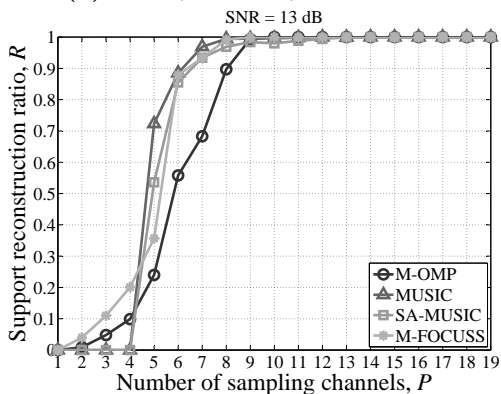
(c) $N = 2$, $\Omega = 0.10$, SNR=13 dB.

Fig. A.4: Empirical reconstruction rate with M-OMP, MUSIC, SA-MUSIC and M-FOCUSS* vs the no. of sampling channels. Optimal sampling patterns are used.
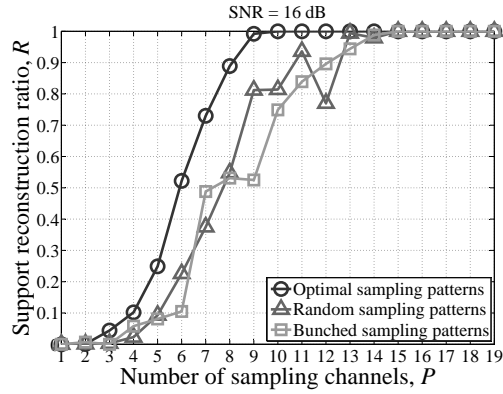
(a) M-OMP, $N = 2$, $\Omega = 0.10$, SNR=16 dB.
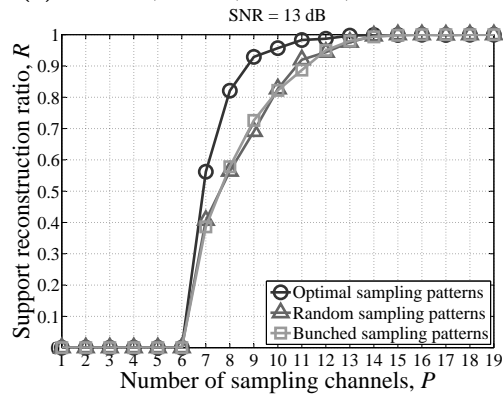
(b) MUSIC, $N = 3$, $\Omega = 0.15$, SNR=13 dB.

Fig. A.5: Empirical reconstruction rate with the selected algorithms for different types of the sampling patterns vs the no. of sampling channels.
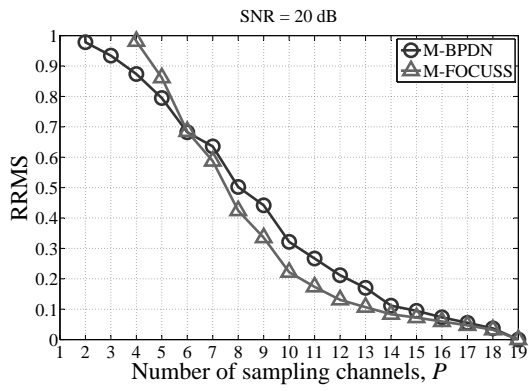
Fig. A.6: RRMS error with M-BPDN and M-FOCUSS vs the no. of sampling channels, $N = 4$, $\Omega = 0.16$, SNR=20 dB. Optimal sampling patterns are used.

Comparison of M-FOCUSS and M-BPDN is presented on Fig. A.6. Reconstruction with M-BPDN results in lower RRMS error when $P < 6$, but in this case RRMS ≥ 0.8. This is a high reconstruction error that makes useless the reconstructed signal because it significantly differs from the input signal. Although the exact value of the acceptable RRMS error is defined by the specific application, we may assume that we are aiming to get RRMS not higher that 0.5. From this perspective M-FOCUSS has better reconstruction performance for all the test signals considered in this research.

5   Conclusions

This paper investigates the performance of commonly used reconstruction algorithms in discrete blind multi-coset sampling. Discrete multi-coset sampling can replace Nyquist-rate sampling in applications with frequency sparse signals.

Simulation results show that use of optimal sampling patterns results in the best reconstruction performance. Bunched and random sampling patterns may lead to the undesirable decrease of the reconstruction performance.

When the number of non-zero slices is known prior to reconstruction, the modification of M-FOCUSS outperforms all other algorithms except for the low noise signals. In that case MUSIC is more beneficial. In order to use SA-MUSIC with the thresholding for the subspace estimation, the thresholding parameter should be picked for each type of a signal (number of bands, dynamic range, level of noise etc). M-OMP is a simple algorithm that can be successfully applied in case of signals with the small number of bands even with relatively high level of noise.

M-FOCUSS and M-BPDN can be used when the number of non-zero slices of the DFT of the sequence of the samples of an input signal is not known prior to the reconstruction. In this case the M-FOCUSS algorithm also shows better performance.

References

[1] H. Landau, "Necessary density conditions for sampling and interpolation of certain entire functions," *Acta Mathematica*, vol. 117, pp. 37–52, 1967.

[2] P. Feng and Y. Bresler, "Spectrum-blind minimum-rate sampling and reconstruction of multiband signals," in *IEEE International Conference on Acoustics, Speech, and Signal Processing*, vol. 3, May 1996, pp. 1688–1691.

[3] P. Vaidyanathan and V. Liu, "Efficient reconstruction of band-limited sequences from nonuniformly decimated versions by use of polyphase filter banks," *IEEE Transactions on Acoustics, Speech and Signal Processing*, vol. 38, no. 11, pp. 1927–1936, 1990.

[4] R. Vaughan, N. Scott, and D. White, "The theory of bandpass sampling," *IEEE Trans. Signal Process.*, vol. 39, no. 9, pp. 1973–1984, Sep. 1991.

[5] M. Mishali and Y. C. Eldar, "Blind multiband signal reconstruction: Compressed sensing for analog signals," *IEEE Trans. Signal Process.*, vol. 57, no. 3, pp. 993–1009, 2009.

[6] Y. Bresler, "Spectrum-blind sampling and compressive sensing for continuous-index signals," in *Information Theory and Applications Workshop*, Jan. 27 2008-Feb. 1 2008, pp. 547–554.

[7] M. Mishali, Y. Eldar, O. Dounaevsky, and E. Shoshan, "Xampling: Analog to digital at sub-Nyquist rates," *IET Circuits, Devices and Systems*, vol. 5, no. 1, pp. 8–20, Jan. 2011.

[8] K. Poulton, R. Neff, B. Setterberg, B. Wuppermann, T. Kopley, R. Jewett, J. Pernillo, C. Tan, and A. Montijo, "A 20 GS/s 8 b ADC with a 1 MB memory in 0.18 μm CMOS," in *IEEE International Solid-State Circuits Conference, ISSCC-2003. Digest of Technical Papers.*, vol. 1, Feb. 2003, pp. 318–496.

[9] S. Cotter, B. Rao, K. Engan, and K. Kreutz-Delgado, "Sparse solutions to linear inverse problems with multiple measurement vectors," *IEEE Trans. Signal Process.*, vol. 53, no. 7, pp. 2477–2488, Jul. 2005.

[10] K. Lee and Y. Bresler, "Subspace-augmented music for joint sparse recovery with any rank," in *IEEE Sensor Array and Multichannel Signal Processing Workshop (SAM), 2010*, Oct. 2010, pp. 205–208.

[11] E. van den Berg and M. P. Friedlander, "SPGL1: A solver for large-scale sparse reconstruction," June 2007, http://www.cs.ubc.ca/labs/scl/spgl1.

[12] ——, "Probing the Pareto frontier for basis pursuit solutions," *SIAM Journal on Scientific Computing*, vol. 31, no. 2, pp. 890–912, 2008.

[13] M. Mishali and Y. Eldar, "Reduce and boost: Recovering arbitrary sets of jointly sparse vectors," *IEEE Transactions on Signal Processing*, vol. 56, no. 10, pp. 4692–4702, Oct. 2008.

[14] E. J. Candès and M. B. Wakin, "An introduction to compressive sampling," *IEEE Signal Process. Mag.*, vol. 25, no. 2, pp. 21–30, Mar. 2008.

Paper B

Reducing the Computational Complexity of Reconstruction in Compressed Sensing Nonuniform Sampling

Ruben Grigoryan, Tobias Lindstrøm Jensen, Thomas Arildsen and Torben Larsen

Abstract

This paper proposes a method that reduces the computational complexity of signal reconstruction in single-channel nonuniform sampling while acquiring frequency sparse multi-band signals. Generally, this compressed sensing based signal acquisition allows a decrease in the sampling rate of frequency sparse signals, but requires computationally expensive reconstruction algorithms. This can be an obstacle for real-time applications. The reduction of complexity is achieved by applying a multi-coset sampling procedure. This proposed method reduces the size of the dictionary matrix, the size of the measurement matrix and the number of iterations of the reconstruction algorithm in comparison to the direct single-channel approach. We consider an orthogonal matching pursuit reconstruction algorithm for single-channel sampling and its modification for multi-coset sampling. Theoretical as well as numerical analyses demonstrate order of magnitude reduction in execution time for typical problem sizes without degradation of the signal reconstruction quality.

1   Introduction

Signals generally must be sampled at the Nyquist rate, otherwise aliasing will prevent correct reconstruction of the signal. However, if we narrow the scope of signals to frequency sparse signals, we can successfully apply sub-Nyquist rate sampling [1, 2]. This type of signal acquisition assumes that the number of the obtained samples (measurements) is lower than the number of Nyquist rate samples. Frequency sparsity implies that the energy of a signal is concentrated in small joint or disjoint parts (i.e. bands or individual tones) of the spectrum. If sub-Nyquist rate sampling is possible, then cheaper analog front ends may be used, or signal acquisition can be accelerated. Sub-Nyquist sampling has evolved from bandpass sampling to various compressed sensing (CS) architectures such as the random demodulator [3], the nonuniform sampler [**?**], the multi-coset sampler [2, 4, 5] and the modulated wideband converter [6].

The key idea of CS is to use advanced reconstruction procedures to compensate for the lack of measurements. In the language of linear algebra, the process of the CS signal reconstruction is the process of solving an under-determined linear system with fewer equations than unknowns. The concept of sparsity is used to establish the rules under which a unique signal reconstruction is possible [7]. By contrast to CS, traditional Nyquist rate sampling corresponds to a system with the isometric matrix that can be easily solved.

An obstacle for real-time CS applications is the high complexity of reconstruction [**?**]. Therefore, it is important to find ways to reduce the computational costs of signal recovery. There are two main groups of reconstruction algorithms [8]: 1) greedy algorithms which find the dominant components of the solution; and 2) relaxation methods which

solve convex (such as ℓ_1-minimization) and non-convex problems.

In this paper, we propose a method that reduces computational complexity of signal reconstruction in single-channel nonuniform sampling (SC-NUS). SC-NUS is one of the CS approaches that can be used for acquisition of frequency sparse signals. SC-NUS selects samples from a Nyquist grid and uses them to recover the whole Discrete Fourier Transform (DFT) of the Nyquist rate samples. Frequency sparse signals that can be acquired with SC-NUS may have both individual tones and bands. However, in some applications such as telecommunications, the energy of a signal is concentrated in a small number of bands rather than in a large number of independent tones. In this case, a multi-coset sampler (MCS) architecture is beneficial [2, 4, 5]. MCS also selects samples from a Nyquist grid, but does it periodically. Assume that a real-valued multi-band signal has to be sensed with SC-NUS with the predefined undersampling ratio. That can be done in two ways: 1) in the direct SC-NUS manner; and 2) in the MCS manner. We show that the computational complexity of the signal reconstruction in MCS is lower than in direct SC-NUS. This reduction of complexity is the result of two factors. First, the size of the measurement and the dictionary matrices in MCS is smaller than the size of the corresponding matrices in SC-NUS. Secondly, the number of iterations performed by the reconstruction algorithms in MCS is lower than the number of iterations in SC-NUS reconstruction. On the whole, we reduce the number of arithmetical operations that are performed at the reconstruction stage. Numerical simulations show that this reduction of computational complexity does not decrease the reconstruction quality. In this paper, we consider the Orthogonal Matching Pursuit (OMP) algorithm for SC-NUS and its modification for MCS. A noise free scenario is assumed for simplicity, but the method can also be applied to the noisy case.

A related method is presented in [**?**], where the authors propose to jointly reconstruct a set of sequentially sampled signals. However, this method works well only if the positions of tones and bands do not change significantly. In [9], the authors pointed out that reconstruction in the modulated wideband converter requires fewer FLoating-point OPerations (FLOP) than reconstruction in the random demodulator. Our proposed method extends this observation.

The outline of the paper is as follows. In Section 2, we describe single-channel nonuniform and multi-coset sampling, and present the main idea of the paper. Analytical and simulation results are shown in Section 3. We conclude the paper in Section 4.

2   Sampling Schemes

2.1   Single-channel nonuniform sampling

SC-NUS acquires only some of the Nyquist rate samples. In the reconstruction procedure, these measurements are used to recover the DFT of samples as they would be acquired at the full Nyquist rate. Therefore, we decrease the average sampling rate be-
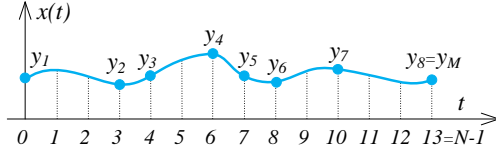
(a) Direct single-channel nonuniform sampling, the SC-NUS pattern $\Lambda = \{0, 3, 4, 6, 7, 8, 10, 13\}$.

(b) Multi-coset sampling, the MCS period $L = 7$, the number of MCS periods $W = 2$, the number of sampling channels $P = 4$, the MCS pattern $\Lambda = \{0, 1, 4, 6\}$.

Fig. B.1: Illustration of SC-NUS and MCS, the Nyquist grid is marked with the dotted lines.

low the Nyquist rate. The process of sampling is illustrated in Fig. B.1a. In total, there are $N = 14$ Nyquist rate samples, and only $M = 8$ of them are acquired by SC-NUS. The so-calle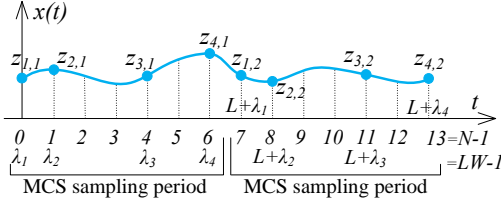d sampling pattern Λ defines which samples are obtained. In SC-NUS, the relation between the measurements and the unknown DFT is

$$\mathbf{y} = \mathbf{A} \cdot \mathbf{x} = \mathbf{D} \cdot \mathbf{F}_N \cdot \mathbf{x}; \tag{B.1}$$

where $\mathbf{y} \in \mathbb{R}^{M \times 1}$ is a vector of the acquired samples, $\mathbf{D} \in \mathbb{Z}^{M \times N}$ is the decimation (measurement) matrix that corresponds to the sampling pattern, $\mathbf{F}_N \in \mathbb{C}^{N \times N}$ is the DFT (dictionary) matrix of order N, and $\mathbf{x} \in \mathbb{C}^{N \times 1}$ is the unknown DFT of the Nyquist rate samples. The vector $\mathbf{x}$ is assumed to be sparse with $K_1 < M$ non-zero elements. The support S is the set of indices of these non-zero elements.

The OMP algorithm [8] can be used to recover the unknown input signal in SC-NUS. A reconstruction with OMP is performed in two steps: 1) OMP finds the support S of $\mathbf{x}$ (see Algorithm 1); 2) the actual values of $\mathbf{x}$ in the support are obtained with the least squares method applied to $\mathbf{y} \approx \mathbf{A}^S \cdot \mathbf{x}_S$. The symbol S in the superscript and in the subscript denotes the column and the row restriction of the matrix and the vector, respectively. In Algorithm 1, we utilize the fact that real-valued signals have conjugate-symmetric DFT [5].

2.2   Multi-coset sampling

MCS also selects the Nyquist rate samples but does it periodically [2, 4, 5]. The principle behind MCS is to use several parallel uniform samplers. These samplers acquire signal's values at the same rate but with different time offsets. The offsets are defined by the MCS pattern $\Lambda = \{\lambda_1, \ldots, \lambda_P\} \subset \{0, 1, \ldots, L-1\}\}$. MCS can be seen as a time-interleaved sampler with P out of L channels. Accordingly, only P samples are selected from every bunch of L consecutive Nyquist-rate samples. L is called the MCS period. The process of MCS is illustrated in Fig. C.3b where $W = 2$ MCS periods are shown. Denote by $z_{p,w} \in \mathbb{R}$, $p \in \{1, 2, \ldots, P\}, w \in \{1, 2, \ldots, W\}$ the wth output sample of the pth sampling channel. In discrete MCS, the relation between the measurements and the unknown DFT is described with the following equation [2, 4, 5]:

$$\mathbf{Y} = \mathbf{B} \cdot \mathbf{X} \tag{B.2}$$

where $\mathbf{Y} \in \mathbb{C}^{P \times W}$ is the known measurements,

$$\mathbf{Y} = \begin{pmatrix} \mathcal{F}_W([z_{1,1} \cdots z_{1,W}]^{\mathrm{T}}) \\ \vdots \\ \mathcal{F}_W([z_{P,1} \cdots z_{P,W}]^{\mathrm{T}}) \end{pmatrix} \circ \begin{pmatrix} \delta_{1,1} & \ldots & \delta_{1,W} \\ \vdots & \ddots & \vdots \\ \delta_{P,1} & \ldots & \delta_{P,W} \end{pmatrix} \tag{B.3}$$

$$\delta_{p,w} = \exp\left[\frac{-2\pi j \cdot \lambda_p \cdot (w-1)}{LW}\right], \tag{B.4}$$

the matrix $\mathbf{B} \in \mathbb{C}^{P \times L}$ is the known matrix that comprises both the measurement and the dictionary matrices. The elements of $\mathbf{B}$ are given by:

$$B_{p,\ell} = \frac{1}{L \cdot T} \exp\left[j\frac{2\pi}{L} \cdot \lambda_p \cdot (\ell - 1)\right] \tag{B.5}$$

and $\mathbf{X} \in \mathbb{C}^{L \times W}$ represents the unknown input signal, $p \in \{1, 2, \ldots, P\}$, $w \in \{1, 2, \ldots, W\}$, $\ell \in \{1, 2, \ldots, L\}$. The matrix $\mathbf{X}$ is assumed to be sparse with $K_2 < P$ non-zero rows. In (C.4), $\mathcal{F}_W([z_{p,1} \cdots z_{p,W}]^{\mathrm{T}})$ is DFT of the samples obtained from the pth sampling channel, $\circ$ denotes the Hadamard product and $\delta_{p,w}$ represents the delay of the wth DFT bin in the pth sampling channel. The Nyquist sampling period T depends on the highest frequency component in the input signal. In total, the duration of the observed signal equals to LWT. Consider the matrix $\mathbf{X}$. If the unknown DFT of the input signal is sliced into L equal parts, then each row of $\mathbf{X}$ is one of these consecutive slices [2, 4, 5]. Signals with a few bands in the spectrum may result in a highly sparse $\mathbf{X}$.

Reconstruction with a greedy method for MCS is similar to the reconstruction for SC-NUS. We use the M-OMP algorithm that is the modification of OMP for multiple-measurement vectors problem [10]. M-OMP finds the support S, the indices of non-zero rows, of $\mathbf{X}$ (see Algorithm 2). Knowing the support, we can reconstruct the unknown signal with the least squares method similar to the SC-NUS case.

Algorithm 1 Find the support S of $\mathbf{x}$ with OMP [8]

Input: $\mathbf{y} \in \mathbb{R}^{M \times 1}, \mathbf{A} \in \mathbb{C}^{M \times N}, K_1 \in \mathbb{N}_1$
Output: $S \in \mathbb{N}_1^{K_1}$
1: $S \leftarrow \emptyset, \mathbf{r} \leftarrow \mathbf{y}, k \leftarrow 0$
2: **for** $k = 1$ to $\lceil K_1/2 \rceil$ **do**
3:     $i_{\max} \leftarrow \operatorname{argmax}_{i \in \{1,\ldots,N\} \setminus S} \langle \mathbf{a}_i^*, \mathbf{r} \rangle$
4:     $i_{\mathrm{sym}} \leftarrow N - i_{\max} + 1$
5:     $S \leftarrow S \cup \{i_{\max}, i_{\mathrm{sym}}\}$
6:     $\mathbf{Q} \leftarrow \text{Gram-Schmidt}(\mathbf{A}^S)$
7:     $\mathbf{r} \leftarrow \mathbf{r} - \mathbf{Q} \cdot \mathbf{Q}^* \cdot \mathbf{r}$
8: **end for**

2.3   Multi-coset reconstruction in single-channel nonuniform sampling

Consider the sampling scenario where SC-NUS acquires multi-band signals. This can be done in two ways: 1) by the direct single-channel sampling that is described by (B.1); and 2) SC-NUS can select samples from the Nyquist grid in the same way as MCS. Therefore, SC-NUS can emulate MCS. In this case, the reconstruction problem (B.1) is replaced by (C.3).

The notable thing is that the reconstruction in MCS has lower computational complexity than the reconstruction in the direct SC-NUS. This reduction of the complexity is the result of two factors:

(1) in MCS, measurement and dictionary matrices are smaller than the corresponding matrices in SC-NUS; in other words, $\mathbf{A} \in \mathbb{C}^{M \times N}$ is replaced by $\mathbf{B} \in \mathbb{C}^{P \times L}$ where $P \ll M$ and $N \ll L$.

(2) in MCS reconstruction, the number of iterations performed by the reconstruction algorithm is lower than the number of iterations in the SC-NUS reconstruction. This happens due to the fact that usually $K_2 \ll K_1$.

The drawback of the proposed method is a decrease in the frequency support resolution. SC-NUS can reconstruct an individual DFT bin, whereas MCS can reconstruct only the whole frequency slice. This trade-off between the support resolution and the reconstruction complexity is out of the scope of the current paper and will be considered in our future research.

2.4   Complexity analysis

By computational complexity of a procedure we assume the number of FLOPs performed in this procedure, and by one FLOP we assume an arithmetic operation per-

---

Algorithm 2 Find the support S of $\mathbf{X}$ with M-OMP [10]

Input: $\mathbf{Y} \in \mathbb{C}^{P \times W}, \mathbf{B} \in \mathbb{C}^{P \times L}, K_2 \in \mathbb{N}_1$
Output: $S \in \mathbb{N}_1^{K_2}$
 1: $S \leftarrow \emptyset$, $\mathbf{R} \leftarrow \mathbf{Y}$, $k \leftarrow 0$
 2: **for** $k = 1$ to $\lceil K_2/2 \rceil$ **do**
 3:    $i_{\max} \leftarrow \operatorname{argmax}_{i \in \{1,\dots,L\} \setminus S} \|\mathbf{b}_i^* \cdot \mathbf{R}\|_2^2$
 4:    $i_{\text{sym}} \leftarrow L - i_{\max} + 1$
 5:    $S \leftarrow S \cup \{i_{\max}, i_{\text{sym}}\}$
 6:    $\mathbf{Q} \leftarrow \text{Gram-Schmidt}(\mathbf{B}^S)$
 7:    $\mathbf{R} \leftarrow \mathbf{R} - \mathbf{Q} \cdot \mathbf{Q}^* \cdot \mathbf{R}$
 8: **end for**

---

formed on two real floating-point numbers. Then, the complexity of the reconstruction in SC-NUS is

$$C^{\text{SC-NUS}} = C^{\text{SC-NUS}}_{\text{OMP}} + C^{\text{SC-NUS}}_{\text{Least Squares}}, \tag{B.6}$$

and the complexity of the MCS reconstruction is described with

$$C^{\text{MCS}} = C^{\text{MCS}}_{(3)} + C^{\text{MCS}}_{\text{M-OMP}} + C^{\text{MCS}}_{\text{Least Squares}}, \tag{B.7}$$

where $C^{\text{MCS}}_{(3)}$ denotes the complexity of the calculations (C.4). Assume that we use SC-NUS and MCS to recover the DFT of the Nyquist rate samples of a multi-band signal. The number of the samples is equal to $N = LW$ with $W \in \mathbb{N}_1$, SC-NUS and MCS are used with the same undersampling ratio $M/N = PW/(MW) = P/L$ and the frequency bands in a signal are aligned with the MCS frequency slices. We say that a band is aligned with a frequency slice if it occupies the whole slice (see Fig. B.2). One MCS slice comprises W DFT bins. If F is the number of bands in the signal, then the number of non-zero elements of $\mathbf{x}$ in (B.1) is equal to $K_1 = 2FW$, where the factor 2 appears due to the symmetry of DFT. At the same time, F bands result only in $K_2 = 2F$ non-zero rows of the matrix $\mathbf{X}$ in (C.3). Knowing the values of M, N, P, L, W, K_1 and K_2, we can compute the complexity of the reconstruction in SC-NUS and MCS. For example, consider the complexity of the stage 3 in Algorithm 1 and Algorithm 2. For OMP, this number is

$$\begin{aligned} C^{\text{OMP}}_{\text{Stage 3}} &\simeq (8M - 2) \sum_{i=1}^{K_1/2} (N - 2(i - 1)) \\ &\simeq 8PF(L - F + 1/W)W^3, \end{aligned} \tag{B.8}$$

and for M-OMP

$$C_{\text{Stage 3}}^{\text{M-OMP}} \simeq (8PW - 2) \sum_{i=1}^{K_2/2} (L - 2(i - 1))$$

$$\simeq 8PF(L - F + 1)W, \tag{B.9}$$

The ratio between these two numbers is

$$C_{\text{Stage 3}}^{\text{OMP}} / C_{\text{Stage 3}}^{\text{M-OMP}} \simeq W^2, \tag{B.10}$$

K_1 and K_2 are even due to the fact that we consider real-valued signals. So, for this stage, the reduction in complexity is the quadratic function of the number W. In MCS, the additional computations (C.4) have to be made prior to reconstruction. However, they have only $O(W \log(W))$ cost. On the whole, the direct counting shows that the MCS reconstruction requires fewer arithmetic operations than the SC-NUS reconstruction (see Section 3). This counting done using the code that computes the complexity according to (B.6) and (B.7). The parts of the code that calculate the costs of the standard operations, such as a matrix multiplication, a QR factorization and a backward substitution, are validated by comparison with the theoretical complexity available in the literature. The least squares solutions are obtained via QR factorization.

In (B.10), we assume that SC-NUS and MCS operates with the same undersampling ratio $M/N = P/L$. That is, we assume that the same sampling ratio results in the same reconstruction quality for both MCS and SC-NUS. We check this assumption with the numerical simulations.

3   Numerical Simulations

The two analyzed signal acquisition methods were implemented and benchmarked in MATLAB.[1] In order to have a well defined number of arithmetic operations, a standard and naïve implementation of QR factorization and a least squares solver have been made [11]. Benchmarking is performed to make an overall numerical evaluation of the potential reconstruction speed-up in MCS compared to the direct SC-NUS.

3.1   Simulation setup

We consider simulation scenarios with multi-band frequency sparse signals. The signals are noise-free, real valued and generated in the time domain as N samples such that $N = LW$. The highest frequency component of a signal does not exceed f_{max}. All bands in a signal have the same bandwidth, B. The average sampling rate f_{samp} is varied from

---

[1]The source code is available online at http://www.sparsesampling.com/discretemulticoset/.
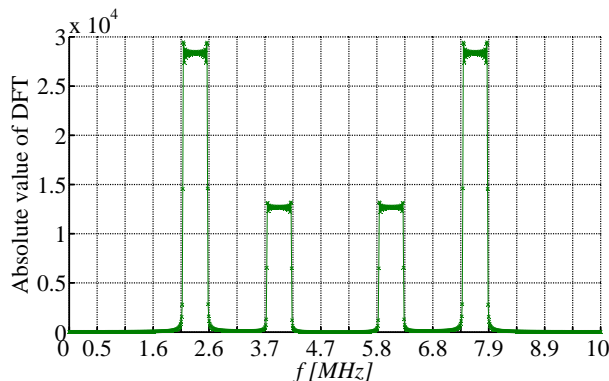
Fig. B.2: Absolute DFT values versus frequency for an illustrative test signal with $F = 2$, $L = 19$, $N = 494$, $K_1 = 104$ and $K_2 = 4$. The vertical grid lines correspond to the MCS frequency slices.

$2f_{\max}/L$ to the Nyquist rate $f_{\mathrm{Nyq}} = 2f_{\max}$ in steps of $2f_{\max}/L$. This shows how the reconstruction quality depends on the sampling rate. The reconstruction quality of one test signal is measured with the relative root mean squared error:

$$E = \begin{cases} \sqrt{\|\widehat{\mathbf{x}} - \mathbf{x}\|_2^2/\|\mathbf{x}\|_2^2}, & \sqrt{\|\widehat{\mathbf{x}} - \mathbf{x}\|_2^2/\|\mathbf{x}\|_2^2} < 1 \\ 1, & \text{otherwise} \end{cases} \qquad (B.11)$$

where $\mathbf{x}$ and $\widehat{\mathbf{x}}$ denote the original and recovered DFT coefficients, respectively. It is useless to consider the values of E greater than 1. Due to the possible spectrum leakage effect, the vector $\mathbf{x}$ is not completely sparse but rather compressible. Therefore, we cannot necessarily expect the error E to converge to zero in our simulations. An example of a test signal with $F = 2$ bands is illustrated in Fig. B.2. The maximum frequency component is less than $f_{\max} = 5$ MHz and the Nyquist rate is $f_{\mathrm{Nyq}} = 10$ MHz. The duration of the signal corresponds to $N = 494$ Nyquist rate samples which is 49.4μs. The bands are placed randomly but always in the centers of the frequency slices. We choose L to be a prime number according to [8]; we use $L = 19$. The width of a frequency slice is thus $2f_{\max}/L \simeq 526$ kHz. The bandwidth of the individual bands of a test signal is set to $B = 486$ kHz. Such a bandwidth together with the spectrum leakage effect results in full occupation of the spectrum slice. The power of the individual bands are picked randomly over a dynamic range of 20 dB. It is assumed that the numbers K_1 and K_2 in Algorithm 1 and Algorithm 2 are known prior to the reconstruction of every signal. Otherwise, the performance of OMP and M-OMP are limited by methods chosen to evaluate the number of non-zero elements in the solution. This can distort the assessment. Simulations were performed for $F = \{1, \ldots, 6\}$ bands in the test signals. For every number of bands, we generate 1000 signal instances which was shown to ensure
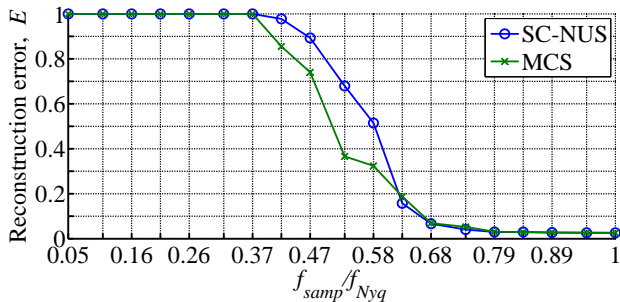
Fig. B.3: Simulated average reconstruction error in SC-NUS and MCS versus average sampling rate. The number of bands is $F = 4$.

convergence of the results.

Selection of proper sampling patterns is itself a nontrivial problem. However, in case of noise free signals random sampling patterns work well for both SC-NUS and MCS [5]. The benchmarks were performed on a computer with an Intel X5670 2.93 GHz CPU running MATLAB R2012a.

3.2   Reconstruction speed-up

As can be seen in Fig. B.3, the proper reconstruction quality is achieved with the same sampling rate for both SC-NUS and MCS. By the proper quality, we mean the error-floor value of E resulting from spectrum leakage which does not depend on the sampling rate. This holds true for all F and ensures that the replacing SC-NUS by MCS does not degrade the recovery quality.

The theoretical and the benchmarked reconstruction speed-up are presented in Fig. B.4. The benchmarked speed-up is the average value of the ratio of the benchmarked signal recovery time in SC-NUS to that in MCS. The theoretical speed-up is the ratio $C^{\text{SC-NUS}}/C^{\text{MCS}}$. As can be seen from the figure, the benchmarked speed-up is $4 - 7$ times lower than the theoretical speed-up. This can be explained by the fact that in the theoretical analysis, we disregard some practical issues such as the memory organization, the processor architecture and the cost of the auxiliary operations. Nevertheless, we do see the same behaviour of the theoretical and benchmark speed-up.

4   Conclusions

This paper proposed a method that decreases the computational complexity of the reconstruction procedure in compressed sensing single-channel nonuniform sampling. We consider sampling of multi-band real-valued signals in noise free environment. The
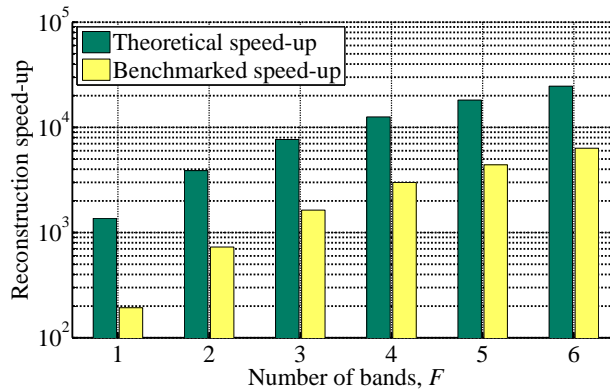
Fig. B.4: Theoretical and benchmarked reconstruction speed-up versus number of bands, F.

core idea of the proposed method is to use the multi-coset sampling approach. The drawback of the proposed method is the reduced frequency support resolution which may be acceptable in many applications. Depending on the number of bands in a signal, the number of arithmetic operations in the signal reconstruction stage is observed to decrease by the orders of magnitudes of 10^3 to 10^4. In addition, the proposed method does not degrade the reconstruction quality in the tested cases.

References

[1] R. Vaughan, N. Scott, and D. White, "The theory of bandpass sampling," *IEEE Trans. Signal Process.*, vol. 39, no. 9, pp. 1973–1984, Sep. 1991.

[2] P. Feng and Y. Bresler, "Spectrum-blind minimum-rate sampling and reconstruction of multiband signals," in *IEEE International Conference on Acoustics, Speech, and Signal Processing*, vol. 3, May 1996, pp. 1688–1691.

[3] J. Tropp, J. Laska, M. Duarte, J. Romberg, and R. Baraniuk, "Beyond Nyquist: Efficient sampling of sparse bandlimited signals," *IEEE Trans. Inf. Theory*, vol. 56, no. 1, pp. 520–544, Jan. 2010.

[4] Y. Bresler, "Spectrum-blind sampling and compressive sensing for continuous-index signals," in *Information Theory and Applications Workshop*, Jan. 27 2008-Feb. 1 2008, pp. 547–554.

[5] M. Mishali and Y. C. Eldar, "Blind multiband signal reconstruction: Compressed sensing for analog signals," *IEEE Trans. Signal Process.*, vol. 57, no. 3, pp. 993–1009, 2009.

[6] M. Mishali, Y. Eldar, O. Dounaevsky, and E. Shoshan, "Xampling: Analog to digital at sub-Nyquist rates," *IET Circuits, Devices and Systems*, vol. 5, no. 1, pp. 8–20, Jan. 2011.

[7] E. J. Candès and M. B. Wakin, "An introduction to compressive sampling," *IEEE Signal Process. Mag.*, vol. 25, no. 2, pp. 21–30, Mar. 2008.

[8] M. Elad, *Sparse and Redundant Representations: From Theory to Applications in Signal and Image Processing*. Springer, 2010.

[9] M. Mishali, Y. Eldar, and A. Elron, "Xampling: Signal acquisition and processing in union of subspaces," *IEEE Trans. Signal Process.*, vol. 59, no. 10, pp. 4719 –4734, Oct. 2011.

[10] S. Cotter, B. Rao, K. Engan, and K. Kreutz-Delgado, "Sparse solutions to linear inverse problems with multiple measurement vectors," *IEEE Trans. Signal Process.*, vol. 53, no. 7, pp. 2477–2488, Jul. 2005.

[11] L. Trefethen and D. Bau, *Numerical Linear Algebra*. Philadelphia: Society for Industrial and Applied Mathematics, 1997.

Paper C

Computational Complexity Reduction in Nonuniform
Compressed Sensing by Multi-Coset Emulation

Ruben Grigoryan, Tobias Lindstrøm Jensen and Torben Larsen

The layout has been revised.

Abstract

Single-channel Nonuniform Sampling (SNS) is a Compressed Sensing (CS) approach that allows sub-Nyquist sampling of frequency sparse signals. The relatively simple architecture, comprising one wide-band sampling channel, makes it an attractive solution for applications such as signal analyzers and telecommunications. However, a high computational cost of the SNS signal reconstruction is an obstacle for real-time applications. This paper proposes to emulate Multi-Coset Sampling (MCS) in SNS acquisition as a means to decrease the computational costs. Such an emulation introduces performance-complexity tradeoffs due to the difference of the SNS and MCS models. We investigate these tradeoffs with numerical simulations and theoretical assessments of the reconstruction complexity in multi-band signals scenarios. These scenarios include different numbers, different widths and positions of the frequency bands and different levels of noise in the signals. For the SNS reconstruction, we consider the accelerated iterative hard thresholding algorithm; for the MCS reconstruction, the multiple signal classification and focal underdetermined system solver algorithms are used. The proposed emulation reduces the computational complexity up to an order of magnitude. For one of the scenarios, the reconstruction quality slightly decreases. For the other scenarios, the reconstruction quality is ether preserved or improved.

1 Introduction

The Nyquist sampling rate is a sufficient but not a necessary condition for an acquisition of sparse signals (see Fig. C.1a) [1, 2]. These signals can be successfully sampled at lower, sub-Nyquist, rates. Today, this approach is called Compressed Sensing (CS) [3–5]. In CS, an acquisition process is described by an underdetermined system of linear equations, where the signal of interest is represented by a sparse or approximately sparse solution [6]. Consequently, a reconstruction in CS is the process of estimating this solution. The CS approach is universal and can be applied in many fields such as in telecommunications [7], image processing [6] and time-delay estimation [8].

Several CS methods have been developed to acquire frequency sparse signals: 1) single-channel nonuniform sampling (SNS) [7, 9, 10]; 2) multi-coset sampling (MCS) [11–13]; 3) random demodulator (RD) [14]; and 4) modulated wideband converter (MWC) [15]. The SNS architecture comprises one wideband sampling channel (see Fig. C.1c). RD and MWC requires premixing of the input signal prior to sampling and a low noise amplifier depending on the power of the input signal. The MCS architecture can be obtained by removing some of the parallel channels of the interleaved Analog-to-Digital Converter (ADC) [11].

With the SNS approach, some applications like signal analyzer and telecommunication can acquire signals with a wider accumulated bandwidth. In most of the modern
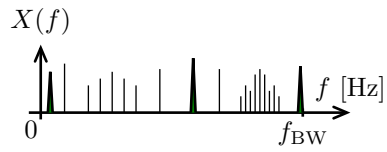
(a) Frequency sparse wide-band signal.
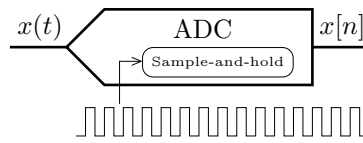
(b) Uniform Nyquist rate sampling.
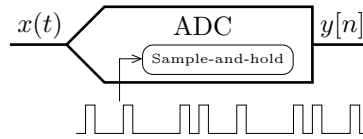
(c) Single-channel Nonuniform Sampling.

Fig. C.1: Illustration of the different single-channel acquisition approaches. Pulse signals represent the moments of sampling.

(a) Multi-band signal

(b) Multi-Coset Sampling architecture.

(c) SNS emulates MCS.
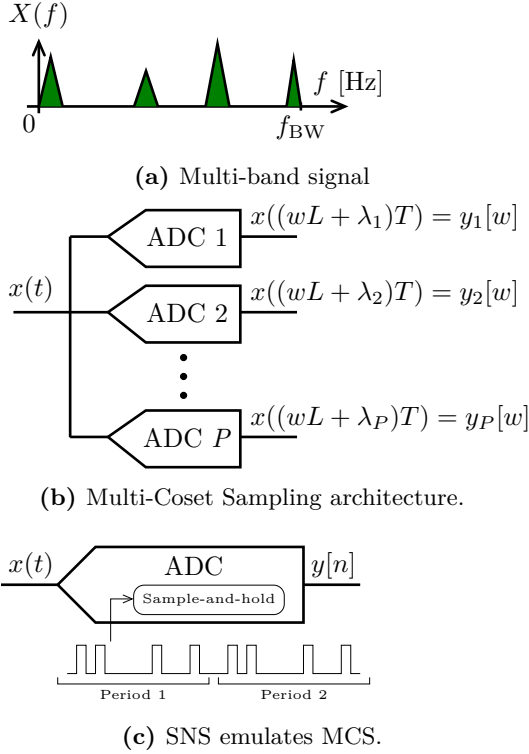
Fig. C.2: Illustration of MCS acquisition. L is the multi-coset sampling period in samples and T is the Nyquist sampling period.

sampling devices, the input bandwidth exceeds the maximum sampling rate [16]. The input bandwidth can also be increased by combining an existing ADC with a specially designed sample-and-hold circuit [7]. Therefore, a device can operate at Nyquist rate up to some limit and then it may switch to CS mode. With the uniform Nyquist rate sampling, a signal with the highest frequency component f_{BW} has to be sampled at a rate greater than $2f_{\mathrm{BW}}$ (see Fig. C.1b). However, with the SNS approach, the average sampling rate can be lower (see Fig. C.1c). As shown in [7], obstacles in using SNS in real-time applications are related to high complexity of the reconstruction (approximately $71 \cdot 10^9$ floating point operations per second to reconstruct a signal comprised of 65536 Nyquist rate samples) and not to the design of the analog front-end. Therefore, it is necessary to decrease the complexity of the SNS reconstruction in order to use CS in real-time applications.

The various signal reconstruction methods can be classified into two groups: optimization methods and greedy methods [17]. The optimization methods, such as ℓ_1 minimization, show a high reconstruction capability, but unfortunately they are computationally expensive and slow [18]. An Orthogonal Matching Pursuit (OMP) is one of the popular greedy algorithms [6, 17]. It is faster than convex optimization but has a lower signal reconstruction performance [6]. The Accelerated Iterative Hard Thresholding (AIHT) [19] and the Approximate Message Passing (AMP) [20] algorithms are greedy methods that both have low computational costs and a high reconstruction capability. However, although the complexity of the reconstruction is reduced, for real-time applications and large problem sizes (for example, length of signals $10^3 - 10^5$ samples) it still may be too high.

In many applications, such as telecommunication, the signals contain several frequency bands (see Fig. C.2a) rather than a large number of independent tones spread over the entire bandwidth. In this case, the MCS acquisition (see Fig. C.2b) is more beneficial from a computational point of view as it operates with a smaller sensing matrix [13]. The architecture in Fig. C.2c is similar to the standard SNS shown in Fig. C.1c with the only difference that the SNS sampling is split into periods similar to what is used in MCS. Hence, the modified architecture in Fig. C.2c is SNS with MCS emulation. The modified architecture allows us to work on substantially smaller sub-problems than the standard SNS thus leading to a lower reconstruction complexity.

Sparsity of a signal in the SNS model equals to accumulated width of tones and bands relative to the total bandwidth. At the same time, sparsity of a signal in the MCS model equals to the ratio of non-zero frequency slices and the total number of slices [12, 13]. Therefore, the same signal may have an MCS representation with higher sparsity than in the SNS representation. At the same time, the performance of the CS reconstruction algorithms depends on the sparsity of the recovered signal [21]. Consequently, the reconstruction performance in these two approaches may also be different even for the same input signals. So, MCS emulation in the SNS acquisition introduces performance-complexity tradeoffs, as on one hand, emulation decreases the computational complexity, but on another hand, it changes sparsity. We investigate these tradeoffs with numerical simulations and theoretical assessments of the reconstruction complexity assuming multi-band signal scenarios. These scenarios include different numbers (from 1 to 4), different widths (4% or 8% of bandwidth) and positions of the bands (at the centers of frequency slices or at the edges) and different levels of noise in signals (SNR$\in \{100, 20, 10\}$ dB). In [22], the authors presented the potential reconstruction speed-up of the MCS emulation in SNS. However, these sampling scenarios were limited to the noise-free signals with bands aligning with the multi-coset frequency slices, and the impact of the emulation on the reconstruction quality was not evaluated in case of other positions and widths of bands. The present paper fills this gap and investigates tradeoffs in detail.

The article is organized as follows. In Section 2, we describe the models of SNS

and MCS. We present the reconstruction algorithms in Section 3. Complexities of the algorithms are assessed in Section 4. The simulation framework is described in Section 5. In Section 6, we present the simulation results and Section 7 concludes the paper.

2   Sampling Approaches and Signal Reconstruction
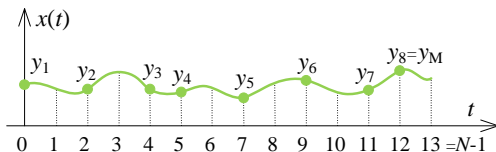
(a) General SNS acquisition, $M = 8$, $\Lambda_{\text{SNS}} = \{0, 2, 4, 5, 7, 9, 11, 12\}$.
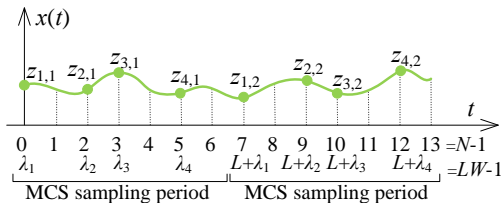
(b) MCS acquisition, $L = 7$, $W = 2$, $P = 4$, $\Lambda_{\text{MCS}} = \{0, 2, 3, 5\}$.

Fig. C.3: Illustration of SNS and MCS. The dotted lines correspond to the Nyquist rate sampling.

2.1   Single-channel nonuniform sampling

SNS consists of one input sampling channel that selects Nyquist rate samples according to a specific nonuniform (but not random) sampling pattern. Then, a reconstruction procedure uses the selected samples to recover all the Nyquist rate samples. Therefore, SNS operates at an average rate below the Nyquist rate. The SNS acquisition process is illustrated in Fig. C.3a. In total, there are N Nyquist rate samples, but SNS acquires $M < N$ of them. Denote by $\mathbb{N}_j^k = \{z \in \mathbb{N} : 0 \leq j \leq z \leq k\}$. The position of the acquired samples is specified by the sampling pattern $\Lambda_{\text{SNS}} \subset \mathbb{N}_0^{N-1}$ with cardinality $|\Lambda_{\text{SNS}}| = M < N$. The model of SNS is [7]:

$$\mathbf{y} = \mathbf{A}(\mathbf{x} + \mathbf{e}) = \mathbf{DF}_{\text{INV}}(\mathbf{x} + \mathbf{e}), \tag{C.1}$$

where $\mathbf{y} \in \mathbb{R}^{M \times 1}$ is a measurement vector, a vector of the the acquired samples, $\mathbf{A} \in \mathbb{C}^{M \times N}$ is called a sensing matrix, $\mathbf{x} \in \mathbb{C}^{N \times 1}$ is a vector containing the Discrete

Fourier Transform (DFT) coefficients of the unknown Nyquist rate samples, $\mathbf{e} \in \mathbb{C}^{N \times 1}$ represents AWGN in the DFT domain, $\mathbf{D} \in \mathbb{Z}^{M \times N}$ is a selection matrix that corresponds to Λ_{SNS} and $\mathbf{F}_{\text{INV}} \in \mathbb{C}^{N \times N}$ is the Inverse DFT (dictionary) matrix of order N.

The unknown vector $\mathbf{x}$ is assumed to be compressible with $K_1 < N$ dominant elements, which implies that K_1 elements are enough to represent the most information in the signal. There is no universal way on how to define K_1. This paper evaluates the number of the dominant DFT bins as:

$$K_1 = \Omega N, \tag{C.2}$$

where $K_1, N \in \mathbb{N}$ and $\Omega \in \mathbb{R}$ is a total occupancy ratio. We call the value N/K_1 the sparsity of a signal in the SNS acquisition. The support of $\mathbf{x}$, the set of the indices of the dominant elements, is denoted by S_1.

2.2   Multi-coset sampling

The main idea of MCS is to use several parallel input channels operating at lower rates rather than one operating at a higher rate (see Fig. C.2b) [11–13]. The samples are acquired periodically with different time offsets. The offsets are defined by the MCS pattern $\Lambda_{\text{MCS}} = \{\lambda_1, \lambda_2, \ldots, \lambda_P\} \subset \mathbb{N}_0^{L-1}$, where $P < L$ is the number of the sampling channels and L is called the MCS period. MCS can be seen as a time-interleaved sampler with P out of L channels. Therefore, only P samples are selected from every bunch of L consecutive Nyquist-rate samples. The process of MCS is illustrated in Fig. C.3b, where W sampling periods are shown. Denote by $z_{p,w} \in \mathbb{R}$, $p \in \mathbb{Z}_1^P, w \in \mathbb{Z}_1^W$ the wth output sample of the pth sampling channel. The discrete model of the MCS acquisition is [11–13]:

$$\mathbf{Y} = \mathbf{B}(\mathbf{X} + \mathbf{E}), \tag{C.3}$$

where $\mathbf{Y} \in \mathbb{C}^{P \times W}$ is a matrix of the known measurements,

$$\mathbf{Y} = \begin{pmatrix} \mathcal{F}([z_{1,1}, \ldots, z_{1,W}]) \\ \vdots \\ \mathcal{F}([z_{P,1}, \ldots, z_{P,W}]) \end{pmatrix} \circ \begin{pmatrix} \delta_{1,1}, & \ldots, & \delta_{1,W} \\ \vdots & \ddots & \vdots \\ \delta_{P,1}, & \ldots, & \delta_{P,W} \end{pmatrix} \tag{C.4}$$

$$\delta_{p,w} = \exp\left[\frac{-j2\pi\lambda_p(w-1)}{LW}\right], \, p \in \mathbb{N}_1^P, w \in \mathbb{N}_1^W, \tag{C.5}$$

where $\mathcal{F}([z_{p,1}, \ldots, z_{p,W}]) \in \mathbb{C}^{1 \times W}$ denotes DFT of the samples obtained from the pth sampling channel, $\circ$ denotes the Hadamard product and $\delta_{p,w}$ represents the delay of the wth DFT bin in the pth sampling channel. The matrix $\mathbf{B} \in \mathbb{C}^{P \times L}$ combines the measurement and the dictionary matrices. The elements of $\mathbf{B}$ are given by:

$$B_{p,\ell} = \frac{1}{LT}\exp\left[j\frac{2\pi}{L}\lambda_p(\ell-1)\right]. \tag{C.6}$$

where $\ell \in \mathbb{N}_1^L$. The Nyquist sampling period T depends on the highest frequency component in the input signal. In total, the duration of the observed signal equals LWT. The matrices $\mathbf{X} \in \mathbb{C}^{L \times W}$ and $\mathbf{E} \in \mathbb{C}^{L \times W}$ represent the unknown input signal and AWGN, respectively. If the unknown DFT of the input signal is sliced into L equal parts, then each row of $\mathbf{X}$ is one of these consecutive slices [11–13]. It is assumed that $\mathbf{X}$ has $K_2 < L$ dominant (in the ℓ_2 sense) rows. The value of K_2 equals to the number of the slices partly or fully occupied by the frequency bands. The ratio K_2/L is a sparsity of a signal in the MCS acquisition. The set of these rows, the support of $\mathbf{X}$, is denoted by S_2. Signals with few bands in the spectrum may result in $\mathbf{X}$ having only few dominant rows.

2.3   MCS emulation in SNS acquisition of multi-band signals

Recovering $\mathbf{x}$ from (C.1) is called a Single-Measurement Vector (SMV) problem and recovering $\mathbf{X}$ from (C.4) is called a Multiple-Measurement Vectors (MMV) problem [23]. In a MMV problem, W solution vectors (columns of $\mathbf{X}$) have to be found. Assume without loss of generality that a frequency sparse multi-band signal is acquired by SNS and MCS with the same average sampling ratio $f_{\text{samp}} = M/N = P/L$, which implies $N = LW$ and $M = PW$. In SNS, signal reconstruction corresponds to estimating a single vector of length LW by $\mathbf{A} \in \mathbb{C}^{PW \times LW}$, while in MCS, reconstruction corresponds to estimating W vectors of length L by $\mathbf{B} \in \mathbb{C}^{P \times L}$. Therefore, the complexity of the reconstruction of the same signal in SNS and MCS is different. Moreover, we can expect that reconstruction in MCS has lower costs for two reasons:

1. Complexity of most of the numerical algorithms depends nonlinearly on the size [24]. For example, matrix multiplication and inversion requires $\mathcal{O}(N^3)$ arithmetical operations, QR factorization – $\mathcal{O}(MN^2)$, fast Fourier transform – $\mathcal{O}(N\log_2 N)$ etc (see [25] for definition of the $\mathcal{O}(\cdot)$ notation). This suggests that recovery of W vectors of length L has a lower computational complexity than the recovery of one vector of length LW.

2. for MCS, there are reconstruction methods reducing the dimension of the MMV problem. This reduction is based on the correlation matrix of the acquired samples [11–13].

Therefore, the MCS emulation in the SNS acquisition can reduce the computational cost of signal reconstruction by replacing problem (C.1) with (C.3). The rest of the paper is dedicated to study of this potential computational saving with respect to the reconstruction quality.

2.4   Considerations on the impact of the MCS emulation in the SNS acquisition

According to (C.1) and (C.3), the SNS model represents DFT bins individually, while in the MCS model, a signal $\mathbf{x}$ is represented by frequency slices (the rows of $\mathbf{X}$). In other words, the MCS acquisition has a lower frequency resolution. As a result, the sparsity of a signal in the SNS model depends only on the total width of bands while the sparsity of a signal in the MCS model depends not only on the width of bands but also on their positions. Therefore, the same signal may have a MCS representation with lower sparsity than in the SNS representation. At the same time, the performance of the CS reconstruction algorithms depends on sparsity of the recovered signal [21]. Consequently, the reconstruction performance in these two approaches may also be different even for the same input signal. So, the MCS emulation in the SNS acquisition introduces performance-complexity tradeoffs, as on one hand, emulation decreases the computational complexity, but on another hand, it changes sparsity. We investigate these tradeoffs with numerical simulations and theoretical assessments of the reconstruction complexity assuming multi-band signal scenarios. These scenarios include different numbers, different widths and positions of the frequency bands and different levels of noise in the signals.

2.5   Reconstruction Performance Metrics

In order to evaluate the reconstruction quality, we have to choose quality metrics. An average relative root mean squared error is a direct way to evaluate a quality of reconstruction of several signals

$$E = \sum_{i=1}^{Q} \frac{\|\mathbf{x}_i - \widehat{\mathbf{x}}_i\|_2}{\|\mathbf{x}_i\|_2}, \tag{C.7}$$

where $\mathbf{x}_i$ and $\widehat{\mathbf{x}}_i$ denote the ith input signal and the recovered signal in the time domain respectively. The number of signals is equal to Q. We can also evaluate the standard deviation of E which shows how reconstruction errors variate from the average value:

$$\sigma = \sqrt{\frac{1}{Q} \sum_{i=1}^{Q} \left(\frac{\|\mathbf{x}_i - \widehat{\mathbf{x}}_i\|_2}{\|\mathbf{x}_i\|_2} - E \right)^2}. \tag{C.8}$$

To give insight on lower bound of E, it is possible to evaluate an "ideal" reconstruction error, E_{ideal}. This error is derived by replacing $\widehat{\mathbf{x}}_i$ with a signal formed by forcing all the elements to zero outside the support S_1 of $\mathbf{x}_i$.

Another metric is a Support Reconstruction Ratio (SRR):

$$\text{SRR} = \frac{\text{no. of the correct reconstructed supports } (S_1 \text{ or } S_2)}{\text{no. of the test signal}} \in [0, 1] \tag{C.9}$$

If SRR=1, reconstruction is successful for all the test signals.

3   Complexity Analysis

3.1   Complexity Metric

In this paper, we want to compare how computational cost of reconstruction in SNS is changed if applying MCS emulation. We define complexity of an algorithm as a total number of floating point operations. This is not the only possible metric of the complexity. The memory bandwidth is a bottleneck of modern CPU and GPU based systems [26]. In other words, it can take more time to transfer data between CPU/GPU and memory than to perform computations on this data. However, there is no straightforward way to evaluate a memory complexity as it depends on the implementation for the specific platform (CPU/GPU/FPGA etc). At the same time, the number of floating operations is widely used as it gives insight how many computational resources are required to run an algorithm [25, 27, 28].

3.2   Reconstruction Algorithms

Several algorithms which can be used in the SNS acquisition exist [6, 17]. The Algorithms based on ℓ_1 minimization have high reconstruction capability [17]. However, they are computationally expensive and slow [18]. The normalized IHT algorithm [29] (and its accelerated version – AIHT [19]) is known to outperform the well-known OMP in terms of reconstruction capability. In its turn, Compressive Sampling Matching Pursuit (CoSaMP) [30] slightly outperforms normalized IHT in noisy scenarios [18]. However, CoSaMP computes a least squares estimate of the solution which for large N and K_1 can be computationally demanding. The AMP algorithm has a reconstruction performance almost equal to CoSaMP [20] and finds the solution with almost the same procedures as in IHT. The difference is in the additional message passing stage. Thus, the complexity of the AMP iterations exceeds the complexity of IHT iterations. Therefore, IHT is an algorithm that has both low computational complexity and high reconstruction quality. In addition, the assessment of the IHT complexity can serve as the lower bound for an assessment of the AMP complexity. We also use the Block sparsity AIHT (B-AIHT). This algorithm is a modification of AIHT that takes into account a fact that non-zero elements may be grouped in blocks.

Iterative algorithms like IHT and M-FOCUSS estimate the solution until the convergence criteria is met. The reconstruction capability of an algorithm can be evaluated with a convergence rate, i.e. a number of iterations which are required to run until some reconstruction quality is met. Alternatively, the number of iterations can be predefined and the reconstruction error is observed. In this article, we use the second approach as it simplifies the complexity analysis.

Algorithm 3 Reconstruct $\mathbf{x}$ with AIHT [19]

Input: $\mathbf{y} \in \mathbb{R}^{M \times 1}$, $\mathbf{A} \in \mathbb{C}^{M \times N}$, $K_1 \in \mathbb{N}_1$, $T_{\text{AIHT}} \in \mathbb{N}_1$
Output: $\mathbf{x} \in \mathbb{C}^{N \times 1}$
 1: $\mu \leftarrow N$, $\mathbf{r} \leftarrow \mathbf{y}$, $\mathbf{x}^{[0]} \leftarrow \mathbf{0}$
 2: **for** $i = 1$ **to** T_{AIHT} **do**
 3:     $\mathbf{x}^{[i]} \leftarrow \mathbf{x}^{[i-1]} + \mu \mathbf{A}^{\text{H}} \mathbf{r}$
 4:     $\mathbf{x}^{[i]} \leftarrow P_{K_1} \langle \mathbf{x}^{[i]} \rangle$
 5:     $\mathbf{r} \leftarrow \mathbf{y} - \mathbf{A} \mathbf{x}^{[i]}$
 6:     **if** $i > 2$ **then**
 7:         $\alpha_1 \leftarrow \dfrac{(\mathbf{A}\mathbf{x}^{[i]} - \mathbf{A}\mathbf{x}^{[i-1]})^{\text{H}}\mathbf{r}}{\|\mathbf{A}\mathbf{x}^{[i]} - \mathbf{A}\mathbf{x}^{[i-1]}\|_2^2}$
 8:         $\widetilde{\mathbf{x}}_1 \leftarrow \mathbf{x}^{[i]} + \alpha_1 (\mathbf{x}^{[i]} - \mathbf{x}^{[i-1]})$
 9:         $\widetilde{\mathbf{r}}_1 \leftarrow \mathbf{y} - \mathbf{A}\widetilde{\mathbf{x}}_1$
10:         $\alpha_2 \leftarrow \dfrac{(\mathbf{A}\widetilde{\mathbf{x}}_1 - \mathbf{A}\mathbf{x}^{[i-2]})^{\text{H}}\widetilde{\mathbf{r}}_1}{\|\mathbf{A}\widetilde{\mathbf{x}}_1 - \mathbf{A}\mathbf{x}^{[i-2]}\|_2^2}$
11:         $\widetilde{\mathbf{x}}_2 \leftarrow \widetilde{\mathbf{x}}_1 + \alpha_2 (\widetilde{\mathbf{x}}_1 - \mathbf{x}^{[i-2]})$
12:         $\widetilde{\mathbf{x}}_2 \leftarrow P_{K_1} \langle \widetilde{\mathbf{x}}_2 \rangle$
13:         $\widetilde{\mathbf{r}}_2 \leftarrow \mathbf{y} - \mathbf{A}\widetilde{\mathbf{x}}_2$
14:         **if** $\|\widetilde{\mathbf{r}}_2\|_2^2 < \|\mathbf{r}\|_2^2$ **then**
15:             $\mathbf{x}^{[i]} \leftarrow \widetilde{\mathbf{x}}_2$
16:             $\mathbf{r} \leftarrow \widetilde{\mathbf{r}}_2$
17:         **end if**
18:     **end if**
19: **end for**

IHT recovers a sparse signal by performing T_{AIHT} iterations that update an approximate solution, preserve only the K_1 largest elements and set other elements to zero [29]. The last operation (thresholding) is denoted by $P_{K_1} \langle \cdot \rangle$ in Algorithm 3. Knowing that $\mathbf{A}$ is a product of the selection matrix and the Inverse DFT matrix, multiplications by $\mathbf{A}$ and $\mathbf{A}^{\text{H}}$ can be performed with IFFT and FFT operations respectively. For the same reason, there is no need to compute a step of the gradient descend at each iteration [19]. AIHT uses a double overrelaxation approach to accelerate the convergence of the algorithm [19]. In this paper, we use the AIHT (see Algorithm 3) and B-AIHT algorithms, which differs from AIHT only in the selection operator $P_{K_1} \langle \cdot \rangle$. In B-AIHT, blocks of the solution vectors that have the highest energy are preserved while other blocks are set to zero.

For the MCS reconstruction, we use the MUSIC algorithm [12] and two modifications of the M-FOCUSS algorithm [23]. These algorithms find the support S_2 of $\mathbf{X}$. Knowing S_2 the actual signal recovery is performed using the least-squares estimation [13].

The MUSIC algorithm finds the support S_2 by estimating the signal and noise subspaces [11]. The general form of this reconstruction method is presented in Algorithm 4.

Algorithm 4 Find the support S of $\mathbf{X}$ with MUSIC [12]

Input: $\mathbf{Y} \in \mathbb{C}^{P \times W}$, $\mathbf{B} \in \mathbb{C}^{P \times L}$, $K_2 \in \mathbb{N}_1$, $T_{\mathrm{QR}} \in \mathbb{N}_1$
Output: $S \in \mathbb{N}_1^{K_2}$
1: $S \leftarrow \emptyset$
2: $\mathbf{R} \leftarrow \mathbf{Y}\mathbf{Y}^{\mathrm{H}}$
3: $\mathbf{U} \leftarrow$ Eigenvalue decomposition$(\mathbf{R}, T_{\mathrm{QR}})$
4: $\mathbf{U}_S \leftarrow \mathbf{U}_{\{1,\dots,K_2\}}$
5: $p_i \leftarrow \|\mathbf{U}_S \mathbf{U}_S^{\mathrm{H}} \mathbf{b}_i\|_2^2$, $i \in \{1, \dots, L\}$
6: $S \leftarrow$ Indices of K_2 largest elements of p_i

Algorithm 5 Find the support S of $\mathbf{X}$ with M-FOCUSS-R [23, 31]

Input: $\mathbf{Y} \in \mathbb{C}^{P \times W}$, $\mathbf{B} \in \mathbb{C}^{P \times L}$, $\lambda \in \mathbb{R}$, $p \in \mathbb{R}, T_{\mathrm{FOC}} \in \mathbb{N}_1$
Output: $S \in \mathbb{N}_1^{K_2}$
1: $\mathbf{X}_{pr} \leftarrow \mathbf{0}$, $\mathbf{Q} \leftarrow \mathbf{0}$, $\mathbf{W} \leftarrow 0$
2: $\mathbf{X} \leftarrow \mathbf{B}^\dagger \mathbf{Y}$
3: **for** $c = 1$ **to** T_{FOC} **do**
4: $\quad \mathbf{W}_{i,i} \leftarrow \|\mathbf{X}(i,:)\|_2^{1-p/2}$, $i \in \{1, \dots, L\}$
5: $\quad \mathbf{B}_{\mathrm{W}} \leftarrow \mathbf{B}\mathbf{W}$
6: $\quad \mathbf{Q} \leftarrow \mathbf{B}_{\mathrm{W}}^{\mathrm{H}}(\mathbf{B}_{\mathrm{W}}\mathbf{B}_{\mathrm{W}}^{\mathrm{H}} + \lambda\mathbf{I})^{-1}\mathbf{Y}$
7: $\quad \mathbf{X} \leftarrow \mathbf{W}\mathbf{Q}$, $\mathbf{X}_{pr} \leftarrow \mathbf{X}$
8: **end for**
9: $q_i \leftarrow \|\mathbf{Q}(i,:)\|_2$, $i \in \{1, \dots, L\}$
10: $S \leftarrow$ Indices of K_2 largest elements of q_i

The span of the signal subspace $\mathbf{U}_S$ is equal to the span of the eigenvectors that correspond to K_2 largest eigenvalues of the so-called correlation matrix $\mathbf{R}$. The correlation matrix should be a full rank matrix. At first glance, the eigenvalue decomposition at Step 3 of Algorithm 4 can be considered as the most computationally costly operation. One of the common ways to compute the eigenvalue decomposition of the Hermitian matrix $\mathbf{R}$ is to transform a matrix into the tridiagonal form and then apply QR iterations converging diagonal elements of the tridiagonal matrix to the eigenvalues [24]. It is not feasible to obtain a closed form expression that gives the sufficient number of QR iterations , T_{QR}, which is sufficient to correctly estimate the signal subspace. Therefore, we obtain T_{QR} empirically by running MUSIC with different number $(1, 2 \dots)$ of the QR iterations. Then, T_{QR} is set to the smallest value that results in the best reconstruction performance. The fixed T_{QR} significantly decreases the complexity of applying MUSIC.

The M-FOCUSS-R algorithm (see Algorithm 5; in line 4 the MATLAB notation

is used to denote a row of $\mathbf{X}$) [31] (R refers to "Restricted") is a modification of M-FOCUSS. In M-FOCUSS-R, K_2 indices of the rows of $\mathbf{Q}$ are assumed to comprise S_2 if they have the largest ℓ_2 norms after T_{FOC} iterations [31]. In [32], the authors suggested that any practical implementation of FOCUSS-like algorithms should comprise thresholding of decaying elements to zero. This motivated M-FOCUSS-R.

Note that the correlation matrix $\mathbf{R}$ in Algorithm 4 can be factorized as:

$$\mathbf{R} = \mathbf{V}\mathbf{V}^{\text{H}} = \mathbf{B}\mathbf{X}\mathbf{X}^{\text{H}}\mathbf{B}^{\text{H}}, \tag{C.10}$$

where $\mathbf{V}$ has P orthogonal columns. As shown in [13], the support of $\mathbf{X}$ equals the support of the matrix $\mathbf{U} \in \mathbb{C}^{P \times L}$ for:

$$\mathbf{V} = \mathbf{B}\mathbf{U}. \tag{C.11}$$

The factorization $\mathbf{R} = \mathbf{V}\mathbf{V}^{\text{H}}$ is performed with the eigenvalue decomposition. Similar to the MUSIC case, we denote by T_{QR} the number of the QR iteration in this decomposition. Equation (C.11) can be solved by any algorithm for sparse MMV problems. In this paper, we use M-FOCUSS-R and denote the overall reconstruction method as M-FOC-COR.

4   Complexity Analysis

For AIHT, B-AIHT, MUSIC, M-FOCUSS-R and M-FOC-COR algorithms, we derive an analytical expression that calculates a number of floating point operations given the size of the problem, average sampling rate, number of non-zero elements and number of iterations.

To simplify the analysis, we assume that $N = 2^n$ for some positive integer n. Then the complexity of the signal reconstruction with AIHT (see Algorithm 3) is assessed to be:

$$\begin{aligned}
C_{\text{AIHT}}^{\text{SNS}} &\simeq T_{\text{AIHT}} C_{\text{Step 3–5}}^{\text{AIHT}} + (T_{\text{AIHT}} - 2) C_{\text{Step 7–14}}^{\text{AIHT}} \\
&\simeq T_{\text{AIHT}} \left[3N + M + 3N\log_2 N \right] \\
&\quad + (T_{\text{AIHT}} - 2) \left[7N + 10M + 3N\log_2 N \right] \\
&\simeq (10 T_{\text{AIHT}} - 14)N + (11 T_{\text{AIHT}} - 20)M \\
&\quad + (6 T_{\text{AIHT}} - 6)N\log_2 N. \tag{C.12}
\end{aligned}$$

The complexity of B-AIHT is approximately to be equal to the complexity of AIHT, as the cost of the selection steps 4 and 12 (selection operator $P_{K_1}\langle \cdot \rangle$) in Algorithm 3 is neglectable in comparison to the cost of FFT and IFFT.

Recall that the least-squares estimation is performed in a MCS acquisition when the support S_2 is found out by a reconstruction algorithm. In this article, the least-norm

and least-squares solutions are obtained via QR factorization. The complexity of the MCS reconstruction with MUSIC is assessed to be:

$$
\begin{aligned}
C_{\text{MUSIC}}^{\text{MCS}} &\simeq C_{\text{MUSIC}}^{S_2} + C_{\text{Least Squares}}^{S_2} \\
&\simeq \frac{4}{3}P^3 + T_{\text{QR}}\Big(2P^3 + \frac{P - P^2}{2}\Big) \\
&\quad + P^2\Big(2W + 2K_2 + 2L - \frac{3}{2}\Big) + P(2K_2^2 + K_2(W + 1)) \\
&\quad + K_2^2 W + K_2\Big(\frac{1}{2} - W\Big).
\end{aligned}
\tag{C.13}
$$

Complexity of the MCS reconstruction with M-FOCUSS-R is assessed to be:

$$
\begin{aligned}
C_{\text{M-FOCUSS-R}}^{\text{MCS}} &\simeq C_{\text{Step 2}}^{\text{M-FOCUSS-R}} + T_{\text{FOC}} C_{\text{Step 6}}^{\text{M-FOCUSS-R}} + C_{\text{Least Squares}}^{S_2} \\
&\simeq P^2\Big(2L + W - \frac{1}{2}\Big) + P\Big(2LW + L + \frac{1}{2}\Big) - LW \\
&\quad + T_{\text{FOC}}\Big(2P^3 + P^2\Big(2L + W + \frac{1}{2}\Big) + M\Big(2LW + L + \frac{1}{2}\Big) - LW\Big) \\
&\quad + K_2^2\Big(2P + W - \frac{1}{2}\Big) + K_2\Big(2PW + P - W + \frac{1}{2}\Big) \\
&\simeq 2T_{\text{FOC}}P^3 + P^2\Big((2L + W)(T_{\text{FOC}} + 1) + \frac{T_{\text{FOC}}}{2} - \frac{1}{2}\Big) \\
&\quad + (T_{\text{FOC}} + 1)\Big(2PLW + PL + \frac{P}{2} - LW\Big) \\
&\quad + K_2^2\Big(2P + W - \frac{1}{2}\Big) + K_2\Big(2PW + P - W + \frac{1}{2}\Big).
\end{aligned}
\tag{C.14}
$$

In MCS, additional computations (C.4) have to be done prior to reconstruction. The complexity of these computations equals the complexity of the P DFT operations and Hadamard product of two P by W matrices. Considering that output samples of ADC are real-valued, the complexity of (C.4) is assessed to be:

$$
C_{(3)}^{\text{MCS}} \simeq P\Big(\frac{3}{2}\widehat{W}\log_2\widehat{W} + W\Big),
\tag{C.15}
$$

where $\widehat{W}$ is a positive integer equal to the next power of two of W.

Equations (C.12)–(C.13) and (C.15) have to be validated before the comparison of complexity of algorithms. Ideally, the validation for the specific implementation has to be performed with the time benchmarking of the actual execution time. However, it is unfeasible to assess the execution time of supplementary operations like function calls, access to memory etc. which causes execution time overhead. Instead, we perform this validation with the relative running time. In particular, we evaluate how the reconstruction time and the number of operations varies as we vary the sampling conditions.

Such a relative comparison removes "biasing" and allows to evaluate the behavior of complexity of algorithms.

While varying the number of bands from 1 to 4, the number of iterations from 1 to 15 and the length of the input signal from 16384 to 32768 samples in the simulation scenario 2) (see Section III), the difference between the benchmarked and the assessed results does not exceed 30%. For example for AIHT, the reconstruction time with 15 iterations is 1.6 times larger than the reconstruction time with 10 iterations, while according to (C.12), the number of the arithmetic operations is increased by a factor of 1.55. This results in the difference of $(1.60 - 1.55)/1.55 \cdot 100\% = 3.2\%$. This is the smallest difference observed.

We can now preliminary and asymptotically compare the computational complexity of different reconstruction procedures. Assume that the length of the acquired signal is $N = LW$, and therefore, $M = PW$. L is the MCS sampling period and specifies the number of frequency slices in the MCS model, W is a number of samples acquired from a single ADC (see Fig. C.2b).

Assume that the problem size N is increasing. For the fixed MCS configuration, this means that L is fixed while W is increasing. Then the ratio of the complexity of AIHT and M-FOCUSS-R asymptotically is:

$$\lim_{W \to \infty} \frac{C_{\text{AIHT}}^{\text{SNS}}}{C_{\text{M-FOCUSS-R}}^{\text{MCS}}} = \lim_{W \to \infty} \frac{(6T_{\text{AIHT}} - 6)LW \log_2(LW)}{C_1 W + 1.5 PW \log_2 W}$$

$$= \lim_{W \to \infty} \left(\frac{(6T_{\text{AIHT}} - 6)LW \log_2 L}{C_1 + 1.5 PW \log_2 W} + \frac{(6T_{\text{AIHT}} - 6)LW \log_2 W}{C_1 + 1.5 PW \log_2 W} \right)$$

$$= \lim_{W \to \infty} \frac{(6T_{\text{AIHT}} - 6)LW \log_2 W}{1.5 PW \log_2 W} = \frac{(6T_{\text{AIHT}} - 6)L}{1.5 P} \geq \frac{6L}{1.5 P} = 4\frac{L}{P}.$$

The previous inequality is true as $L > P$ and $T_{\text{AIHT}} > 1$ for sub-Nyquist sampling; C_1 is a constant depending on P, T_{FOC} and K_2. Therefore, complexity of the reconstruction with AIHT is asymptotically higher than with M-FOCUSS-R.

Following the same idea, the ratio of the complexity of AIHT and MUSIC asymptotically equals to:

$$\lim_{W \to \infty} \frac{C_{\text{AIHT}}^{\text{SNS}}}{C_{\text{MUSIC}}^{\text{MCS}}} = \lim_{W \to \infty} \frac{(6T_{\text{AIHT}} - 6)LW \log_2(LW)}{C_3 W + 1.5 PW \log_2 W}$$

$$= \lim_{W \to \infty} \frac{(6T_{\text{AIHT}} - 6)L \log_2 W}{C_3 + 1.5 P \log_2 W} = \frac{(6T_{\text{AIHT}} - 6)L}{1.5 P} \geq \frac{6L}{1.5 P} = 4\frac{L}{P},$$

where C_3 depends on P, T_{QR} and K_2. Therefore, the complexity of AIHT is also asymptotically higher than the complexity of MUSIC.

This preliminary comparison supports the idea that the MCS emulation reduces the reconstruction complexity.

5   Simulation Framework

This section describes the simulation framework that is used to evaluate the impact of the MCS emulation to reconstruction quality and computational complexity.

5.1   Sampling Scenarios and Test Signal Description

As mentioned in 2.4, the MCS emulation introduces performance-complexity tradeoffs related to changes of sparsity in the SNS and MCS representations of input signals. In order to investigate these tradeoffs, we consider three simulation scenarios with real-valued multi-band signals. These scenarios highlight how reconstruction performance and complexity are affected by the MCS emulation. Three simulation scenarios are:

1. Narrow bands placed at the centers of the frequency slices (see example on Fig. C.4a). Each band occupies 4% of the whole bandwidth. In this case, $N/K_1 > L/K_2$, i.e. the sparsity of a test signal in SNS is higher that the sparsity in MCS. We may expect a better reconstruction performance in the SNS acquisition.

2. Wide bands occupy the whole multi-coset frequency slices (see example on Fig. C.4b). Each band occupies 8% of the whole bandwidth. Sparsity of the SNS and MCS representation is approximately equal, $N/K_1 \approx L/K_2$.

3. Wide bands intersect the boundaries of the frequency slices (see example on Fig. C.4c). Each band occupies 8% of the whole bandwidth. Sparsity in SNS is higher than in MCS, $N/K_1 > L/K_2$, but both sparsities are less than in the previous scenarios.

The difference between the first and the second scenario is that K_1 is increased while K_2 remains unchanged. In the third scenario, K_1 is fixed while K_2 is changed.

For each type of the test signals, 100 random instances were created and sampled. For each random instance, K_2 is known and K_1 is estimated prior to reconstruction. Otherwise, the performance of the reconstruction algorithms would be affected by the performance of the methods finding the number of the dominant DFT bins and frequency slices. The reconstruction time was benchmarked with 10 times averaging.
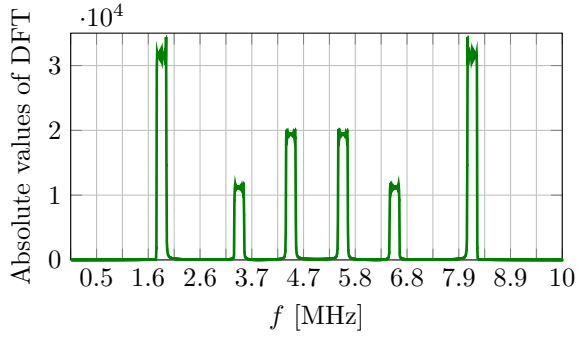
(a) Narrow bands are placed at the centers of the frequency slices, $F = 3$, $\Omega = 0.12$, $K_1 = 3934$, $K_2 = 6$, SNR $= 100$ dB.
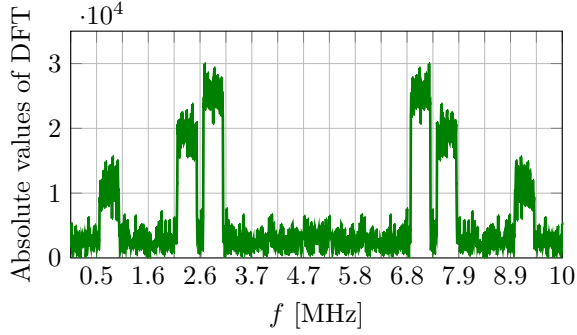
(b) Wide bands occupy the whole frequency slices, $F = 3$, $\Omega = 0.24$, $K_1 = 7866$, $K_2 = 6$, SNR $= 10$ dB.
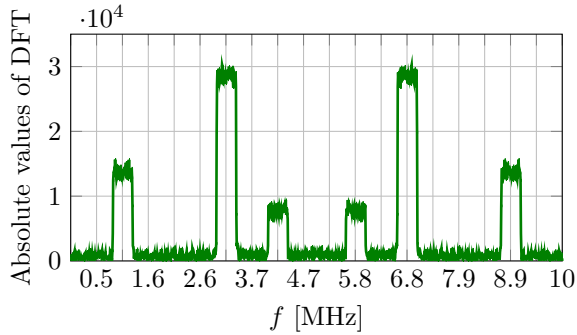
(c) Wide bands intersect the boundaries of the frequency slices, $F = 3$, $\Omega = 0.24$, $K_1 = 7866$, $K_2 = 12$, SNR $= 20$ dB.

Fig. C.4: Frequency domain illustration of examples of input test signals, $L = 19$. The vertical grid lines mark the frequency slices.

5.2   Signal and Sampling Parameters

According to [6], a prime value of the multi-coset sampling period L results in the largest value of the spark of $\mathbf{B}$, which is spark($\mathbf{B}$) $= P + 1$. We set the multi-coset sampling period to $L = 19$. Recall that according to (C.3), the overall number of the frequency slices in test signals equals L.

The AIHT algorithm uses IFFT and FFT operations which in MATLAB are fastest for input vectors with the length equal to a power of two. In order not to artificially increase the reconstruction time for the SNS acquisition, we use $N = 2^{15} = 32768$. For the MCS acquisition, we use $N = LW = 19 \cdot 1725 = 32775$, as the number of samples should be divisible by L.

Samples are taken at the rate $f_{\mathrm{NYQ}} = 10\,\mathrm{MHz}$. Consequently, in test signals, there are no components with frequencies equal or higher than $f_{\max} < f_{\mathrm{NYQ}}/2 = 5\,\mathrm{MHz}$. The width of a frequency slice equals $f_{\mathrm{NYQ}}/L \simeq 526\,\mathrm{kHz}$.

We used test signals with a different number of bands, $F \in \{1, 2, 3, 4\}$. As $L = 19$, one frequency slice has a width of $1/L \cdot 100\% = 0.05\%$ of the bandwidth $f_{\max}$. Recall that a real-valued signal have a symmetrical spectrum. Then, the corresponding occupancy ratio for scenario (1) is $\Omega = \{0.04, 0.08, 0.12, 0.16\}$ and for the scenario (2) and (3) $\Omega = \{0.08, 0.16, 0.24, 0.32\}$. The average powers of the bands are picked randomly from the uniform distribution over the dynamic range of $20\,\mathrm{dB}$.

Additive white Gaussian noise was added to the signals in order to evaluate the behavior of the reconstruction algorithms in a noisy environment. We consider three levels of noise corresponding to SNR $\in \{100, 20, 10\}\,\mathrm{dB}$.

5.3   Sampling patterns

The sampling patterns for MCS were selected by brute force search for the lowest condition numbers for all combinations of P from L [11]. For the SNS patterns, the brute force search is not applicable due to the large value of N. Instead, we use the approach presented in [7]. Basically, this approach is a random search for patterns Λ having the most smooth distribution of the absolute values of the DFT coefficients.

5.4   Reconstruction Considerations

One of the simulation objectives is to compare the reconstruction quality in SNS and MCS. In other words, to find out what minimum sampling rates are sufficient to reconstruct a signal with an acceptable quality for different test cases. We run simulations, where we increase the average sampling rate f_{samp} from f_{samp}/L to f_{NYQ} and reconstruct a set of test signals with SNS and MCS.

For the MCS acquisition, we assume that the lowest sufficient sampling rate is achieved if SRR equals to 1, i.e. when the slice support S_2 is found correctly for all the signal instances. In the presence of noise, we do not expect to recover the support

S_1 absolutely correctly due to the fact that noise is masking some of the DFT bins. Therefore, we cannot use SRR in SNS for the reconstruction criteria as we do in MCS. Instead, we evaluate a reconstruction quality with E and σ. We assume that in SNS an acceptable reconstruction quality is achieved when the average value of E does not exceed the corresponding value in the MCS acquisition with the lowest sufficient sampling rate.

6   Simulation Results

The simulations were performed on Intel Xeon X5670 2.93 GHz CPU, MATLAB R2012a and Ubuntu 12.04 LTS[1]. The simulation framework generates test signals with different parameters (number of bands, position of bands, occupancy ratio, SNR, length of signals etc) and then, simulate the SNS and MCS acquisition with different reconstruction algorithms and sampling rates. The software also plots the simulation results including the reconstruction performance, the benchmarked execution time and the theoretical computational complexity. For each combination of parameters, 100 test signal were used. According to our observations, this number is sufficient to get reproducible and converged results. Due to the limited paper space, we cannot present all the simulation results. However, the presented results describe the difference in the behavior of the SNS and MCS acquisition in terms of complexity and performance.

6.1   Reconstruction performance

In Fig. C.5, examples of the empirical dependency of E, σ and the support reconstruction ratio versus the average sampling rates are illustrated. A number that follows the name of an algorithm denotes the number of iterations in the corresponding reconstruction method. E_{ideal} is provided for reference.

As can be seen in Fig. C.5a, a five times increase of the number of iterations in AIHT results in significant reconstruction improvements. However, B-AIHT-25 does not perform as well as AIHT-25 because it tries to reconstruct more dominant values than are actually presented in the test signals with narrow bands placed at the centers of the frequency slices. This example illustrates that AIHT outperforms its block version for simulation scenario (1). For simulation scenario (2), AIHT-5, AIHT-25 and B-AIHT-5 perform similarly (see Fig. C.5b). The fact that B-AIHT-5 has a slightly better reconstruction performance than AIHT-25 indicates a slight inaccuracy of the K_1 estimation with (C.2) due to the spectrum leakage. A universal correction factor cannot be introduced to (C.2) as an impact of the spectral leakage on K_1 depends on the number of bands and the spectral occupancy ratio. For all the algorithms, the reconstruction
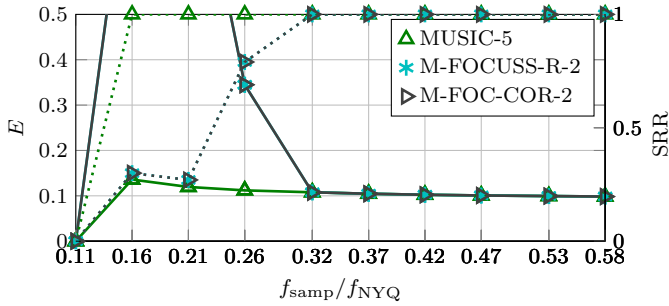
---

[1]The source code is available online at http://dx.doi.org/10.5278/VBN/MISC/CRSNS, DOI: 10.5278/VBN/MISC/CRSNS.
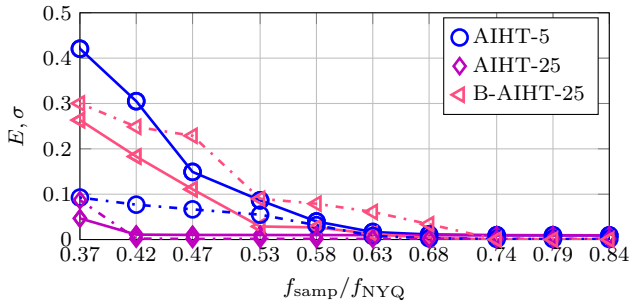
(a) The simulation scenario 1) with SNS, $E_{\text{ideal}} = 0.01$, $F = 3$, $\Omega = 0.12$, $\text{SNR} = 100$ dB.
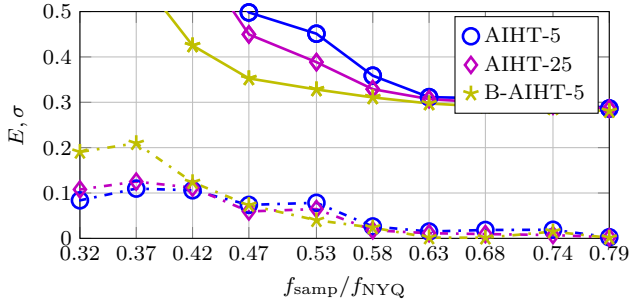
(b) The simulation scenario 2) with SNS, $E_{\text{ideal}} = 0.27$, $F = 2$, $\Omega = 0.16$, $\text{SNR} = 10$ dB.

(c) The simulation scenario 2) with MCS, $E_{\text{ideal}} = 0.09$, $F = 1$, $\Omega = 0.08$, $\text{SNR} = 20$ dB.

Fig. C.5: Simulated reconstruction error, E (solid lines), computed standard deviation, σ (dash-dotted lines) and SRR (dotted lines) versus the sampling ratio $f_{\text{samp}}/f_{\text{NYQ}} = M/N = P/L$.

Table C.1: The lowest sufficient $f_\text{samp}/f_\text{NYQ}$ for the scenario (1)

F	SNR	AIHT-5	AIHT-15	AIHT-25	B-AIHT-5	B-AIHT-15	B-AIHT-25	MUSIC-5	M-FOCUSS-R-4	M-FOC-COR-6
	100	0.26	0.26	0.26	0.32	0.26	0.21	0.16	0.32	0.32
1	20	0.26	0.26	0.26	0.32	0.26	0.21	0.21	0.32	0.32
	10	0.26	0.26	0.26	0.32	0.26	0.26	0.21	0.32	0.32
	100	0.58	0.47	0.42	0.63	0.63	0.63	0.42	0.53	0.53
3	20	0.58	0.47	0.42	0.63	0.63	0.63	0.42	0.53	0.53
	10	0.63	0.53	0.53	0.63	0.63	0.63	0.63	0.53	0.53

Table C.2: The lowest sufficient $f_\text{samp}/f_\text{NYQ}$ for the scenario (2)

| F	SNR	AIHT-5	AIHT-15	AIHT-25	B-AIHT-5	B-AIHT-15	B-AIHT-25	MUSIC-5	M-FOCUSS-R-4	M-FOC-COR-6
	100	0.58	0.53	0.53	0.53	0.53	0.53	0.32	0.47	0.42
2	20	0.58	0.53	0.53	0.53	0.53	0.53	0.32	0.47	0.42
	10	0.63	0.63	0.58	0.53	0.53	0.53	0.63	0.47	0.42
	100	0.74	0.68	0.68	0.74	0.68	0.63	0.53	0.58	0.58
4	20	0.74	0.68	0.68	0.74	0.68	0.63	0.58	0.63	0.63
	10	0.84	0.74	0.74	0.74	0.68	0.63	0.95	0.63	0.63

errors converge to $E_\text{ideal} = 0.27$ but do not reach it due to noise folding, which is a known problem in CS [**?**, 12]. Fig. C.5c presents the MCS simulation results for test scenario (1). The MUSIC-5 algorithm has the highest reconstruction performance: it reconstructs signals that occupy 8% of the bandwidth only with 16% of the Nyquist rate samples. This result agrees with [12]. The reconstruction errors E converge to $E_\text{ideal} = 0.95$. It is also notable that M-FOCUSS-R and M-FOC-COR-2 have the same reconstruction quality for all the sampling rates.

Tables I–III contain the sufficient sampling rates for the three simulation scenarios. As can be seen in Table I, the AIHT algorithm in scenario (1) does not have an absolute advantage over B-AINT and the MCS reconstruction algorithms. MUSIC outperforms AIHT in all the cases except when $F = 3$.

For scenario (2) (see Table II), the MCS approach outperforms the SNS acquisition. However, the MUSIC algorithm has a low reconstruction capability and requires almost

Table C.3: The lowest sufficient $f_{\text{samp}}/f_{\text{NYQ}}$ for the scenario (3)

F	SNR	AIHT-5	AIHT-15	AIHT-25	B-AIHT-5	B-AIHT-15	B-AIHT-25	MUSIC-5	M-FOCUSS-R-4	M-FOC-COR-6
	100	0.32	0.32	0.32	0.47	0.42	0.37	0.32	0.32	0.32
1	20	0.32	0.32	0.32	0.47	0.42	0.37	0.37	0.32	0.32
	10	0.37	0.32	0.32	0.47	0.42	0.42	0.58	0.32	0.32
	100	0.68	0.63	0.63	0.74	0.74	0.74	0.68	0.58	0.58
3	20	0.68	0.63	0.63	0.74	0.74	0.74	0.79	0.63	0.63
	10	0.74	0.68	0.68	0.79	0.79	0.79	–	0.68	0.68
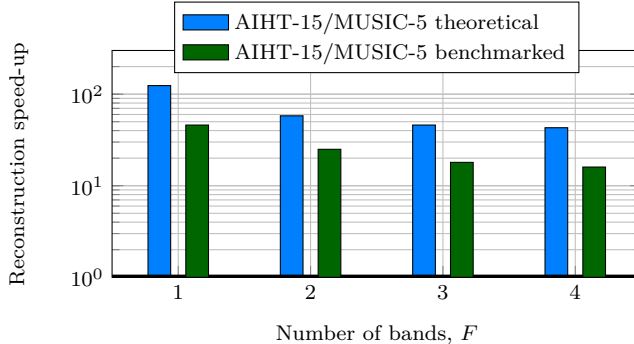
Fig. C.6: Theoretical and benchmarked reconstruction speed-up vs. number of bands for the scenario (1), SNR=100 dB. For all F, the sampling rates for MUSIC-5 are lower than the sampling rates for AIHT-15.

the Nyquist rate sampling in case of $F = 4$ (a relative large number of non-zero slices $K_2 = 14$–16) and low SNR=10 dB.

The MCS approach also outperforms SNS in case of the simulation scenario (3) (see Table III). While MUSIC fails to converge to the stable recovery for $F=3$ and SNR=10 dB, M-FOCUSS-R and M-FOC-COR perform as good as the SNS methods.

In general, M-FOCUSS-R and M-FOC-COR are robust to noise, while MUSIC has the best performance in low noise cases.

6.2 Reconstruction complexity

The theoretical and the benchmarked speed-ups that have been achieved with the MCS emulation are illustrated in Fig. C.6–C.8. The benchmarked speed-up is the ratio of
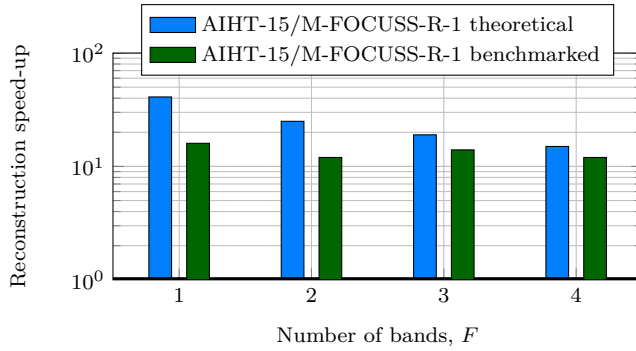
Fig. C.7: Theoretical and benchmarked reconstruction speed-up vs. number of bands for the scenario (2), SNR=20 dB. For all F, the sampling rates for M-FOCUSS-R-1 are less or equal than the sampling rates for AIHT-15.
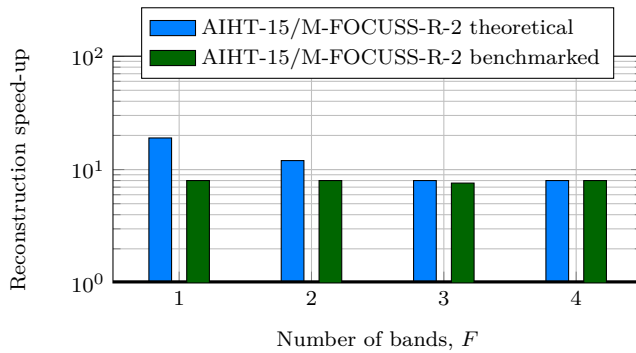
Fig. C.8: Theoretical and benchmarked reconstruction speed-up vs. number of bands for the scenario (3), SNR=10 dB. For all F, the sampling rates for M-FOCUSS-R-4 are less or equal than the sampling rates for AIHT-15

the SNS and MCS reconstruction time. For example in scenario (2), AIHT-15 in average reconstructs a signal with $F{=}2$, $\Omega{=}0.08$ and SNR=10 dB in 100 ms, while the reconstruction time for MUSIC-5 is 4 ms. Therefore, the benchmarked reconstruction speed-up is $100/4{=}25$ times. The theoretical speed-ups of the SNS reconstruction with the MCS emulation are computed with (C.12)–(C.13) and (C.15). For the same example, AIHT-15 performs $47 \cdot 10^6$ operations, while MUSIC-5 performs $0.53 \cdot 10^6$. So, the theoretical speed-up is $47/0.53 \approx 90$ times. The difference between the theoretical and the benchmarked speed-up can be explained by the fact that in the theoretical assessment we do not consider some practical issues such as the time needed for data transferring, function calls etc. The speed-up illustrated in Fig. C.6–C.8.

7   Conclusion

This paper proposed a MCS emulation as a means to reduce the computational complexity in a SNS acquisition of frequency sparse multi-band signals. We investigated the performance-complexity tradeoffs of this emulation for three sampling scenarios which include variable number of bands (from 1 to 4), different relative widths of bands (4% or 8% of the total signal bandwidth per band), positions of the frequency bands (at the centers or at the boarders of the frequency slices) and different level of noise in signals (SNR $\in \{100, 20, 10\}$ dB). Numerical simulations showed that the conventional SNS approach has a slightly better performance than the proposed SNS with the MCS emulation in two cases: i) signals with two narrow bands placed at the centers of frequency slices and SNR $= 10$ dB; and ii) signals with two wide bands that intersect the frequency slices and SNR $= 10$ dB. In other cases, the MCS sampling rates are less of equal to the SNS sampling rates, so that the MCS emulation preserves or improves the reconstruction quality. Numerical simulations and the theoretical assessments show that the MCS emulation reduces the reconstruction complexity by orders of 10 for all the considered sampling scenarios.

8   Acknowledgements

References

[1] A. Kohlenberg, "Exact interpolation of band-limited functions," *Journal of Applied Physics*, vol. 24, no. 12, pp. 1432 –1436, dec 1953.

[2] R. Vaughan, N. Scott, and D. White, "The theory of bandpass sampling," *IEEE Trans. Signal Process.*, vol. 39, no. 9, pp. 1973–1984, Sep. 1991.

[3] E. J. Candès and M. B. Wakin, "An introduction to compressive sampling," *IEEE Signal Process. Mag.*, vol. 25, no. 2, pp. 21–30, Mar. 2008.

[4] E. J. Candès, J. Romberg, and T. Tao, "Robust uncertainty principles: exact signal reconstruction from highly incomplete frequency information," *IEEE Transactions on Information Theory*, vol. 52, no. 2, pp. 489–509, 2 2006.

[5] D. Donoho, "Compressed sensing," *IEEE Transactions on Information Theory*, vol. 52, no. 4, pp. 1289–1306, 4 2006.

[6] M. Elad, *Sparse and Redundant Representations: From Theory to Applications in Signal and Image Processing.*   Springer, 2010.

[7] M. Wakin, S. Becker, E. Nakamura, M. Grant, E. Sovero, D. Ching, J. Yoo, J. Romberg, A. Emami-Neyestanak, and E. Candè, "A nonuniform sampler for wideband spectrally-sparse environments," *IEEE J. Emerg. Sel. Topic Circuits Syst.*, vol. 2, no. 3, pp. 516–529, Sep. 2012.

[8] K. Gedalyahu and Y. Eldar, "Time delay estimation: Compressed sensing over an infinite union of subspaces," in *IEEE International Conference on Acoustics Speech and Signal Processing*, 2010, pp. 3902–3905.

[9] P. Maechler, N. Felber, H. Kaeslin, and A. Burg, "Hardware-efficient random sampling of Fourier-sparse signals," in *IEEE International Symposium on Circuits and Systems (ISCAS)*, May 2012, pp. 269–272.

[10] M. Trakimas, R. D'Angelo, S. Aeron, T. Hancock, and S. Sonkusale, "A compressed sensing analog-to-information converter with edge-triggered SAR ADC core," *IEEE Transactions on Circuits and Systems I: Regular Papers*, vol. 60, no. 5, pp. 1135–1148, May 2013.

[11] P. Feng and Y. Bresler, "Spectrum-blind minimum-rate sampling and reconstruction of multiband signals," in *IEEE International Conference on Acoustics, Speech, and Signal Processing*, vol. 3, May 1996, pp. 1688–1691.

[12] Y. Bresler, "Spectrum-blind sampling and compressive sensing for continuous-index signals," in *Information Theory and Applications Workshop*, Jan. 27 2008-Feb. 1 2008, pp. 547–554.

[13] M. Mishali and Y. C. Eldar, "Blind multiband signal reconstruction: Compressed sensing for analog signals," *IEEE Trans. Signal Process.*, vol. 57, no. 3, pp. 993–1009, 2009.

[14] J. Tropp, J. Laska, M. Duarte, J. Romberg, and R. Baraniuk, "Beyond Nyquist: Efficient sampling of sparse bandlimited signals," *IEEE Trans. Inf. Theory*, vol. 56, no. 1, pp. 520–544, Jan. 2010.

[15] M. Mishali, Y. Eldar, O. Dounaevsky, and E. Shoshan, "Xampling: Analog to digital at sub-Nyquist rates," *IET Circuits, Devices and Systems*, vol. 5, no. 1, pp. 8–20, Jan. 2011.

[16] Kester, W.A. and Analog Devices, *Data Conversion Handbook*, ser. Analog Devices. Elsevier, 2005. [Online]. Available: http://books.google.dk/books?id=0aeBS6SgtR4C

[17] Y. C. Eldar and G. Kutyniok, *Compressed Sensing: Theory and Applications*. Cambridge University Press, 2012.

[18] T. Blumensath and M. Davies, "Normalized iterative hard thresholding: Guaranteed stability and performance," *IEEE Journal of Selected Topics in Signal Processing*, vol. 4, no. 2, pp. 298–309, 2010.

[19] T. Blumensath, "Accelerated iterative hard thresholding," in *Signal Process.*, vol. 92, no. 3, 2012, pp. 752–756.

[20] D. L. Donoho, A. Maleki, and A. Montanari, "Message-passing algorithms for compressed sensing," in *Proceedings of the National Academy of Sciences of the United States of America*, vol. 106 no. 45, 2009, pp. 18 914 –18 919.

[21] D. Donoho and J. Tanner, "Precise undersampling theorems," *Proceedings of the IEEE*, vol. 98, no. 6, pp. 913 –924, june 2010.

[22] R. Grigoryan, T. Jensen, T. Arildsen, and T. Larsen, "Reducing the computational complexity of reconstruction in compressed sensing nonuniform sampling," in *21st European Signal Processing Conference (EUSIPCO)*, 2013.

[23] S. Cotter, B. Rao, K. Engan, and K. Kreutz-Delgado, "Sparse solutions to linear inverse problems with multiple measurement vectors," *IEEE Trans. Signal Process.*, vol. 53, no. 7, pp. 2477–2488, Jul. 2005.

[24] L. Trefethen and D. Bau, *Numerical Linear Algebra*. Philadelphia: Society for Industrial and Applied Mathematics, 1997.

[25] T. H. Cormen, C. E. Leiserson, R. L. Rivest, and C. Stein, *Introduction to Algorithms*, 3rd ed. The MIT Press, 2009.

[26] F. Alted, "Why modern CPUs are starving and what can be done about it," *Computing in Science & Engineering*, pp. 68–71, Mar.–Apr. 2010.

[27] D. E. Knuth, *The Art of Computer Programming*. Addison-Wesley Publishing Company, 1969, vol. 1.

[28] M. Abramov, *Lecture Notes on Algorithms Complexity*. Moscow Center for Continuous Mathematical Education (MCNMO), 2009.

[29] T. Blumensath and M. E Davies, "How to use the iterative hard thresholding algorithm," in *SPARS'09 - Signal Processing with Adaptive Sparse Structured Representations*, Saint Malo, France, 2009.

[30] D. Needell and J. A. Tropp, "Cosamp: Iterative signal recovery from incomplete and inaccurate samples," *Applied and Computational Harmonic Analysis*, vol. 26, no. 3, pp. 301–321, 2009.

[31] R. Grigoryan, T. Arildsen, D. Tandur, and T. Larsen, "Performance comparison of reconstruction algorithms in discrete blind multi-coset sampling," in *IEEE International Symposium on Signal Processing and Information Technology (ISSPIT)*, 2012, pp. 147–152.

[32] I. Gorodnitsky and B. Rao, "Sparse signal reconstruction from limited data using FOCUSS: a re-weighted minimum norm algorithm," *IEEE Trans. Signal Process.*, vol. 45, no. 3, pp. 600–616, Mar. 1997.